

STUDYING LONG TERM LI-ION ELECTROLYTE  
DEGRADATION USING LITHIUM ION DIFFERENTIAL  
THERMAL ANALYSIS

by

Michael Bauer

Submitted in partial fulfilment of the requirements  
for the degree of Master of Science

at

Dalhousie University  
Halifax, Nova Scotia  
August 2018

© Copyright by Michael Bauer, 2018

# Table of Contents

<b>List of Tables.....</b>	<b>vii</b>
<b>List of Figures .....</b>	<b>viii</b>
<b>Abstract .....</b>	<b>xii</b>
<b>List of Abbreviations and Symbols Used.....</b>	<b>xiii</b>
<b>Acknowledgements.....</b>	<b>xv</b>
<b>Chapter 1: Introduction.....</b>	<b>1</b>
<b>Chapter 2: Experimental Techniques .....</b>	<b>4</b>
2.1 Li-ion Differential Thermal Analysis.....	4
2.1.1 Theoretical Background .....	4
2.1.2 Description of Apparatus .....	10
2.1.3 Measurement Protocol.....	13
2.1.4 Positive Peak Behaviour.....	16
2.1.5 Curve Interpretation .....	20
2.1.6 Measurement Sensitivity .....	22
2.1.7 Replicability .....	25
2.2 Other Experimental Techniques.....	26

2.2.1	Differential Scanning Calorimetry .....	27
2.2.2	Gas Chromatography.....	28
2.2.3	Mass Spectrometry.....	29
2.2.4	Gas Chromatography-Mass Spectrometry .....	31
2.2.5	ICP-OES.....	31

### **Chapter 3: Li-ion Cells .....33**

3.1	Electrodes .....	34
3.1.1	Negative Electrode .....	35
3.1.2	Positive Electrode.....	36
3.2	Separators .....	37
3.3	Electrolytes in Li-ion Cells .....	37
3.3.1	Solid Electrolyte Interphase .....	38
3.3.2	Requirements in Electrolyte Design.....	39
3.3.3	Ion Transport Properties.....	40
3.3.4	Lithium Salts .....	42
3.3.5	Additives .....	43
3.4	Electrolyte Degradation.....	45
3.4.1	Parasitic Reactions .....	46
3.4.2	Transesterification.....	48

**Chapter 4: The LiPF<sub>6</sub>-DMC Phase Diagram .....52**

4.1 Motivation ..... 52

4.2 Construction of Phase Diagrams ..... 55

4.3 High Concentration Regions ..... 59

**Chapter 5: Long Term Electrolyte Degradation.....63**

5.1 Physical Properties of Dry Cells ..... 63

5.2 Electrolyte Produced ..... 64

5.3 Cell Preparation Method ..... 67

5.4 Cycling Protocol..... 68

5.5 Testing Protocol ..... 68

5.5.1 Primary Test – Results ..... 69

5.5.2 Secondary Test – 2%VC High Voltage ..... 76

5.6 Replica Cells ..... 78

5.6.1 Ex-situ Study of Electrolyte ..... 79

5.6.2 Electrolyte Extraction Process ..... 79

5.6.3 Use of GC-MS and ICP-OES..... 79

5.6.4 Results of Ex-Situ Testing..... 80

5.6.5 Replication of Determined Electrolyte State..... 82

**Chapter 6: Results and Discussion .....86**

6.1	Comparison of Primary Test to EC:EMC DTA .....	86
6.2	Liquidus Point Movement versus Cycle Life.....	90
6.3	Electrolyte Changes in an Improved Cell Chemistry.....	96
<b>Chapter 7: Conclusion .....</b>		<b>100</b>
7.1	Conclusions.....	100
7.2	Future Work .....	101
7.2.1	Development of Additional Phase Diagrams .....	101
7.2.2	Observation of Dramatic Changes in the Electrolyte.....	102
7.2.3	Low Salt Tests.....	105
7.2.4	Cylindrical Cell Performance Post DTA.....	106
7.2.5	Exploration of Ternary Phase Diagrams .....	108
7.2.6	Additive Study.....	109
7.2.7	Software Development.....	109
7.2.8	Concentration Gradients and Room Temperature Cell Failure.....	110
7.2.9	Heat Capacity/Background Slope .....	111
7.2.10	Enthalpy of Fusion vs Composition.....	112
7.2.11	Finer Study of Post-Eutectic Regions .....	113
7.2.12	Extended Tests of Binary Phase Diagrams .....	114
7.2.13	Careful Study of Early Cell Life .....	115

7.2.14	Storage versus Cycling.....	116
7.2.15	Methyl Acetate Cells.....	117
7.2.16	Anode Free Cells.....	117
7.2.17	Positive Peak Investigation .....	118
7.2.18	Melting Points of Linear Carbonates .....	119
7.2.19	Electrolyte Evolution of EC:DMC.....	120
<b>Bibliography .....</b>		<b>122</b>
<b>Appendix A: Solvent Melting Points.....</b>		<b>128</b>
<b>Appendix B: Permissions.....</b>		<b>130</b>

## List of Tables

Table 5.1: A brief summary of the physical properties of the cells used in this thesis.....	64
Table 5.2: Names, structures, and melting points of chemicals discussed in this thesis. .	66
Table 5.3: The results of the GC-MS and ICP-OES tests conducted on the VC cells ex-situ. .....	81
Table 5.4: The results of the GC-MS and ICP-OES tests conducted on the PES-211D cells. .....	81
Table 6.1: A comparison of the EC:EMC ratios of the opened cells, in terms of lost EMC content.....	86

## List of Figures

Figure 2.1: A solvent-solvent phase diagram between EC and EMC, with several points filled in that show the effect of LiPF <sub>6</sub> salt in the solvent.....	6
Figure 2.2: DTA data for 1 M LiPF <sub>6</sub> in DMC. The left panel shows the data as immediately generated by the DTA system, the middle panel shows the DTA curve, and the right panel shows the LiPF <sub>6</sub> -DMC phase diagram.....	7
Figure 2.3: A solvent-solvent phase diagram between EC and DMC, with all phases labelled, and the eutectic at 0.292 mole fraction of DMC. ....	9
Figure 2.4: A schematic diagram of the DTA apparatus used in this thesis.....	10
Figure 2.5: A schematic diagram of the components inside the DTA Dewar .....	11
Figure 2.6: A schematic diagram of the inside of the DTA cryostat used in this thesis... ..	12
Figure 2.7: An 18650 form factor cell, run three times, with heating rates of 1.0 °C/min, 0.5°C/min, and 0.25°C/min.....	16
Figure 2.8: A DTA curve with a positive peak being removed.....	18
Figure 2.9: A cell, before and after a peak removal run on the feature at -85°C.....	19
Figure 2.10: Liquidus and solidus determination on a sample dataset of 0.4 M LiPF <sub>6</sub> in DMC. ....	20
Figure 2.11: The linear background integration method of interpreting the area under the peak on a sample dataset of 0.4 M LiPF <sub>6</sub> in DMC. ....	21
Figure 2.12: A comparative study between DTA and DSC on 1 M 3:7(w%) EC:EMC. . .	23
Figure 2.13: A comparison of electrolyte mass to DTA peak integration area for a set of 18650 cells. ....	24
Figure 2.14: A comparison of electrolyte mass to DTA peak integration area for a set of pouch cells, as conducted by Ryan Day.....	25
Figure 2.15: Data from two successive DTA tests performed on one cell. ....	26
Figure 2.16: A diagram of the basic components of a Gas Chromatography device. ....	28
Figure 2.17: A diagram of the basic components of a quadrupole mass analysis device. ....	30
Figure 2.18: A diagram of the basic components of the ICP-OES system.....	32



Figure 3.1: A schematic diagram of a Li-ion cell.....	33
Figure 4.1: The conductivity of a sample of 1M LiPF <sub>6</sub> in DMC and a DTA curve of a cell containing 1 M LiPF <sub>6</sub> in DMC.....	53
Figure 4.2: The conductivity and DTA curve of 1 M LiPF <sub>6</sub> in 80:10:10 DMC:EC:EMC, against temperature. ....	55
Figure 4.3: A set of DTA curves for LiPF <sub>6</sub> -DMC electrolytes between 0 and 2M, at intervals of 0.2 M.....	57
Figure 4.4: The LiPF <sub>6</sub> -DMC phase diagram from 0 to 24% LiPF <sub>6</sub> by weight. ....	58
Figure 4.5: Part of the high concentration region of the LiPF <sub>6</sub> -DMC space, alongside the lower concentration data.....	60
Figure 4.6: A speculative phase diagram of the LiPF <sub>6</sub> -DMC system that includes regions of very high salt content. ....	61
Figure 5.1: A typical DTA curve from a 1 M 3:7 (w%) EC:EMC LiPF <sub>6</sub> pouch cell. ....	69
Figure 5.2: Cycling (left) and DTA (right) data for cell 52367, an NMC532/NG cell with 1.0 M LiPF <sub>6</sub> in 3:7 w% EC:EMC + 2VC electrolyte, cycled to 4.1V. ....	70
Figure 5.3: Cycling (left) and DTA (right) data for cell 52371, an NMC532/NG cell with 1.0 M LiPF <sub>6</sub> in 3:7 w% EC:EMC + 2VC electrolyte, cycled to 4.2V. ....	70
Figure 5.4: Cycling (left) and DTA (right) data for cell 52375, an NMC532/NG cell with 1.0 M LiPF <sub>6</sub> in 3:7 w% EC:EMC + 2VC electrolyte, cycled to 4.3V. ....	71
Figure 5.5: Cycling (left) and DTA (right) data for cell 52377, an NMC532/NG cell with 1.0 M LiPF <sub>6</sub> in 3:7 w% EC:EMC + 2VC electrolyte, cycled to 4.4V. ....	71
Figure 5.6: Cycling (left) and DTA (right) data for cell 52383, an NMC532/NG cell with 1.0 M LiPF <sub>6</sub> in 3:7 w% EC:EMC + 2VC electrolyte, cycled to 4.1V. ....	72
Figure 5.7: Cycling (left) and DTA (right) data for cell 52386, an NMC532/NG cell with 1.0 M LiPF <sub>6</sub> in 3:7 w% EC:EMC + PES-211D electrolyte, cycled to 4.1V.....	72
Figure 5.8: Cycling (left) and DTA (right) data for cell 52390, an NMC532/NG cell with 1.0 M LiPF <sub>6</sub> in 3:7 w% EC:EMC + PES-211D electrolyte, cycled to 4.2V.....	73
Figure 5.9: Cycling (left) and DTA (right) data for cell 52393, an NMC532/NG cell with 1.0 M LiPF <sub>6</sub> in 3:7 w% EC:EMC + PES-211D electrolyte, cycled to 4.3V.....	73
Figure 5.10: Cycling(left) and DTA(right) data for cell 52399, an NMC532/NG cell with 1.0 M LiPF <sub>6</sub> in 3:7 w% EC:EMC + PES-211D electrolyte, cycled to 4.4V.....	74

Figure 5.11: Cycling(left) and DTA(right) data for cell 52401, an NMC532/NG cell with 1.0 M LiPF <sub>6</sub> in 3:7 w% EC:EMC + PES-211D electrolyte, cycled to 4.5V.....	74
Figure 5.12: Cycling(left) and early DTA data(right) from cell 64928, a 1.0 M LiPF <sub>6</sub> in 3:7 EC:EMC 2VC 4.5 V NMC532/NG cell. ....	76
Figure 5.13: Cycling(left) and late DTA data(right) from cell 64928, a 1.0 M LiPF <sub>6</sub> in 3:7 EC:EMC 2VC 4.5 V NMC532/NG cell.. ....	77
Figure 5.14: Cycling(left) and DTA data(right) from cell 64929, a 1.0 M LiPF <sub>6</sub> in 3:7 EC:EMC 2VC 4.5 V NMC532/NG cell.. ....	77
Figure 5.15: A comparison of the DTA data generate by the last test of cell 52367, a 1.0 M LiPF <sub>6</sub> in 3:7 EC:EMC NMC532/NG cell cycled to 4.1V, and a replica cell.....	83
Figure 5.16: A comparison of the DTA data generate by the last test of cell 52371, a 1.0 M LiPF <sub>6</sub> in 3:7 EC:EMC NMC532/NG cell cycled to 4.2V, and a replica cell.....	84
Figure 5.17: A comparison of the DTA data generate by the last test of cell 64929, a 1.0 M LiPF <sub>6</sub> in 3:7 EC:EMC NMC532/NG cell cycled to 4.5V, and a replica cell.....	85
Figure 6.1: DTA data collected on cells with a 33.3:66.6 ratio of EC:EMC and variable amounts of LiPF <sub>6</sub> . ....	87
Figure 6.2: DTA data collected on cells with 1.0 M LiPF <sub>6</sub> in EC:EMC cells with variable amounts of EC.....	88
Figure 6.3: The relationship between decreasing LiPF <sub>6</sub> molarity and the liquidus temperature for the 3:7 EC:EMC LiPF <sub>6</sub> electrolyte, as determined by Ryan Day. ....	90
Figure 6.4: Liquidus points versus cycle count for a selection of the cells in the primary test, in shown in section 5.5.1. ....	91
Figure 6.5: Approximate LiPF <sub>6</sub> molarity, calculated by neglecting the influence of EMC loss on the measured liquidus temperature. ....	93
Figure 6.6: The molarity-cycle count data for the less regularly tested cells overlaid against the data shown in Figure 6.5.....	94
Figure 6.7: Cycling data for cells 63397, 63399, 63401, 63403, 63404, 63405.....	98
Figure 6.8: DTA data for cells 63397, 63399, 63401, 63403, 63404, and 63405. ....	99
Figure 7.1: A closeup of the cycling data and the relevant DTA curves of cell 64928, a 4.5 V VC cell. ....	103
Figure 7.2: DTA curves of low salt tests. ....	106

Figure 7.3: Cycling data from cylindrical cells that displayed slight improvement after DTA testing.....	107
Figure 7.4: A comparison of the background slopes observed in cells with different chemistries. ....	111
Figure 7.5: A comparison of the DTA curves of three cells with different salt concentrations and identical solvent compositions. ....	113

## Abstract

Lithium ion cells contain liquid electrolytes that degrade over the lifetime of the cell. Though the results of this degradation are well understood, the pathways are not. Lithium ion differential thermal analysis (Li-ion DTA) is a non-destructive in-situ method for probing the state of an electrolyte in a cell. This functions by controlled cooling and heating through the freezing point of the electrolyte. The temperature signal of the cell will then show phase transitions that can be associated with the components of the electrolyte.

This thesis discusses several experiments using this method. These are: a proof of concept of the creation of salt-solvent diagrams, a long term study of the effects of cycling on standard electrolytes, a short term test, that examines the effects of high voltage on electrolyte composition. These experiments have resulted in the creation of a method to study electrolyte molarity *in situ*.

## List of Abbreviations and Symbols Used

AG	Artificial graphite
CCCV	Constant current constant voltage
CE	Coulombic efficiency
DEC	Diethyl carbonate
DEOHC	Diethyl-2,5-dioxahexane carboxylate
DMC	Dimethyl carbonate
DMOHC	Dimethyl-2,5-dioxahexane carboxylate
DSC	Differential scanning calorimetry
DTA	Differential thermal analysis
DTD	1,3,2-Dioxathiolane-2,2-dioxide (also ethylene sulfate)
EC	Ethylene carbonate
EMC	Ethyl methyl carbonate
EMOHC	Ethyl methyl-2,5-dioxahexane carboxylate
FEC	Fluoroethylene carbonate
GC	Gas chromatography
GC-MS	Gas chromatography coupled with mass spectrometry
ICP-OES	Inductively coupled plasma optical emission spectrometry
LCO	LiCoO <sub>2</sub>
LiBOB	Lithium bis(oxalato)borate (LiB(C <sub>2</sub> O <sub>4</sub> ) <sub>2</sub> )
LiFSI	Lithium bis(fluorosulfonyl)imide (LiN(SO <sub>2</sub> F) <sub>2</sub> )
LiTFSI	Lithium bis(trifluoromethanesulfonyl)imide (LiN(SO <sub>2</sub> CF <sub>3</sub> ) <sub>2</sub> )
LMO	Li <sub>1+x</sub> Mn <sub>2-x</sub> O <sub>4</sub>
LN <sub>2</sub>	Liquid nitrogen

MS	Mass spectrometry
NCA	$\text{Li}(\text{Ni}_{1-x-y}\text{Co}_x\text{Al}_y)\text{O}_2$
NG	Natural graphite
NMC	$\text{Li}(\text{Ni}_{1-x-y}\text{Mn}_x\text{Co}_y)\text{O}_2$
NMC532	$\text{Li}(\text{Ni}_{0.5}\text{Mn}_{0.3}\text{Co}_{0.2})\text{O}_2$
OCV	Open circuit voltage
PES	Prop-1-ene-1,3-sultone
PES-211D	Additive blend 2% PES + 1% DTD + 1% TTSPi
SEI	Solid electrolyte interphase
TTSPi	Tris(trimethylsilyl) phosphite
VC	Vinylene carbonate
M	Molarity
m	Molality
$n$	Free ion number
$r$	Solvation radius
$t$	Time
$Z$	Atomic valence number
$\epsilon$	Dielectric constant
$\eta$	Viscosity
$\mu$	Ionic mobility
$\sigma$	Conductivity

## **Acknowledgements**

I am very grateful to the people who have lent their help and support to me over these past years. First and foremost among them is my supervisor, Jeff Dahn, for his patience, guidance, and passion, throughout this project. I would also like to thank Lauren Thompson, for her part in conducting the ex-situ tests shown in this work. As well, thanks go to thank Simon Trussler and Simon de Vet for their assistance in fabricating parts needed for this work, as well as Michel Johnson and David Stevens, whose technical knowledge helped keep the equipment functional. I would also like to thank everyone in the Dahn Lab, for the help and inspiration they have provided. Finally, I would also like to thank my family for their support and enthusiasm throughout my degree.

## **Chapter 1: Introduction**

Lithium ion cells are one of the most common power storage systems for applications requiring portability, long term rechargeability, and high energy density. They are used to power everything from laptops, to phones, tablets, toys, implantable medical devices, power tools, electric vehicles, and even houses. Each of these applications has specific requirements in terms of the challenges faced. To this end, Li-ion batteries must be developed to have the highest possible energy density, longevity, current rate, safety, and affordability.

Unlike conventional non-rechargeable batteries, Li-ion cells do not have a set chemistry; there are many components of Li-ion cells that can be optimized for different applications. Further, though much work has been done in studying the mechanisms by which Li-ion cells function, a complete model for all interactions that can occur between the components of a cell has not been, and may never be, developed. Thus, determination of the best cells often involves some degree of trial and error. Further complicating this is that many of the methods used in determining the state of the trialed components are only possible ex-situ. Thus, cells must be created, cycled, and destroyed, to understand their behaviour, and the interactions in the cell itself. This has led to a search for methods by which the state of the cell could be probed without destroying the cell. Lithium ion differential thermal analysis (Li-ion DTA) is one such method. This thesis will explain the mechanisms and utility of this method and demonstrate its use in several areas. Though the proper name is Li-ion DTA, this thesis will refer to this system as “DTA”, for brevity.



This thesis presents and demonstrates several valuable uses of DTA, including the use and value of compositional phase diagrams in cell design, and the study of the electrolyte degradation of a series of cells cycled to high temperature and voltages.

Chapter 2 introduces the theoretical basis of the experimental systems being used in this thesis. This includes Li-ion DTA, as well as the various *ex situ* systems. As well, commentary is given as to compositional phase diagrams, how they relate to electrolyte, and how they can be used in conjunction with DTA to study the state of electrolyte *in situ*. This chapter also introduces the experimental DTA apparatus, as well as protocols developed, and analysis tools used.

Chapter 3 introduces the components of Li-ion cells. Commentary is given on all parts of the cell, but special attention is given to the electrolyte. This section also outlines degradations observed in the electrolyte that can be observed by DTA and how these features indicate cell aging.

Chapter 4 introduces the salt-solvent phase diagram. These phase diagrams are vital to the full evaluation of DTA curves. In the past, these diagrams have been generated via DSC testing, but they can also be made using DTA. This process is demonstrated in this chapter via the creation of a binary salt-solvent phase diagram of dimethyl carbonate (DMC) and LiPF<sub>6</sub>.

Chapter 5 introduces the sets of cells produced, including the electrolytes used. This section also outlines the physical properties of the cells, and the protocol for filling with electrolyte, preparation for testing, and the cycling protocol. Two main experiments are detailed: a long term cycling test, and a short term high voltage cycling test. This chapter also presents the replica cell concept and results. These replica cells are used to

confirm the results of the *ex situ* electrolyte analysis with reference to the last of the DTA tests conducted on the cell.

Chapter 6 presents the analysis conducted on the cells, as well as the interpretation of the results of the experiments. This is primarily focused on the location of the liquidus peak, and how this reflects the mechanism by which the electrolyte degrades over time.

Chapter 7 presents the conclusions made from the work, as well as outlines for new projects to be done in the future. These include the production of more phase diagrams, the analysis of subtle features in salt-solvent phase diagrams, examinations of specific regions of ternary solvent diagrams, the behaviour of post-eutectic electrolytes in commercial cells, among many other projects.

## **Chapter 2: Experimental Techniques**

This work uses and references several experimental techniques. The primary experimental technique used is Li-ion differential thermal analysis (DTA), but several other systems were used and referenced, including differential scanning calorimetry (DSC), gas chromatography (GC), mass spectrometry (MS), and inductively coupled optical emission spectrometry (ICP-OES). Of these, DTA, ICP-OES, and GC-MS were used in this thesis; DSC was only referenced as a benchmark for comparison and confirmation in previous work.<sup>1</sup>

### **2.1 Li-ion Differential Thermal Analysis**

#### **2.1.1 Theoretical Background**

Li-ion Differential thermal analysis is a non-destructive method for studying the state of the electrolyte in a Li-ion cell. Although there are numerous methods for studying the electrolyte that is or was present in a cell, most of these methods involve removing the electrolyte from the cell. This process destroys the cell, and thus prevents further cycling and electrolyte evolution. With DTA, the cell remains intact, with no perturbation to further cycling. Thus, DTA can be used to perform multiple studies of a cell's electrolyte over the course of a cell's cycle life. The resultant data, when used alongside compositional phase diagrams detailing the phase behaviour of the original electrolyte, can be interpreted to show the amount of electrolyte remaining, the amounts of salt remaining, and the overall composition of the solvent component of the electrolyte.

There are several basic components needed to conduct a DTA test. These components are as follows: a sample cell to be tested, a reference cell filled with a liquid

with a very low freezing point, and a thermally isolated device that can hold, and measure the temperature of, a reference and sample cells in an airtight helium environment that can be cooled and heated to and from cryogenic temperatures at a constant rate.

A DTA test involves the use of such a device to cool and heat both the sample and reference cells to and from a temperature at which the sample is frozen, but the reference is still in its liquid phase. The heating process will drive the sample cell electrolyte through at least one phase transition, during which the sample cell's heating rate will slow down or stop with respect to the reference cell and the environment. Thus, the temperature signal of the sample cell will show the temperatures at which the sample cell electrolyte undergoes a phase transition. The temperature signal of the reference cell will show how an electrolyte with a similar mass and heat capacity would behave under the same conditions with no phase transition. The difference between these temperature signals is plotted against the sample cell's temperature, forming what is called a DTA curve. This curve shows peaks at each phase transition temperature, that are, if analyzed fully, proportional to the enthalpy change caused by the phase transition of one material in the sample cell. Thus, if the phase transitions and enthalpies of fusion of all materials in the sample cell are well understood, the DTA curve can be analyzed to obtain information as to the composition and mass of the sample cell electrolyte.

Heavily cycled Li-ion cells contain a few main solvents, one or more lithium salts, and some number of reaction side products, normally present in concentrations of a few percent. Exact study of each of these side reaction products by DTA is not practical, as each would affect the others in unique ways. A practical system of analysis would give an

estimate of the amount of the main expected solvents present, as well as the expected salt concentration, and an estimation as to the total mass of remaining electrolyte.

Understanding the phase transitions present in an electrolyte with even a few components is not trivial and requires the creation of compositional phase diagrams. These diagrams show the phase behaviour of an electrolyte mixture versus temperature. While a pure solvent has just one liquid-solid phase transition, a binary solvent has a complex phase diagram. Figure 2.1 shows a binary solvent-solvent phase diagram, where the liquidus and solidus lines indicate the boundaries between the phases. These are the points where the first and last freezing occurs, or vice versa, in terms of temperature.

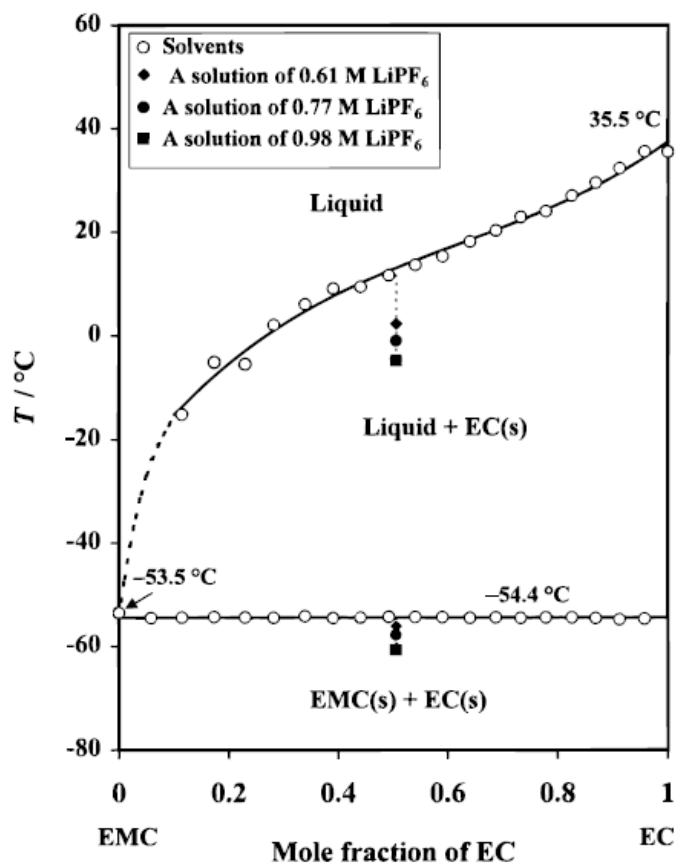


Figure 2.1: A solvent-solvent phase diagram between EC and EMC, with several points filled in that show the effect of LiPF<sub>6</sub> salt in the solvent. Reproduced with permission from *J. Electrochem. Soc.*, **147** 1688-1694. Copyright 2000, The Electrochemical Society

Figure 2.1 shows a binary compositional phase diagram developed by Ding *et al.* for the mixture of ethylene carbonate (EC) and ethyl methyl carbonate (EMC).<sup>2</sup> This diagram shows that, when a binary solvent mixture is cooled to the liquidus curve, the solvent undergoes an initial freezing event where some of the EC freezes out. This leaves the remaining liquid with a lower concentration of EC, and thus a lower freezing point than the original mixture. Thus, a sample in the region between the solidus and liquidus lines will consist of some combination of the liquid phase of EMC and EC, as well as solid EC. When the sample is cooled to the solidus, all EC is frozen, and the EMC in the sample will freeze all at once, as would a conventional single solvent at its melting point. In the opposite case, when a solid mixture of EC and EMC is heated to the solidus, some of the EMC melts, followed quickly by EC melting through the region before the liquidus curve, at which point the EC is done melting.

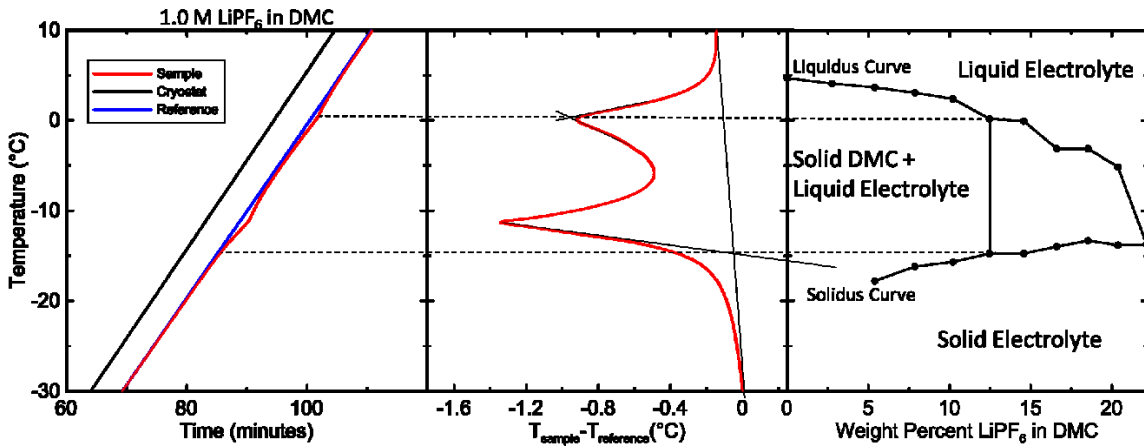


Figure 2.2: DTA data for 1 M LiPF<sub>6</sub> in DMC. The left panel shows the data as immediately generated by the DTA system, the middle panel shows the DTA curve, and the right panel shows the LiPF<sub>6</sub>-DMC phase diagram.

The left panel of Figure 2.2 shows the real temperature data collected during a DTA run of 1 M LiPF<sub>6</sub> in DMC. As the sample is heated to its solidus temperature, a sharp peak is created, followed by a broader liquidus feature, whose peak is at the liquidus line, as in

the middle panel. These two temperatures, the low temperature onset of the solidus, and the temperature of the peak of the liquidus, can then be compared against a phase diagram of the electrolyte system, to determine the composition of the sample cell electrolyte.

These diagrams are also useful for Li-ion cell design. In solutions primarily composed of one solvent, the liquidus temperature will be close to the melting point of the dominant solvent. As the ratio of one solvent to the other solvent increases, the liquidus line will be further depressed toward the solidus. At a certain level of concentration, the liquidus depression will be such that the liquidus and solidus curves will meet, as shown at 0.292 mole fraction of DMC to EC in Figure 2.3. This point is called the eutectic, the composition at which the mixture will have its lowest possible initial freezing point. Thus, the eutectic gives the widest practical temperature range for a Li-ion cell.

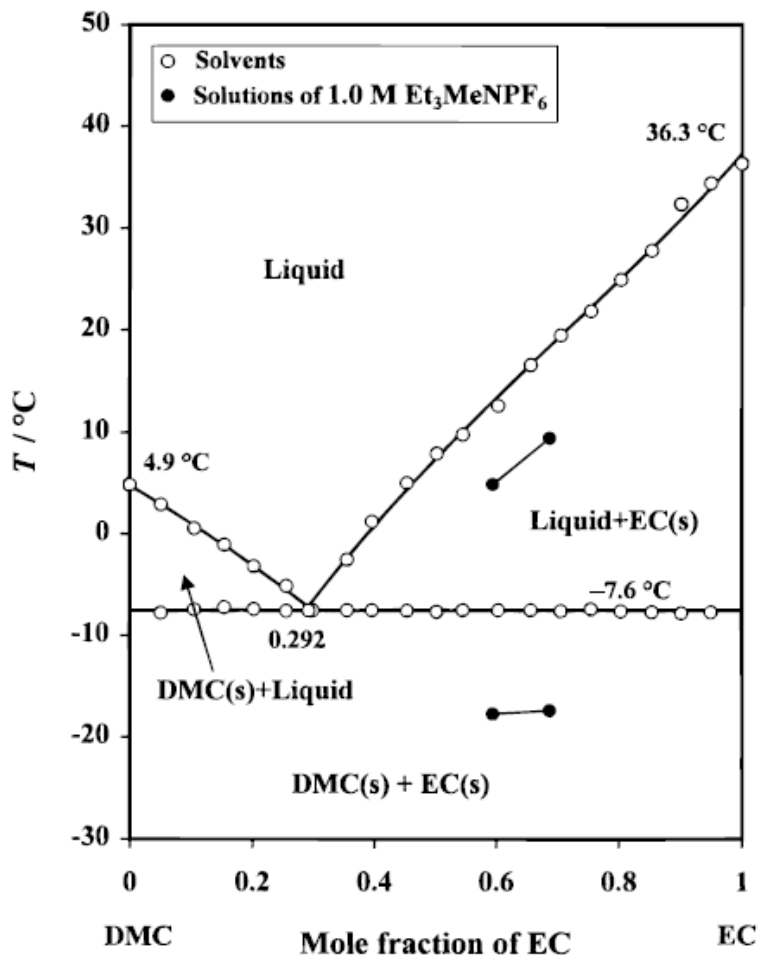


Figure 2.3: A solvent-solvent phase diagram between EC and DMC, with all phases labelled, and the eutectic at 0.292 mole fraction of DMC. Reproduced with permission from *J. Electrochem. Soc.*, **147** 1688-1694. Copyright 2000, The Electrochemical Society

Several valuable observations can be made from a DTA curve. First, if the background is subtracted, the amount of remaining electrolyte can be determined approximately, by comparison to a fresh cell of the same original electrolyte. Second, the locations of the peaks can be compared between cells to determine the relative amount of a remaining component. An often observable metric is the location of the liquidus feature. As the salt content impacts the location of the liquidus as shown in Figure 2.3, movement to higher temperatures can indicate salt consumption in the cell.



### 2.1.2 Description of Apparatus

The specific design of a DTA apparatus can be changed to accommodate different cell sizes and controllers, if the general principles described in section 2.1.1 are observed. The apparatus presented here, used to generate the data shown in this thesis, uses in house software, as well as custom built equipment and commercial hardware. The apparatus was originally developed by Day *et al.*<sup>1</sup> A schematic diagram of the entire apparatus is shown in Figure 2.4, with diagrams showing more detail on the components inside the Dewar in Figures 2.5 and 2.6.

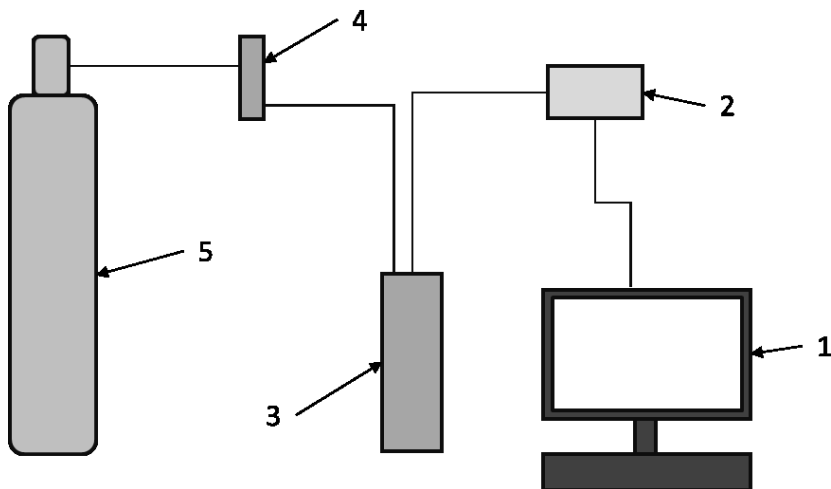


Figure 2.4: A schematic diagram of the DTA apparatus used in this thesis. Programs on the computer (1), control the temperature controller (2), which monitors and controls the temperature of the cryostat in the liquid nitrogen (LN<sub>2</sub>) filled Dewar (3). The cryostat is filled with helium gas from the tank (5), the flow of which is controlled by the rotameter (4).

In the apparatus used here, cooling is provided via contact with a copper post in the LN<sub>2</sub> Dewar. The apparatus is controlled by a LakeShore model 338 Temperature Controller and code written in Visual Basic running on the computer. The helium flow is controlled via a Matheson gas rotameter at 80 ml/min throughout the testing procedure. The helium gas itself is 99.995% pure and supplied by Praxair.

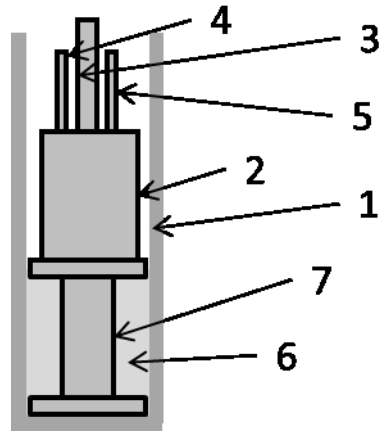


Figure 2.5: A schematic diagram of the items inside of the Dewar(1). The cryostat (2) is connected to the controller via the wires in a thin walled stainless steel tube (3). The cryostat is filled with helium via the in and out tubes (4,5). The cryostat is thermodynamically coupled to a LN<sub>2</sub> reservoir (6) by a copper post (7) submerged in the LN<sub>2</sub>.

Figure 2.5 shows that the Dewar contains the cryostat, LN<sub>2</sub>, and a copper post. The cryostat consists of an airtight aluminum can containing the temperature probe, shown in Figure 2.6, with wiring leading to the control systems shown in Figure 2.4 and helium tubing leading in and out of the top. The copper post serves to provide thermal contact between the cryostat and the LN<sub>2</sub>. Without the post, the cryostat would require regular attention to stay in proper thermal contact with the LN<sub>2</sub>.

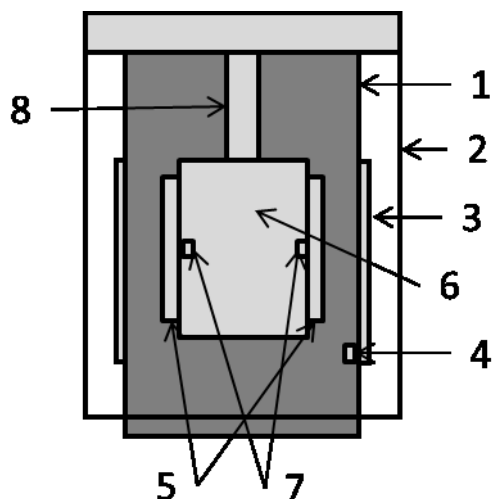


Figure 2.6: A schematic diagram of the inside of the cryostat used in this thesis. The cryostat can (1) is surrounded by insulating alumina wool (2), heated by a small heater tape (3), and its temperature is measured by a small resistor (4). The can also contains the reference and sample cells (5) on a polypropylene mount (6). The temperature of the cells is monitored by small resistance temperature devices (RTD) in the mount (7). The mount is connected to the cryostat via a thin walled stainless-steel tube (8)

The pouch cell probe system used in this thesis, shown in Figure 2.6, consists of a hollow polypropylene mount, filled with alumina wool for temperature insulation, a sample cell and a reference cell all of which is connected via thin walled stainless steel tubing to the stainless steel cryostat lid. In this work, the reference cell contained 1.0 M  $\text{LiPF}_6$  in methyl acetate (MA), which has a liquidus temperature of  $\sim -105^\circ\text{C}$ , considerably lower than the solidus of any combination used in this thesis. The cell temperatures are monitored by contact with  $100\ \Omega$  platinum resistors and the cryostat's temperature is measured by another resistor of the same type, affixed to the inside surface. The sample mount itself is custom built for the currently used geometry of cells, but it can be easily replaced by fabricating a new mount, for any desired geometry. The cryostat is filled with helium gas, for greater thermal conductivity, and heated externally via an Electroflex 30 W heating

tape. As an aside, the cryostat temperature does not serve as a good reference, as it is too far decoupled from the cells, and is susceptible to minor temperature fluctuations.

While the cryostat described here tests pouch cells, two other cryostats have been used in work done concurrently with this thesis, for testing cylindrical 18650 (18 by 65 mm) and 2170 (21 by 70 mm) cells. These cryostats can be hooked up to the larger testing apparatus easily.

### **2.1.3 Measurement Protocol**

DTA measurements consist of linear cooling down to a lower setpoint temperature, a hold for some time at that setpoint, and linear heating to room temperature. The lower setpoint temperature should be several degrees lower than the solidus temperature of the electrolyte, to allow the cell to reach a linear heating rate before the phase transition begins. Cells with different form factors, or sizes and shapes, take different amounts of time to reach a linear heating rate. While pouch cells take around five minutes, cylindrical cells take around twenty minutes. Pouch cells with an electrolyte based on 3:7 EC:EMC solvent should have a lower setpoint of  $-100^{\circ}\text{C}$ , while cells based on EC:DMC or DMC should have lower setpoints of  $-70^{\circ}\text{C}$  or  $-45^{\circ}\text{C}$ , respectively.

For reliable, repeatable DTA data to be obtained, the DTA test procedure must be standardized. In the case of a pouch cell, a sample cell is selected and cleaned of any material on an arbitrarily chosen face. Then, the positive and negative tabs are folded down on opposite sides of the cell and taped down, to prevent accidental discharge of the cell during handling. Then, the remaining head space of the pouch cell is folded away from the testing face. A small amount of Apezion N low-temperature thermal grease is applied to

the cell, which gives better thermal contact between the cell and the RTD mount. The cell is then placed on the polypropylene mount, such that the grease is directly over the RTD, and the corners of the cell are square with the corners of the cell mount. Bread ties are used to affix the cells to the mount. These ties hold the cells in place, provide pressure toward the RTDs, and do not provide significant thermal contact between the cells. Ideally, the same bread ties would be used without modification for all cells of one type, to better standardize the contact pressure between the cell and the RTD surface.

The cryostat is then closed; the four hex screws are driven to finger tightness, then given another quarter turn for an airtight seal. Following this, the cryostat must be filled with helium gas, to create a good thermal connection between the cells and the cryostat. This is done by setting the cryostat to 160 ml/min, filling to approximately 4 atm helium and releasing the atmospheric valve, repeating this eight times, and resetting the rotameter down to 80 ml/min for the duration of the run.

Once the cryostat is filled with helium, the lower and upper setpoints and temperature rates in cooling and heating are specified. In this thesis, cell cooling was done at 3.0°C/min, while heating was done at 1.0°C/min. The cooling rate should be linear, and heating rate should be kept as low as possible. An extremely rapid temperature change in the cooling curve might disturb the crystallization of the electrolyte, which could lead to poor quality data, but speed is not a significant concern. This is not trivial and requires careful adjustment of the cryostat inside the Dewar, to manipulate the cryostat's contact with the copper post. However, any deviation in the heating rate would lead to non-linear temperature regions, rendering the dataset unreliable, and therefore useless. Once the cryostat has reached the setpoint, it is lifted away from the copper post. The heater cannot

provide enough power to heat the cryostat while it is in thermal contact with the LN<sub>2</sub>, so thermal contact must be broken. This should be done during the hold, as the movement will temporarily upset the heating rate. Once the cryostat is back to room temperature, the test is complete.

While this thesis used heating and cooling rates of 1.0°C/min and 3.0°C/min, these are not required, and can be changed based on the requirements of the experiment. Low cooling rates do not significantly affect the DTA signal, but high cooling rates tend to be unstable. Thus, they take considerable care to maintain linear cooling while having only minimal benefits in terms of time saved. However, the heating rate is very important. Each decrease in heating rate corresponds to a considerable increase in the resolution of the DTA curve. Figure 2.7 shows that, at lower heating rates, the same peaks are visible, but the features are more accurate, especially the high temperature side of the liquidus feature. Theoretically, this slope should be vertical. It is a slope due to finite heating rates. As well, the reduction in peak size is due to the increase in time taken. At lower heating rates, less frozen electrolyte is melting at any given time, thus reducing the temperature deviation in the sample cell, and thus the height of the peak.

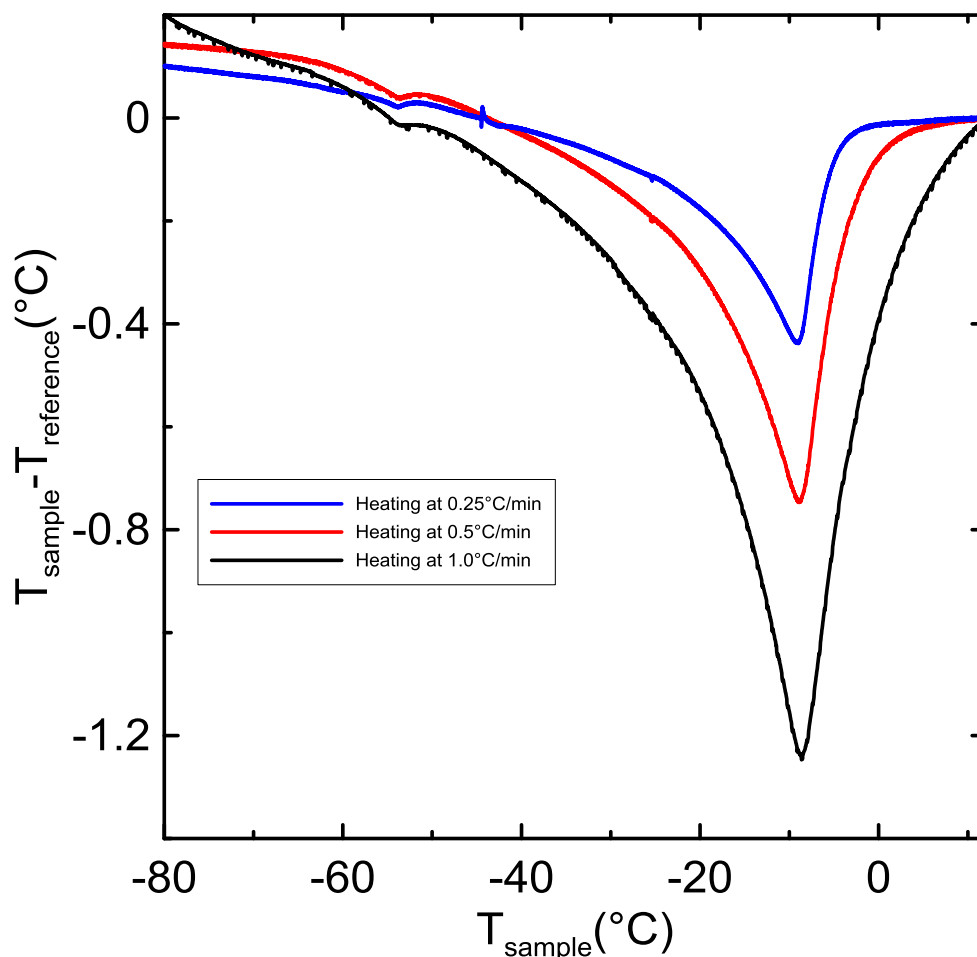


Figure 2.7: An 18650 form factor cell, run three times, with heating rates of 1.0 °C/min, 0.5°C/min, and 0.25°C/min. Decreasing heating speed allows for greater resolution of melting behaviour.

However, though the benefit to data fidelity is significant, so too is the increase in time taken. The work presented in this thesis uses a 1.0°C/min heating rate. This is a largely arbitrary choice, that balances the data quality and time taken to measure one cell.

#### 2.1.4 Positive Peak Behaviour

Several DTA tests, some in this thesis and some performed concurrently, were noted to show positive peaks that appeared repeatably on successive tests. These features suggest that the electrolyte underwent some exothermic phase transition. This phase

transition was hypothesized to be from an amorphous solid electrolyte state to a crystalline one. This is in analogy to more well-known amorphous-crystalline transitions in amorphous silicon alloys.<sup>3,4</sup> Carlsson *et al.* describe an exothermic phase transition called polymorphous crystallization, where silicon/non-metal alloys show phase transitions between a high free energy amorphous phase and a lower free energy crystalline phase.<sup>4</sup> This sort of behaviour would explain the positive peaks observed here.

While these peaks were initially ignored, a cell series showing them consistently in the low temperature background necessitated their removal, to determine the baseline of the DTA curve. The proposed method to correct for the feature is to heat the amorphous solid electrolyte through the crystallization, and then cool the cell down to the lower setpoint and proceed as normal through the heating curve.



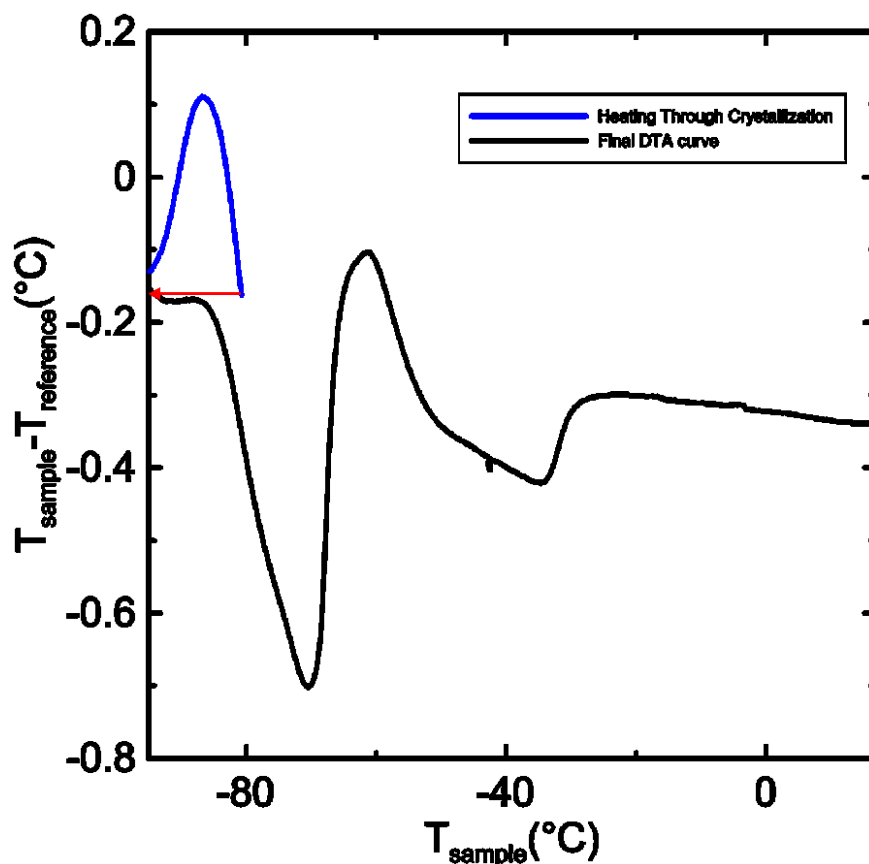


Figure 2.8: A DTA curve with a positive peak being removed. The red arrow represents the cell returning to the lower setpoint.

The removal of these peaks tends to cause slight changes in the rest of the curve, and their appearance at the lower end of curves tends to leave the background of the data occluded. Thus, it is best to remove them, where possible. A protocol was developed to remove the positive peak from the curve; first, the cell is run as normal, to determine the temperatures at which the positive peak occurs and establish where the low temperature background should be. Then, the cell is cooled to a temperature below the positive peak and heated to the temperature where the positive peak joined the background. Then, the cell is cooled back down to the original low temperature and heated to room temperature as normal. Though these peaks can appear in the middle of the curve, they are only removed when appearing outside the main features, as removing them inside the main

features does not work well. Though this behaviour was observed throughout the work composing this thesis, the protocol was developed after the bulk of the work presented was completed.

Figure 2.9 shows an example of the protocol as used on a cell. Note that the elimination results in several changes to the DTA curve, especially in the size of the two main features.

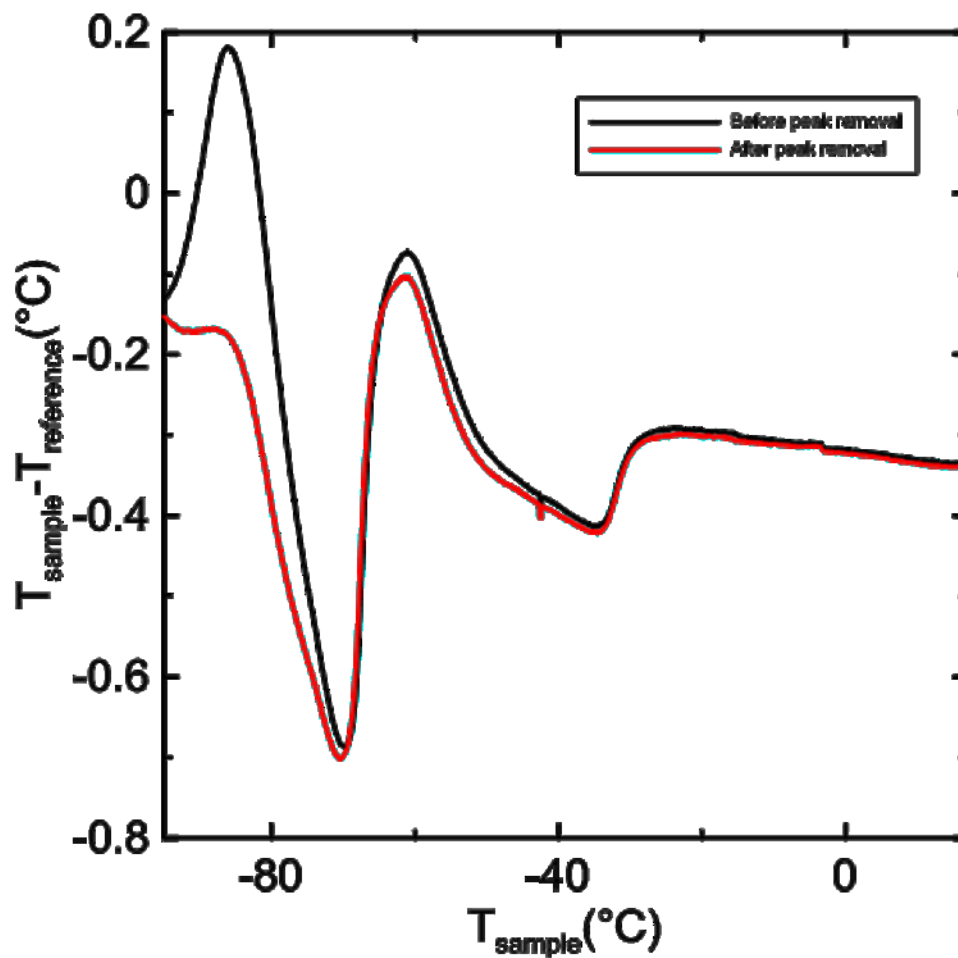


Figure 2.9: A cell, before and after a peak removal run on the feature at -85°C. Note the increase in the size of both primary features after the peak removal run. The second positive peak, at -60 degrees, was not removed. This sample is 1.2 M  $\text{LiPF}_6$  in 3:7 EC:EMC (w%) +2%VC+1%DTD.

### 2.1.5 Curve Interpretation

As of this writing, there are a few simple methods of quantifying the behaviour of a DTA curve. The first is peak interpretation. This thesis follows the method described by Ding *et al.*<sup>5</sup> In this method, the solidus and liquidus features are read off of the temperature curve by the location of the onset of the feature, and the intersection of the onset and offset linear portions of the liquidus feature. This is shown in Figure 2.10, with a sample dataset.

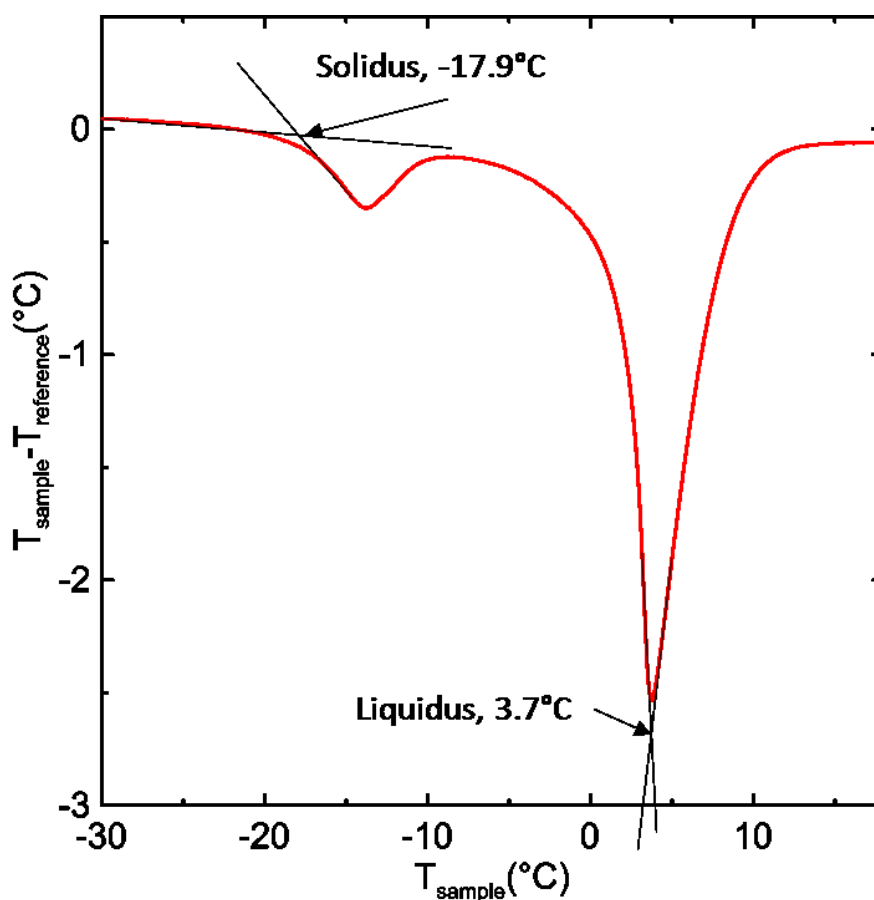


Figure 2.10: Liquidus and solidus determination on a sample dataset of 0.4 M  $\text{LiPF}_6$  in DMC. The solidus temperature is determined by the onset temperature of the lowest temperature feature, while the liquidus temperature is determined by the peak position of the highest temperature feature.

The other method by which DTA curves can be interpreted is their area. The area of interest is the one bounded by the curve and the background. Here, the background is assumed to be linear.<sup>1</sup> The area under the curve of a DTA feature is proportional to the enthalpy of fusion of the material undergoing the phase change. Thus, if the material is well understood and if it is tested with a reference sample cell, the electrolyte mass can be determined by integration of the DTA curve. An example of the peak integration used is shown in Figure 2.11. The sample shown in Figure 2.10 and Figure 2.11 is a cell with 0.4 M LiPF<sub>6</sub> in DMC.

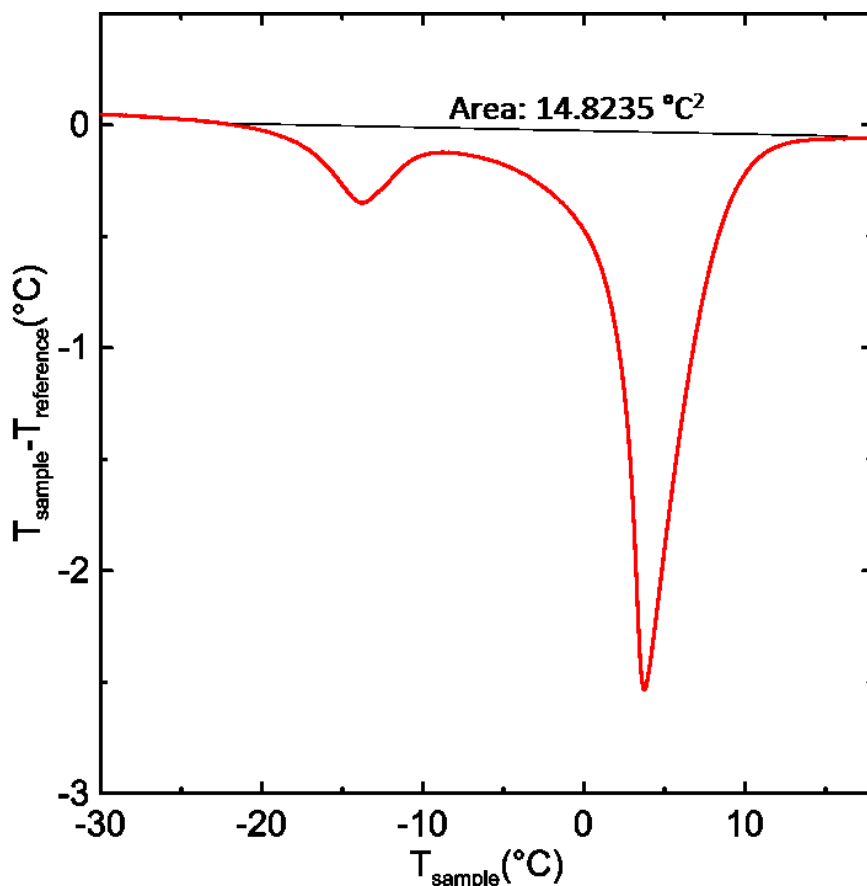


Figure 2.11: The linear background integration method of interpreting the area under the peak on a sample dataset of 0.4 M LiPF<sub>6</sub> in DMC.

### 2.1.6 Measurement Sensitivity

As some of the results that can be obtained from DTA tests cannot be verified by other methods, their accuracy cannot be directly determined. For example, there are no other methods to detect the solidus or liquidus temperatures of the electrolyte in a whole cell, so no verification can be done as to the accuracy of those experiments. Two exceptions are direct comparative tests between DTA tests conducted on a cell and DSCs test conducted on an electrolyte from the same sample, and peak area versus electrolyte mass tests, where the cell is filled with a known mass of electrolyte and tested immediately. Finally, comparisons can be made between successive DTA tests, to ensure that results are consistent.

In terms of general sensitivity, no DSC tests were conducted during the work comprised by this thesis with which a DTA test could be compared. The only comparative tests conducted between DSC and DTA were completed by Day *et al.*<sup>1</sup> Figure 2.12 shows the result of one such comparison, that shows that DTA has good agreement with DSC.

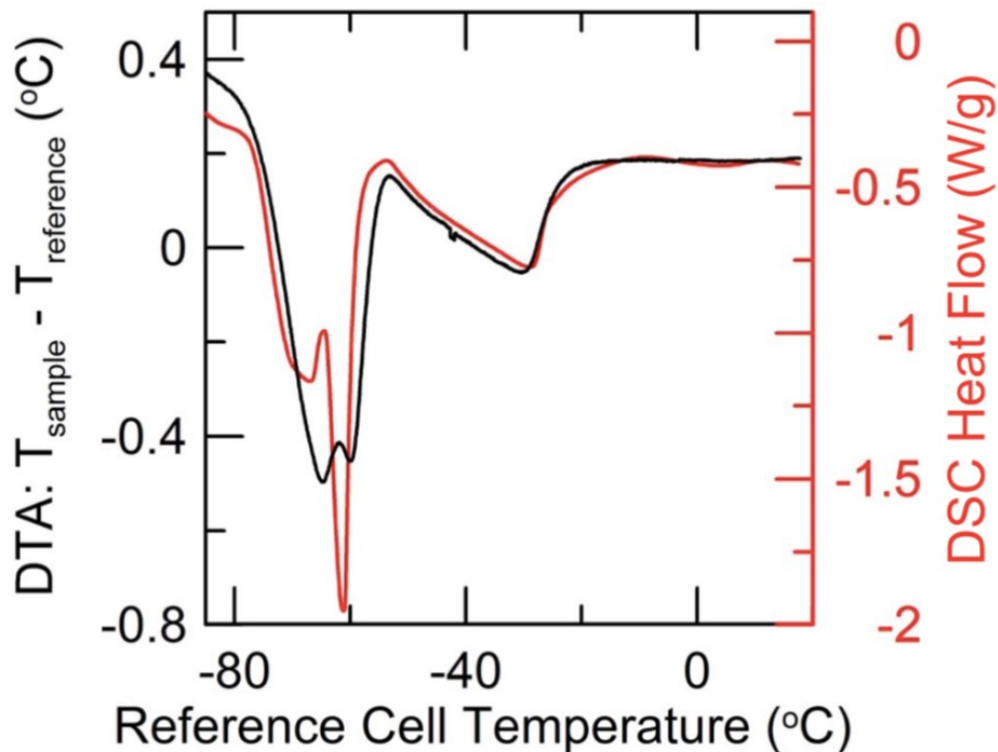


Figure 2.12: A comparative study between DTA and DSC on 1 M 3:7(w%) EC:EMC. Reproduced with permission from *J. Electrochem. Soc.*, **162**, A2577–A2581. Copyright 2015, The Electrochemical Society.

As for peak area tests, there has been some interest in the ability of DTA to test the health of a commercial cell by determining the amount of electrolyte remaining in the cell, especially in the case of commercial form factors. Extracting all the electrolyte from the cell is difficult and the ability to determine the amount of electrolyte remaining without opening the cell would be valuable. To do this effectively, DTA must be able to consistently determine the amount of electrolyte in a cell. To this end, several 18650 cells were filled with varying amounts of electrolyte, tested with DTA, and the known electrolyte masses plotted against the areas under the integration curves. The areas were determined as described in section 2.1.5, with two linear backgrounds selected: one from -70 to 15°C, and another from -50 to 15°C. The results of this test are shown in Figure 2.13.

This shows that the DTA peak area is proportional to the electrolyte mass, for like electrolytes.

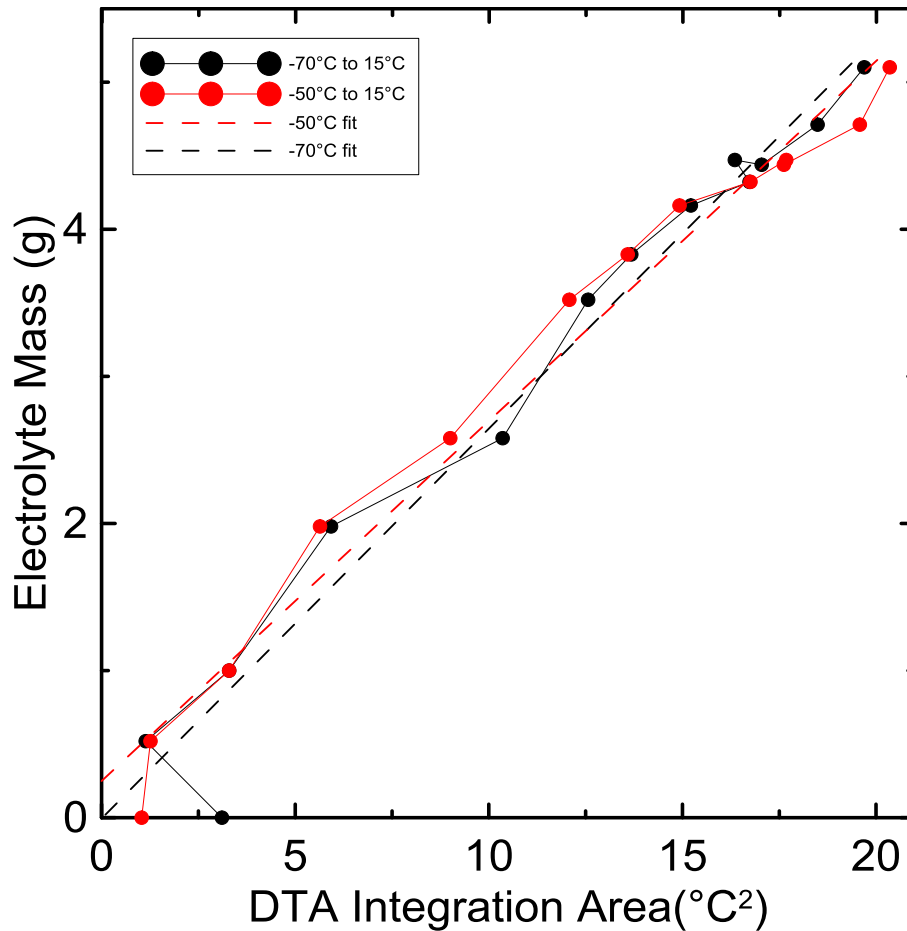


Figure 2.13: A comparison of electrolyte mass to DTA peak integration area for a set of 18650 cells. The peak integration was conducted against a linear background between the temperatures indicated.

A similar, less extensive test was conducted on a pouch cell DTA apparatus by Ryan Day, which produced the data shown in Figure 2.14. This data was treated with a spline background subtraction, which has been left out of recent work, due to new results that suggest the possibility that the background may be related to heat capacity, as discussed in section 7.2.9.

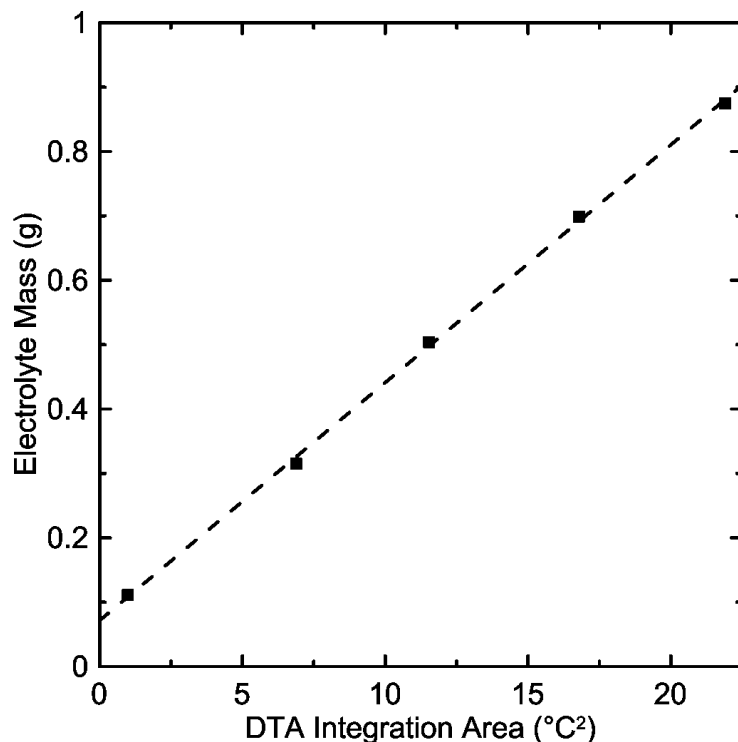


Figure 2.14: A comparison of electrolyte mass to DTA peak integration area for a set of pouch cells, as conducted by Ryan Day.

As of this writing, no tests of this type have been conducted on the 2170 apparatus.

### 2.1.7 Replicability

DTA curves are generally very replicable but are more reliable at higher temperatures. Small deviations in the heater behaviour at low temperatures can lead to small deviations in slope that can cause minor disagreement between successive tests. Figure 2.15 shows two successive tests performed on one cell. Note the perfect agreement in the position of the high temperature feature at  $\sim 20^{\circ}\text{C}$ , and slight disagreement at low temperatures. Small deviations in the behaviour of the heater during the low temperature setpoint can cause minor deviations in the background, which can cause these sorts of changes in the raw data.



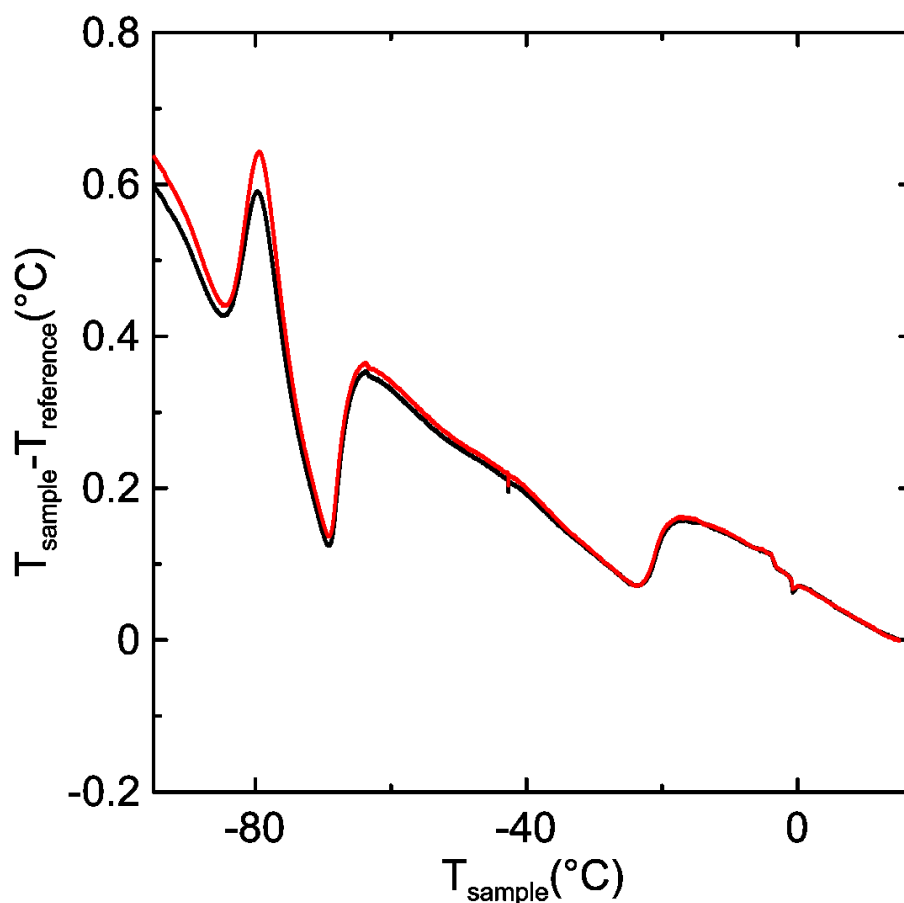


Figure 2.15: Data from two successive DTA tests performed on one cell with the red line showing the second test. This shows that successive tests almost perfectly capture the liquidus point, with some error in the peak positions of the low temperature features.

## 2.2 Other Experimental Techniques

The techniques described here are the more conventional, ex-situ methods used in analysis of the electrolytes produced in this work: DSC, GC-MS, and ICP-OES. DSC was not used directly in this work, but it was used in the original development of the system<sup>1</sup> and is directly relevant to the type of work done here. GC-MS was used for ex-situ study of the solvent portion of the electrolyte, while ICP-OES was used to study the LiPF<sub>6</sub> concentration. The full process and analysis used here is discussed in section 5.6.1.

### 2.2.1 Differential Scanning Calorimetry

Differential Scanning Calorimetry (DSC) is a more conventional method of studying the phase transition behaviour of a sample of material. In DSC, a sample of a few milligrams of some substance is heated and cooled at set rates through its phase changes. Depending on the DSC system, either the power needed to change the temperature a known amount, or the temperature change due to a known change in heat flow is recorded.<sup>6</sup> The DSC in this lab uses a heater to maintain a constant heating rate in the sample, while measuring the power required to do so. When plotted as power versus sample temperature, this data will show features at the temperatures at which the sample underwent a phase change. If the components are well known, this data can be used to determine the relative amounts of material in the sample, as well as the purity of a sample.<sup>6</sup>

While DSC is a more mature and well understood system than Li-ion DTA, it has several drawbacks in the context of battery development. First, as DSC is conducted on small samples of material, the electrolyte must be extracted from the cell to undergo a DSC test. As this process destroys the cell, a test can only be conducted on any given cell at one point in its lifetime. This precludes any study of cell degradation with respect to age. Second, as DSC requires extraction of the electrolyte, it cannot be used to determine the amount of electrolyte remaining. This prevents any study of the amount of electrolyte being consumed. Third, pure substances can undergo supercooling effects due to a lack of nucleation sites.<sup>7</sup> While these effects are much more pronounced in the cooling process, the variable solid states can melt in different ways, preventing repeatability. By contrast, the carbon in the negative electrode of a Li-ion cell acts as a sufficient nucleation material to hinder or prevent supercooling effects.<sup>1</sup>

In general, though DSC is very useful in the study of phase diagrams, the lack of direct applicability to the cell system limits its utility in this work. While DSC was used in some of the work referenced here, it was not used in the course of the work presented here.

### 2.2.2 Gas Chromatography

Gas chromatography uses a gaseous mobile phase, usually a non-reactive gas such as  $N_2$ , He, or  $H_2$ , alongside a liquid stationary phase that has a different level of affinity with each component of the eluent, to separate components of a sample.<sup>8</sup>

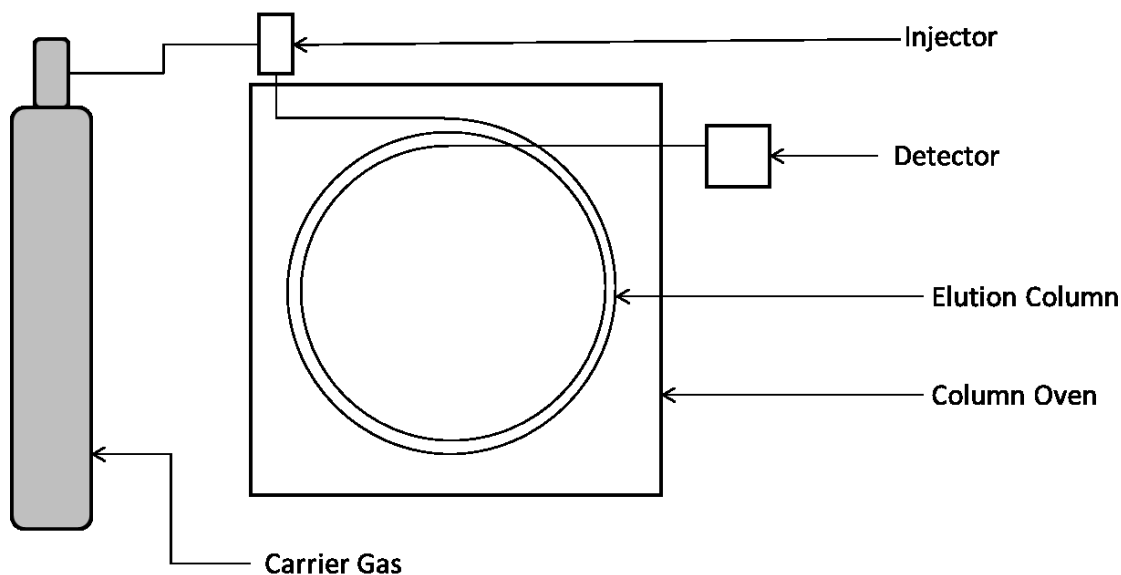


Figure 2.16: A diagram of the basic components of a Gas Chromatography device.

Figure 2.16 shows a simple diagram of a GC system. A sample, referred to as the eluent and composed of multiple analytes, is injected into the column, usually composed of silica.<sup>8</sup> The interior of the column is covered in the stable stationary phase, and heated to a temperature just above the boiling point of the most stable analyte. Thus, the eluent boils immediately and adsorbs onto the stationary phase, with each analyte reaching a

different equilibrium between the mobile and stationary phases. Then, the ratio of the analyte in the stationary phase to that in the mobile phase is proportional to the time taken for a specific analyte to elute through the column:<sup>8,9</sup>

$$t' = \frac{i_s}{i_m} t_m \frac{V_s}{V_m}, \quad (1)$$

where  $t'$  is the retention time of an analyte,  $t_m$  is the time taken for an analyte to pass through the column if it doesn't interact, and  $i_s$ ,  $i_m$ ,  $V_s$ , and  $V_m$  are the ratios and volumes of the stable and mobile phases, respectively.

Thus, the analytes in a sample can be separated and directed into a quantitative detector system, such as a mass spectrometer.<sup>8</sup>

### 2.2.3 Mass Spectrometry

Mass spectrometry (MS) is a quantitative tool for studying the components of a sample. MS can give information as to the concentrations of the components in a sample. Modern MS systems come equipped with mass spectral libraries for many organic compounds so that unknown components can be determined by a search-match procedure.

Mass spectrometers have four primary components; a sample inlet, ionizer, mass analyzer, and detector, which the sample moves through sequentially. The sample inlet and detector are straightforward; they are some injection device and an ion detector. The ionizer uses a heated filament and electron accelerator to bombard the injected sample with electrons.<sup>8</sup> This bombardment serves to ionize the sample, at which point the ionized particles are focused into a beam and directed into the analyzer. The analyzer contains one of several devices capable of separating particles out by their mass. Time of flight and quadrupole analysis are two of the more commonly used systems for this analysis.

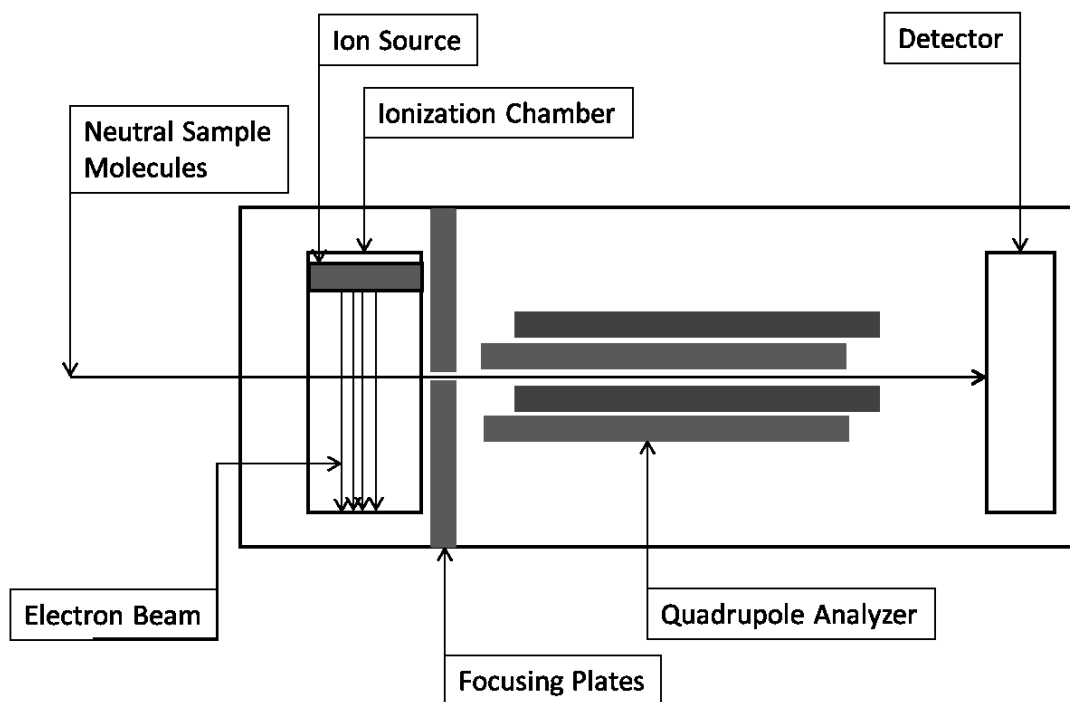


Figure 2.17: A diagram of the basic components of a quadrupole mass analysis device.

The system used in this work uses a quadrupole analyzer, as depicted in Figure 2.17. This system uses four parallel conductors, two with a constant potential and two with an alternating potential. As the analyte particles are charged, they will track towards the rods. The quadrupole analyzer can implicitly determine the charge/mass ratio of an ion by scanning through different potentials, creating different electric fields for the charged particles to fly through, and measuring the field that forces the ions away from the detector. As the ion detector records the number of ions that make it through the analyzer, the system can determine the number of ions, as well as their charge/mass ratio. By referring to a database giving the charge/mass ratios corresponding to different materials, quantitative information can be gained as to the composition of the sample.<sup>8</sup>

#### **2.2.4 Gas Chromatography-Mass Spectrometry**

GC-MS is a powerful, quantitative tool for chemical analysis. This system couples a gas chromatograph's ability to separate components of a liquid sample with the analytical capabilities of a mass spectrometer. GC-MS is used in this work as an ex-situ method for determining the relative solvent composition of electrolytes extracted from Li-ion cells.

#### **2.2.5 ICP-OES**

Inductively coupled plasma optical emission spectroscopy, or ICP-OES, is an ex-situ method of detecting metal content in samples. A solution containing some trace elements is converted into an aerosol and injected into a plasma arc, which vaporizes the aerosol and excites the released atoms. These released atoms will emit photons with characteristic energies. A portion of the emitted photons is then captured by an optical device, the desired wavelength is selected for, amplified, processed, and stored on a computer. The spectrum of the emitted photons is then analyzed to determine the composition of the original sample.<sup>8</sup> A basic diagram of the general system is shown in Figure 2.18.

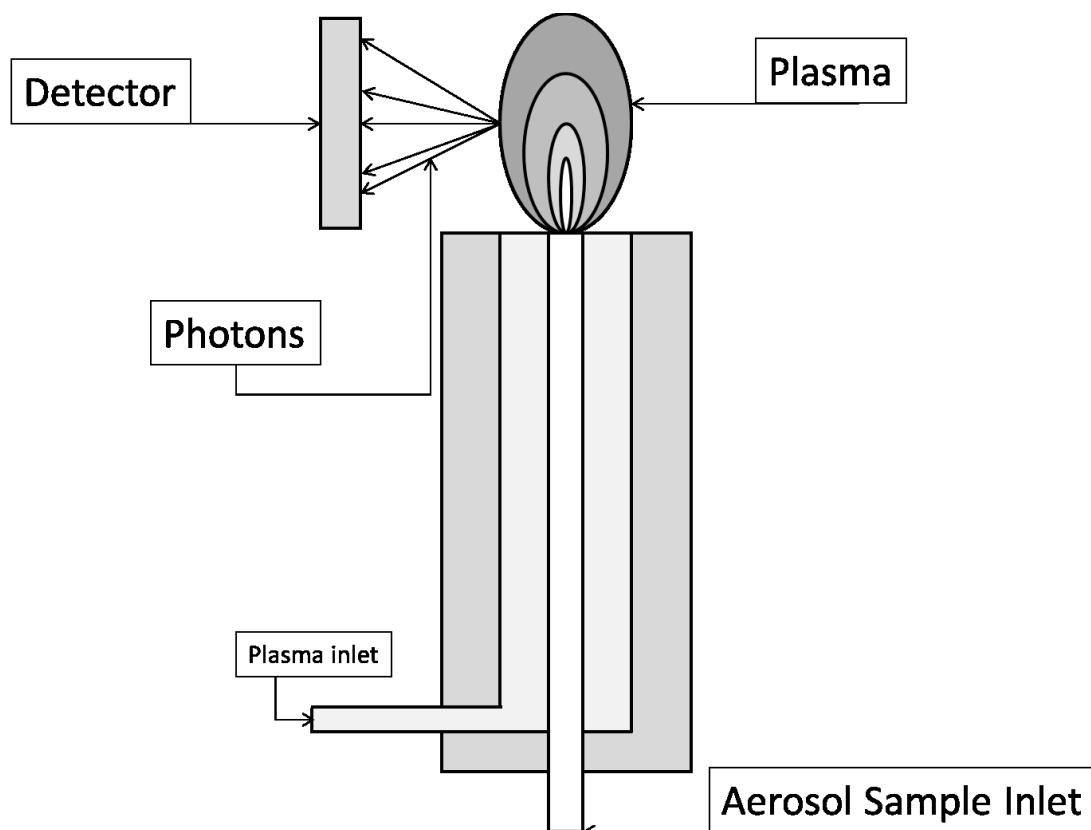


Figure 2.18: A diagram of the basic components of the ICP-OES system.

In this work, ICP-OES is used to detect the lithium content in electrolyte extracted from cells. When used correctly, the method will generate reliable results for the lithium content in a given electrolyte. However, in the protocol used in this work, several calibration solutions must be prepared, which, along with the electrolyte sample, must be handled perfectly. Even the smallest error in the sample preparation introduces large error to the result. By contrast, collection of a DTA signal requires only an intact cell, does not do any damage to the cell's cycling performance, and can be reproduced reliably. As discussed in section 2.1.1, if the experimentalist has access to the proper phase diagrams, the salt content in a Li-ion cell can be determined in a repeatable manner by DTA.

## Chapter 3: Li-ion Cells

Li-ion cells are lithium based rechargeable electrochemical devices with a wide variety of configurations and specializations. All Li-ion cells rely on the exchange of lithium atoms between lithium storage structures.

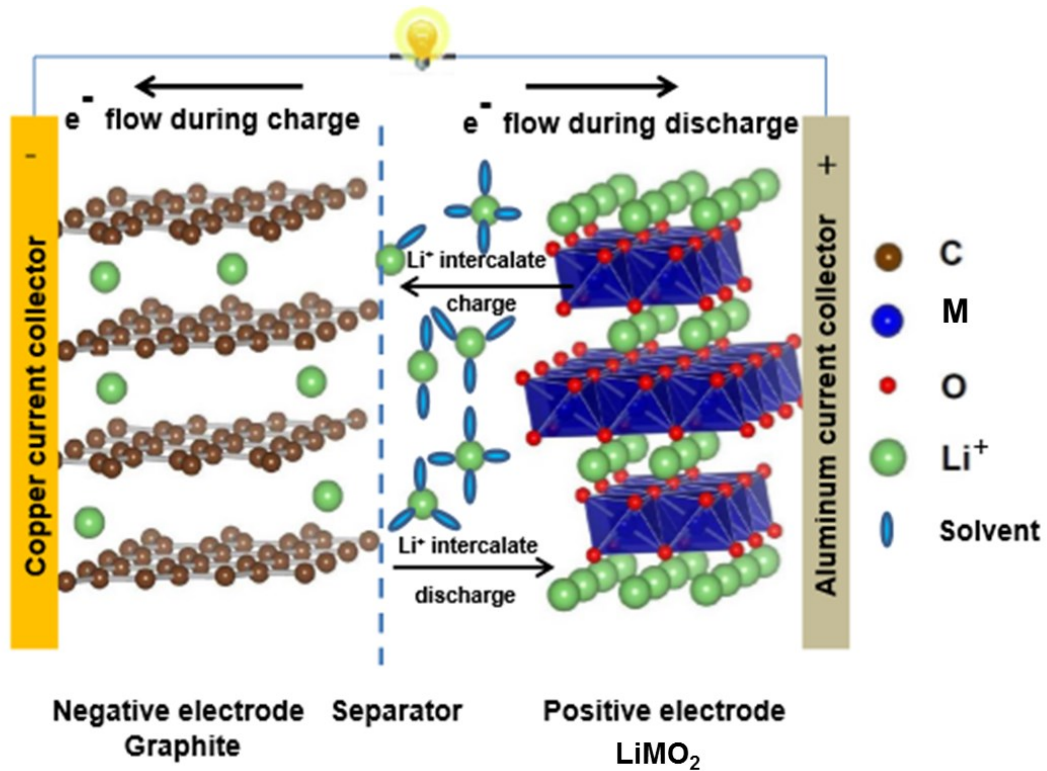


Figure 3.1: A schematic diagram of a Li-ion cell. The electrodes store Li<sup>+</sup> ions, while the current collectors provide direct electrical connection to the outside circuit, and the separator and solid electrolyte interphases prevent rapid chemical reactions between the components of the cell. Reproduced with permission from Deijun Xiong, STUDIES OF THE EFFECTS OF ELECTROLYTE ADDITIVES ON LITHIUM-ION CELL PERFORMANCE, Preliminary Report, Dalhousie University, Halifax, NS (2014)

Figure 3.1 shows a schematic of a Li-ion cell. The typical Li-ion cell is composed of a sealed container holding a positive and negative electrode that store Li<sup>+</sup> ions, each bound to metallic current collectors that are connected to the external circuit, immersed in a nonaqueous lithium salt electrolyte through which Li<sup>+</sup> ions move, and separated by a thin microporous film. During charge, some external current drives electrons across the



external circuit, driving  $\text{Li}^+$  ions from the positive electrode to the negative, to ensure charge neutrality. This drives the potentials of the positive and negative electrodes up and down, with respect to  $\text{Li}/\text{Li}^+$ . During discharge, some external load allows electrons to move from the negative electrode to the positive, which releases  $\text{Li}^+$  ions from the negative electrode to move to the positive electrode. This drives the potentials of the positive and negative electrodes down and up, with respect to  $\text{Li}/\text{Li}^+$ . This movement of  $\text{Li}^+$  ions and electrons allows for energy to be stored almost reversibly. The separator and is electrically insulating, and thus prevents shorting due to contact between the electrodes.

Much work has been done in the development of a great number of electrodes and electrolytes, each with their own advantages.<sup>7,10,11</sup> This allows for a great deal of variety in the cells that can be made. A cell could be made that emphasizes power output, lifetime, affordability, energy density, or a general middle ground. As each component will interact with each other, the design of cell to fit any specific parameter is not trivial.

### **3.1 Electrodes**

Most positive and negative electrodes currently used are layered host materials that can reversibly store and release  $\text{Li}^+$  ions. The electrode itself is usually composed of 96% active material, with about 2% each binder and conductive additive. These additives help the electrode stay together and remain physically and electrically connected to a current collector, and thus the external circuit.<sup>12</sup> Li-ion cell capacity degradation is understood to occur primarily at the electrodes, due to loss of available  $\text{Li}^+$  ions to reactions with the electrolyte.<sup>13</sup> Thus, improving the performance and longevity of electrode materials is of great importance.

### 3.1.1 Negative Electrode

Lithium atoms are very light and very reactive, properties which allow them to transfer significant amounts of charge per unit weight. Thus, lithium is the ideal element for storing electrical charge in a rechargeable format. However, while lithium is the best element for charge transfer, the development of a rechargeable battery was not simple. The first lithium batteries were developed in the 1950s after the first nonaqueous electrolytes were developed, with which lithium would not react.<sup>7</sup> These first lithium batteries used lithium metal as the negative electrode material.<sup>7,10</sup> Though these cells showed promise, a pure lithium negative electrode is very unstable, and can produce reactive dendrites of lithium during the charging process due to uneven lithium deposition.<sup>14</sup> A system comprised of an uncharged lattice where lithium ions could be reversibly inserted and extracted, or intercalated, was developed to prevent dendrite formation. In most current commercial applications, the uncharged negative electrode lattice is composed of some form of graphite. Graphite electrode properties vary based on the source of the material, but in general, graphite has many advantages, such as low cost, extremely long cycle life, and relatively high specific capacity for its long cycle life.<sup>10</sup>

Lithium intercalation into bulk graphite involves the insertion of lithium ions into the interstitial sites between individual aligned graphene sheets.<sup>15</sup> These interstitial sites are not filled at random; rather, they are filled in stages. At low voltage vs  $\text{Li/Li}^+$ , the electrode has one filled lithium gallery per graphene layer, resulting in a composition of  $\text{LiC}_6$ .<sup>10</sup> As the voltage increases, the electrode moves into stage two, where every other gallery is occupied, then stage three, where every third gallery is occupied, and so on, until the electrode is free of Li. The opposite is true for decreasing voltage vs  $\text{Li/Li}^+$ .

Intercalation of  $\text{Li}^+$  into graphite is very reversible, and thus graphite can be used in cells designed to have a long lifetime. However, the specific capacity of graphite is relatively low, in comparison to compounds that use other strategies for lithium storage; while graphite has a theoretical maximum specific capacity of 372 mAh/g,<sup>10</sup> silicon has a theoretical maximum capacity of 3580 mAh/g, which it reaches by alloying with Li.<sup>16,17</sup> However, silicon electrodes undergo significant structural changes during cycling, in order to reach this capacity. Most importantly, the electrode will expand up to 300%.<sup>17</sup> This causes the electrode to expand and contract with each cycle, which can lead to cracking during discharge, significantly damaging the electrode's ability to store lithium. This damage can lead to rapid loss of capacity.<sup>17,18</sup> Though there is much research being done to find a replacement material for graphite with higher theoretical capacity, graphite remains the negative electrode material of choice for most applications.<sup>19</sup>

### **3.1.2 Positive Electrode**

Most positive electrode materials used in Li-ion batteries consist of some form of layered lithium transition metal oxide. Intercalation of the positive electrode works similarly to that of the negative electrode, with  $\text{Li}^+$  ions slotting into sites between sheets of metal oxide. The exact organization of the sites and sheets varies, depending on the metal-oxide used. The first Li-ion positive electrode to be used commercially, and one of the most common in use today,<sup>19-21</sup> is  $\text{LiCoO}_2$ , also called LCO. While LCO offers both safety and high energy density, cobalt is expensive and the safety and energy density can be further improved.<sup>10,19</sup> Alternatives include  $\text{LiNi}_{1-x-y}\text{Mn}_x\text{Co}_y\text{O}_2$  (NMC),  $\text{LiNi}_{0.8}\text{Co}_{0.15}\text{Al}_{0.05}\text{O}_2$  (NCA), and  $\text{LiMn}_2\text{O}_4$  (LMO). These structures all offer benefits and

drawbacks; NMC is very tunable, and is safer, but its cost and capacity depend on the amount of cobalt used,<sup>10,19</sup> NCA has higher capacity, but shows significant loss of capacity during charge-discharge cycling over 40°C,<sup>19</sup> and LMO, though inexpensive and non-toxic due to the lack of cobalt, has poor longevity in Li-ion cells.<sup>10,19,22</sup>

### **3.2 Separators**

Li-ion cells utilize a thin, porous, electronically insulating separator material, often polyethylene or polypropylene, to prevent direct electrical contact between the positive and negative electrodes. A good separator must be porous enough to allow for ionic transport in the cell, but be inert to the electrolyte.<sup>7,10,23</sup> Separators are vital to the Li-ion cell, but are not involved in electrolyte degradation, and are thus unimportant to Li-ion DTA experiments.

### **3.3 Electrolytes in Li-ion Cells**

Li-ion cells require an electronically insulating, ionically conducting medium through which Li<sup>+</sup> ions can be transferred from one electrode to the other. In the case of Li-ion cells, this medium is usually a liquid electrolyte, composed of some combination of cyclic and linear organic solvents, lithium salts, and other chemicals in small concentrations. Lithium salts are used to impart ionic conductivity and allow for Li<sup>+</sup> ion transport. The solvent component is usually comprised of a combination of two or more solvents with different properties, that combine to form compromises of their better qualities, while avoiding the worse ones. The other chemicals, commonly called additives, are a wide variety of types of chemicals, used to modify specific properties of the cell, while not interfering with the properties of the bulk electrolyte.

### 3.3.1 Solid Electrolyte Interphase

Though negative electrodes composed of graphite avoid dendrite formation, lithiated graphite is very reactive. At low voltage vs  $\text{Li}/\text{Li}^+$ , the electrode will reduce many organic solvents. In some cases, solvent molecules will even intercalate alongside the  $\text{Li}^+$  ions, exfoliating the graphite surface.<sup>21</sup> These processes cause rapid and irreversible degradation of both the electrode and electrolyte, starting from the first charge. In the 1990s, ethylene carbonate (EC) was found to form a passivating layer of ionically conductive, electronically insulating material on the negative electrode during the first charge. This layer then prevented further reductive reactions, and allowed for long lived cells.<sup>24</sup> This layer is called the solid electrolyte interphase (SEI). However, pure EC freezes at  $34.6^\circ\text{C}$ ,<sup>25</sup> rendering it solid at room temperature. An electrolyte with only EC solvent would have very low ionic conductivity.<sup>7</sup> Thus, optimization of stable, useful electrolytes for use in Li-ion cells began.

The SEI is a subject of considerable study in the electrochemical literature as its study is vital for the development of long lived, high energy density cells.<sup>7</sup> As the intercalation process in graphite only causes 10% volume expansion, the structure of the SEI is not stressed by repeated cycles.<sup>26</sup> However, minor side reactions, referred to as parasitic reactions, can occur between the electrolyte and the electrode despite the insulating nature of the SEI. These reactions have many effects on the cell, including the gradual expansion of the SEI, the trapping of  $\text{Li}^+$  ions, and gradual changes to the chemistry of the electrolyte. The SEI is also important to the development of high energy density cells, as the higher voltages vs  $\text{Li}/\text{Li}^+$  can induce oxidative reactions that are prevented by another SEI at the positive electrode. Finally, though it was previously believed that EC

was required to develop the SEI, certain additive blends may be able to accomplish the same effect.<sup>27</sup>

Though the SEI is important to the consideration of Li-ion electrolyte chemistries, Li-ion DTA cannot probe it directly. The closest DTA can come to direct examination is by a pair of tests before and after the first charge. The differences in the DTA curves could then show which components of the bulk electrolyte reacted to form a solid state. This process, though potentially valuable, is not a focus of this work, and has not yet been studied.

### **3.3.2 Requirements in Electrolyte Design**

There are many solvents that have been used for Li-ion cells. Selection of these solvents holds to several design parameters, starting with stability. At a fundamental level, solvents for use in Li-ion cell electrolytes must be kinetically stable at voltages between 0 and  $\sim 4.5$  V vs Li/Li<sup>+</sup>, since the electrodes potentially span that range. They must then be inert to all cell components, be safe (non-toxic, low autoignition temperature, non-explosive), be stable in a practical temperature range (up to  $\sim 70^\circ\text{C}$ ), and be environmentally friendly, or at least benign. These are all vital metrics of cell function; lacking any of them will disqualify a solvent. Thus, these factors act to select for what electrolyte blends are viable, rather than what blends are ideal.

There are several other metrics that can be tuned more reliably than the rather simple problem of safety. These include the operational temperature range, the dielectric constant and viscosity. The operational temperature range is the range within which the electrolyte is liquid. The viscosity and dielectric constant come together to determine the

ionic conductivity, related to the ease by which ions can move through the electrolyte. While all solvents have different properties, a combination of two solvents with different melting points, viscosities, or dielectric constants will create a mixed solvent with properties of both.

The melting temperature of the electrolyte is important when determining the temperature range the cell can tolerate, as below this temperature, the electrolyte will lose conductivity. The upper temperature limit is usually 60°C and limited by electrolyte decomposition. For example, an electrolyte containing a high quantity of a solvent like ethyl methyl carbonate, whose melting point is low (-55°C), such as a 3:7 weight percent mixture of EC to EMC, will have an operational range of about -30°C to 60°C. However, an electrolyte with a greater concentration of a solvent like dimethyl carbonate (DMC), with a higher melting point (4.6°C), such as a 3:7 weight ratio of EC to DMC, will have an operational range of -5°C to 60°C, due to the high melting point of the DMC. While the boiling point of an electrolyte might come into play, other components of the cell usually have much lower upper temperature limitations. For example, DMC has a rather low boiling point among organic solvents, at 91°C,<sup>25</sup> but LiPF<sub>6</sub> begins to degrade around 70°C. One would not likely create a solvent solution that could boil before the salt began to degrade.

### **3.3.3 Ion Transport Properties**

The primary role of the electrolyte after formation of the SEI is in transporting Li<sup>+</sup> ions between the positive and negative electrodes. There are several properties of solvents used in Li-ion electrolytes that define how well a solvent does this. The most important of

these are the viscosity and dielectric constant, which determine the ionic conductivity of the solvent. A solvent's dielectric constant quantifies the solvent's ability to dissolve salts into their constituent cations and anions; high dielectric constants are good. A solvent's viscosity is the measure of the fluidity of the solvent; low viscosity is good. Many cyclic carbonates useful in Li-ion cells are strongly polar, giving them very high dielectric constants and high viscosity. EC is one such solvent, and while it helps to form a good SEI, its high viscosity limits ion conductivity. However, the viscosity and dielectric constant of a mixture of two solvents is can be modelled in terms of the properties of the base solvents, as in equations 2 and 3<sup>7</sup>:

$$\varepsilon_s = x_1\varepsilon_1 + x_2\varepsilon_2, \quad (2)$$

$$\eta_s = \eta_1^{x_1}\eta_2^{x_2}, \quad (3)$$

where  $\varepsilon_s$ ,  $\eta_s$  and  $x_i$  are the dielectric constant, viscosity and volume fraction of the mixed solution, and  $\varepsilon_i$ ,  $\eta_i$  and  $x_i$  describe the dielectric constant, viscosity and volume fraction of the  $i^{th}$  component, respectively. This behaviour is caused by the way solvent mixtures behave around ionic solutes. More polar cyclic compounds are more attracted to the salt ions and can thus flow more easily through the less viscous solvent. Conventionally, the less viscous solvents are linear carbonates, which have lower dielectric constants and viscosities than cyclic carbonates. Thus, non-ideal properties can be balanced by the addition of another nonaqueous solvent with complementary properties.

Ionic conductivity quantifies the ability of the electrolyte to conduct ions between the electrodes in the cell. As with the viscosity and dielectric constant, the ionic conductivity can be modelled, as shown by equation 4<sup>7</sup>:



$$\sigma = \sum_i n_i \mu_i Z_i e. \quad (4)$$

In this equation,  $n_i$ ,  $\mu_i$ , and  $Z_i$  describe the number of free ions per unit volume, ionic mobility, and valence of ionic species  $i$ , respectively. While the dielectric constant determines  $n_i$ , the viscosity determines the mobility, as in equation 5<sup>7</sup>:

$$\mu_i = \frac{1}{6\pi\eta r_i}, \quad (5)$$

where  $r_i$  is the solvation radius, according to the Stokes-Einstein equation.

Salt concentration also affects viscosity and ionic conductivity. Increasing salt concentration increases viscosity, as the additional ions reduce overall fluidity, but the ions introduced by the salt also increase the number of charge carriers, thus increasing ionic conductivity.<sup>28</sup> At low salt concentrations, adding salt will increase the electrolyte's ion conductivity. At higher concentrations, the increased viscosity overcomes the contribution from the additional charge carriers, and the electrolyte reaches a maximum conductivity, unique to the solvent mixture.<sup>28</sup>

This work focuses on EC and EMC in the primary research, with some attention to DMC. The work concerning DMC is a development of a compositional phase diagram of DMC and LiPF<sub>6</sub>, discussed in chapter 4. The work concerning EC and EMC is a survey of the degradation of Li-ion cell electrolytes at over long cycle lifetimes, as discussed in chapter 5.

### 3.3.4 Lithium Salts

While there are several possible lithium salts, there are a few important requirements imposed upon a Li-ion cell solute. Lithium salts used in Li-ion electrolytes

must be able to dissolve completely in the solvent, have a non-toxic anion, be thermally stable, and be inert to the rest of the cell, including the solvent and electrodes. These requirements have led to the field of lithium salts being whittled down to a handful of viable compounds, including  $\text{LiBF}_4$ ,  $\text{LiPF}_6$ ,  $\text{LiAsF}_6$ ,  $\text{LiN}(\text{SO}_2\text{F})_2$  (LiFSI),  $\text{LiN}(\text{SO}_2\text{CF}_3)_2$  (LiTFSI),  $\text{LiB}(\text{C}_2\text{O}_4)_2$  (LiBOB), and  $\text{LiClO}_4$ . Of these,  $\text{LiPF}_6$  is the most viable; though it does not excel in any one area, it is the best overall,<sup>7,10</sup> and has seen the most use in commercially available Li-ion cells.<sup>21</sup> The cells used in this thesis employ  $\text{LiPF}_6$ .

### 3.3.5 Additives

Additives are chemicals added to a Li-ion cell electrolyte in small relative quantities – on the order of a few percent – that have significant effects on cell performance. Their low concentration means that they usually have little effect on the bulk properties of the electrolyte, such as viscosity, conductivity, and melting point. Most additives are consumed in the formation cycle of the first charge and create a more stable SEI than would be created by standard solvent. As the long-term degradation of the SEI is a significant factor in Li-ion cell death, a more stable SEI makes for a longer lived cell. Thus, additives can be used to subtly modify an electrolyte, without sacrificing the desired solvent properties, or significantly changing manufacturing procedures.

Many chemicals have been used as additives, such carbonate solvents,<sup>21,29</sup> various sulfur containing compounds,<sup>30–32</sup> and even some lithium salts.<sup>33</sup> This thesis utilizes four additives in two sets. The first is a single additive; vinylene carbonate (VC). The second set is a blend of three individual additives, Prop-1-ene-1,3-sultone (PES), Tris-(trimethylsilyl)-phosphite (TTSPi), and 1,3,2-Dioxathiolane-2,2-dioxide (DTD, or

ethylene sulfate), in a ratio of 211 by weight. These two sets are referred to, in this thesis, as VC and PES-211D.

Vinylene carbonate is one of the most commonly used additives.<sup>32</sup> Vinylene carbonate is referred to as a reduction type additive. This means that it has a higher reduction potential than the bulk solvent. Thus, on the first charge, the VC in an electrolyte will preferentially reduce into a film on the negative electrode, before the rest of the solvent is affected. This improves the negative electrode SEI and inhibits further reduction at that electrode. Further, this SEI has been shown to be resistant to degradation by PF<sub>5</sub> and suppress the formation of LiF.<sup>34</sup> In experiment, VC has been shown to increase coulombic efficiency – the ratio of the discharge capacity to the capacity of the previous charge – as well as reduce charge endpoint capacity slippage, increase cycle life,<sup>35</sup> and reduce impedance at the positive cathode,<sup>21,36</sup> while exhibiting no negative effects on the cell as a whole.<sup>21</sup>

While VC is a well understood, commercially developed additive, PES-211D is an example of a blend that is not as well understood, but shows better overall performance, especially at higher voltage. However, each component has been shown to yield significant benefits by themselves. PES has been shown to form an SEI on the positive and negative electrodes, while producing less gas and showing better cycling performance at elevated temperatures than similar cells cycled with VC.<sup>37,38</sup> DTD has been less studied, but has been shown to form an SEI film that can compete with VC.<sup>31,32</sup> TTSPi has been shown to reduce impedance, parasitic reaction rates, and charge endpoint capacity slippage.<sup>39</sup> PES-211D was developed as an additive blend by Wang *et al.*, in a larger work attempting to develop competitive additive blends for Li-ion cells.<sup>40</sup> It was the best performing of all the

additive blends in the work, and performed considerably better than the VC standard, especially in terms of gas production and cycle life at high temperature.<sup>40</sup>

As the mechanisms by which electrolyte additives function are not systemically understood, there is no framework for finding new additives. Thus, development in this area is mostly trial and error. As this trial consists of making cells with test additives and cycling them until differences can be determined, exploration of new additives is not simple or fast. However, Li-ion DTA could be used to develop an understanding of the effects additives have on electrolyte state, as described in section 7.2.6.

### **3.4 Electrolyte Degradation**

The ideal Li-ion cell would not experience any loss of performance and would thus last forever. For this to happen, the components of the cell would have to remain inert to each other, with only the desired intercalation reactions occurring. However, there are several unwanted reactions that occur in the cell, that cause gradual degradation of performance, until the eventual death of the cell. Two of these, transesterification and parasitic reactions, can involve the electrolyte.<sup>13</sup> Parasitic reactions are a broad class of unwanted reactions that occur at the electrode interface that involve the electrolyte and active  $\text{Li}^+$  ions.<sup>13,41,42</sup> Transesterification, in the context of Li-ion cells, is a set of reactions in the bulk electrolyte that occur between solvent molecules, often initiated by products of parasitic reactions, which result in their transformation into other solvents.<sup>43</sup> These reactions will only be discussed in reference to their effects on the electrolyte, and this thesis will discuss parasitic reactions and transesterification as distinct processes.

### 3.4.1 Parasitic Reactions

As parasitic reactions occur inside the cell, individual processes often cannot be singled out and observed directly. However, there are a variety of methods to detect them indirectly. These are usually conducted as measurements of deviation from optimal cycling behaviour. For example, parasitic reactions can create gas in the cell, unlike Li intercalation, so an increase in the gas content of a cell indicates the occurrence of parasitic reactions.<sup>44</sup> Parasitic reactions can also change the coulombic efficiency of a cell, so careful measurement of a cell's charge transfer can show the degree to which parasitic reactions have occurred. Finally, parasitic reactions can cause slow degradation of a cell's cycling capacity in storage, especially at high temperatures and pressures, so stored cells can be monitored to observe the degree to which parasitic reactions occur.<sup>45,46</sup> However, these methods only serve to determine whether or not parasitic reactions have occurred, and to what degree they have done so. Precise measurement of the heat flow in the cell can be used to directly study the rate to which parasitic reactions are occurring, but even that method cannot show what exact reactions are occurring.<sup>47,48</sup>

DTA can only measure the changes in an electrolyte that occur over long time scales. There are no plans to increase sensitivity to where the minute cycle-to-cycle changes can be detected, but plans have been made to study electrolytes before and after formation, as in section 7.2.6. Further, only the changes to the liquid electrolyte can be directly measured; the liquid, solid and gaseous state reaction products are not usually analyzable by DTA. Generated liquid products are usually present in only a few percent,<sup>49</sup> which would affect DTA signals slightly,<sup>5</sup> the gaseous products may not have a phase transition in the temperature range of interest, and if the solid state products did go through

a phase transition, the enthalpy changes would likely be too complex and subtle to be interpreted.

Several forms of parasitic reactions involve irreversible processes that consume the bulk electrolyte. The broad forms discussed here are the solvent consumption process of SEI growth, and electrolyte oxidation at high cell potentials.<sup>13</sup>

When a cell is charged or discharged, small amounts of intercalated  $\text{Li}^+$  ions will irreversibly react at the negative electrode SEI to thicken the passivating layer. As this process traps active  $\text{Li}^+$  ions in the SEI, it induces capacity loss. This reaction requires an electron contribution from the negative electrode, that must diffuse through the SEI; as the SEI grows with  $t^{1/2}$ ,<sup>41</sup> this process will slow as the cell ages.<sup>13</sup> As this process does not involve  $\text{Li}^+$  ions originally solvated in the electrolyte, the salt content of the electrolyte is not changed. However, as this mechanism involves the reduction of electrolyte molecules, the salt:solvent ratio in the electrolyte can change, making it detectable by DTA.

One goal of Li-ion cell design is the increase of energy density. One way to do this is to increase the voltage of the positive electrode. However, the organic compounds that compose the bulk of the electrolyte material in a formed cell have certain windows of kinetic stability, usually between 0-4.5 V vs  $\text{Li}/\text{Li}^+$ , outside which they are susceptible to oxidation or reduction.<sup>13</sup> While these oxidative reactions can proceed along many pathways, there are two of note that will be described here. The first is that, in high potential cells, the positive electrode can oxidize the electrolyte at the positive electrode, despite the electronically insulating SEI. This will cause some amount of solvent to oxidize, turn into some other molecules, and emit the equivalent amount of  $e^-$  into the electrode during every cycle. These  $e^-$  will then remove a  $\text{Li}^+$  ion from the electrolyte and into the negative

or positive electrode by charge neutrality, depending on whether the cell is under a load or in open circuit conditions.<sup>13</sup> Thus, this process consumes solvent molecules and a number of  $\text{Li}^+$  ions at most equal to the number of  $e^-$  released by solvent oxidation. Both the solvent and  $\text{Li}^+$  consumption can be detected by DTA but differentiating between the effects is not trivial. A second oxidative reaction scheme involves a shuttle process, where the oxidized solvent molecule travels to the negative electrode and is reduced. In some cases, this process is reversible, and results only in self discharge, as the solvent reaction drives charge transport in the cell. However, in a cell in open circuit conditions, the more likely result is the solvent reaction product staying on the negative electrode after the reduction reaction, thus consuming solvent and driving self-discharge. This process will only consume solvent and is thus detectable by DTA.

There are many forms of parasitic reactions; many of which consume some component of the cell. While DTA measurements are not precise enough to determine the exact reactions taking place, the general trends of electrolyte depletion can be used to correlate trends in cell degradation to the electrolyte consumption processes occurring in the electrolyte.

### **3.4.2 Transesterification**

Transesterification is a process by which esters transform into other esters. In the case of Li-ion cells, this process can lead to an overall change in the composition of the electrolyte, independent of changes due to reactions at the electrodes. This change is not ideal, as the solvent composition is usually fine-tuned for the desired properties.<sup>7</sup>

There are many different kinds of transesterification reactions that can occur in a Li-ion cell depending on the electrolyte chemistry used.<sup>7,50,51</sup> Examples are between two

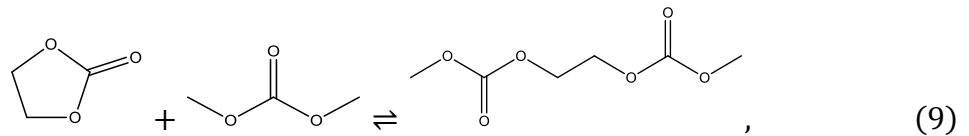
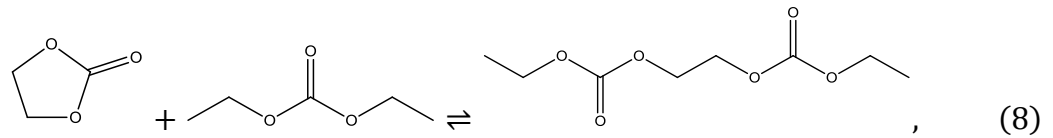
EMC molecules to form DMC and diethyl carbonate (DEC), and between EC and EMC, DMC, or DEC, to form ethyl methyl-2,5-dioxahexane carboxylate (EMOHC), dimethyl-2,5-dioxahexane carboxylate (DMOHC) and diethyl-2,5-dioxahexane carboxylate (DEOHC), which are also called bis-carbonates. These processes are linked and follow several reactions. The first is a transesterification equilibrium between EMC, DEC, and DMC, following equation 6:<sup>52</sup>



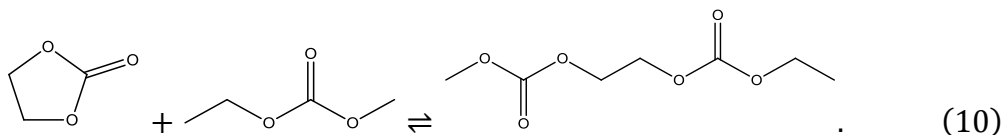
At low temperatures, this reaction only occurs in the presence of lithium alkoxides, which are parasitic reaction products formed at low potentials vs Li/Li<sup>+</sup>.<sup>53-56</sup> However, the transesterification reaction can also occur at high temperature, when the carbonates are combined with LiPF<sub>6</sub>, as in many Li-ion cells.<sup>51,56</sup> Equation 7 shows the equilibrium between LiPF<sub>6</sub>, PF<sub>5</sub>, and LiF, which is driven to the right by the decomposition of LiPF<sub>6</sub>.<sup>34</sup>



The PF<sub>5</sub> produced from equation 7 can also drive the transesterification reaction in 6. A second, more complex, transesterification process occurs between EC and the linear carbonates: both the EMC, which is already present, and those produced by equation 6. These processes follow equations 8-10:







These processes produce DEOHC, DMOHC, and EMOHC, respectively.

These processes are well known to occur; DEC, DMC, and bis-carbonates are found in cycled cells not initially containing those solvents.<sup>36,49,51,52,54,56,57</sup> As with the reaction shown by equation 6, the reactions shown by equations 8-10 are driven by different mechanisms, depending on the temperature of the electrolyte. Kim *et al.* and Sasaki *et al.* show that the formation of the bis-carbonates, as well as DEC and DMC in EC/EMC electrolytes is initiated by lithium alkoxides carrying out nucleophilic reactions involving the solvent molecules, first creating intermediaries from the linear carbonates, and then opening the EC ring, allowing for the bis-carbonates to be formed from their combination.<sup>53,54</sup> Sloop *et al.* show that equations 8-10 can occur in heated solutions of EC/DMC and LiPF<sub>6</sub>.<sup>57</sup> Sloop, Abraham, and Zhang *et al.* explain this phenomenon by stating that the PF<sub>5</sub> produced in the high temperature degradation of the LiPF<sub>6</sub> as per equation 7 acts to polymerize EC, by removing one of the C-O bonds, thus opening the ring and allowing it to react with one of the linear carbonates present in the electrolyte.<sup>43,51,57</sup>

Sasaki *et al.* also carry out an extensive investigation into the transesterification products formed in several combinations of lithium alkoxide, LiPF<sub>6</sub> salt, and various solvents, and conclude that lithium alkoxide is the active species, at low temperature while PF<sub>5</sub> acts as a catalyst to the reaction.<sup>54</sup> This investigation shows that, while lithium alkoxides can drive the reactions, transesterification occurs much faster in the presence of

PF<sub>5</sub>, which lead to electrolytes being relatively stable at low temperatures, as LiPF<sub>6</sub> is stable below 55°C.<sup>43</sup>

Though they are known to be created in Li-ion cells, DMOHC, DEOHC, and EMOHC have not been studied extensively, and their exact effects on the electrolyte are not well known. However, as they are quite viscous, they would reduce the overall conductivity of the electrolyte.<sup>54</sup> Further, the full causal relationship between these changes in electrolyte and cell degradation is not understood.<sup>43</sup> Finally, though EMOHC is described in the literature,<sup>42,50,52,53</sup> it was not found in the electrolyte analysis carried out in this thesis.

If reactions 8-10 are followed exactly, with uniform consumption of electrolyte components due to parasitic reactions, the relative proportions of the electrolyte at the end of cycling can be predicted. An aged electrolyte should have some amount of consumed EMC, along with the same number of moles of EMOHC, DMC, DEC, DMOHC, and DEOHC, collectively. DMC and DEC should be present in an amount equal to the lost EMC, minus the amounts of EMOHC and DMOHC and DEOHC, respectively. As well, the EC concentration will be reduced by the amount of DMOHC, DEOHC, and EMOHC present. This would suggest that EMC consumption would outpace the EC consumption, as EMC is involved in more active processes. This deviation in the EC:EMC ratio is not ideal for DTA analysis, as it introduces new degrees of freedom to the degradation process; changing solvent component ratios may influence the DTA curves in unexpected ways.

## Chapter 4: The LiPF<sub>6</sub>-DMC Phase Diagram

While section 2.1.1 discussed solvent-solvent phase diagrams, salt-solvent phase diagrams are also of importance to DTA. Salt-solvent diagrams are similar in principle to solvent-solvent diagrams but are more directly applicable to Li-ion cells, as they consider the effects of the lithium salt on the phase transitions of the solvent. These diagrams are also more complex than solvent-solvent diagrams, particularly in the post-eutectic region.

### 4.1 Motivation

Though development of phase diagrams is vital for the interpretation of DTA curves, salt-solvent phase diagrams are also valuable for cell design in general. These diagrams can show the viable temperature range for a cell by determining the liquidus temperature of the underlying electrolyte. Once the temperature has dropped below the liquidus temperature, small amounts of frozen material begin to form. These small amounts of material cause the ionic conductivity of the electrolyte to drop rapidly.

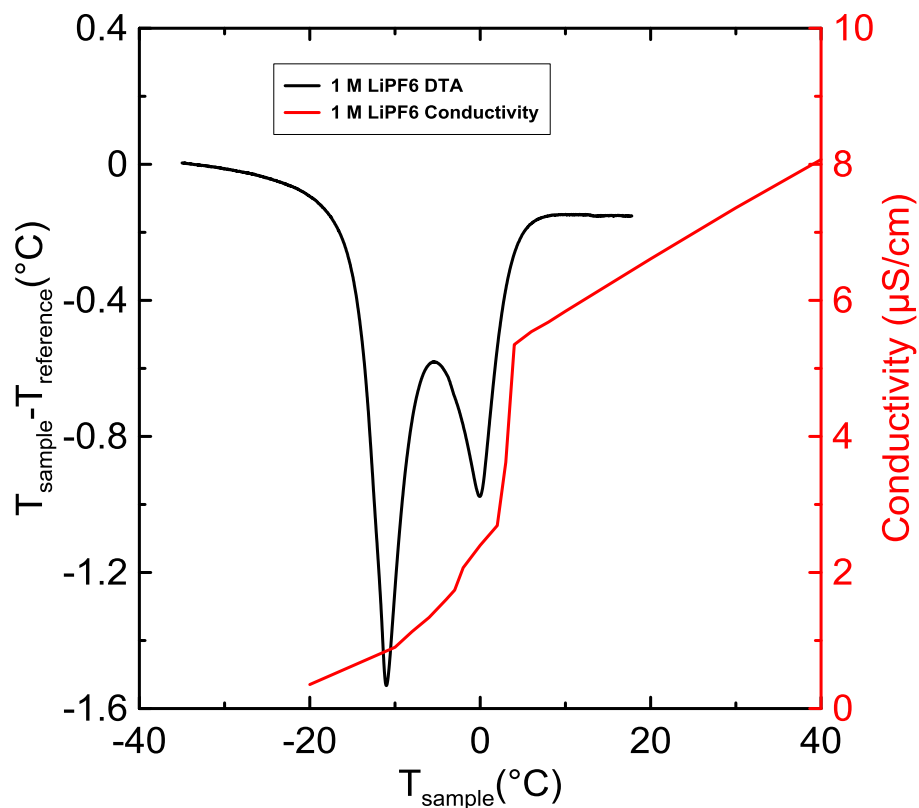


Figure 4.1: The conductivity of a sample of 1M LiPF<sub>6</sub> in DMC and a DTA curve of a cell containing 1 M LiPF<sub>6</sub> in DMC. The conductivity drop is caused by DMC freezing out of the sample at the liquidus point. This data was previously published by the author in *J. Electrochem. Soc.*<sup>58</sup>

Figure 4.1 shows that the conductivity of a 1M LiPF<sub>6</sub> sample of DMC drops considerably at 0.1°C, near the liquidus temperature of the electrolyte. This limits the functional operating temperature of a cell to the range of temperatures above the liquidus. As the conductivity of a cell's electrolyte cannot easily be tested once the cell has been assembled, this method can thus be used to determine a cell's effective temperature range. As many commercial cells contain high concentrations of DMC, functional temperature range is an active concern. One such solvent mixture is 80:10:10 DMC:EC:EMC, whose high DMC content gives a high liquidus temperature. Figure 4.2 shows the conductivity of this solvent mixture as it passes the liquidus temperature. If a battery pack of this

chemistry were to be used in a car, and if said pack were to go below  $-4^{\circ}\text{C}$ , for example in a Canadian winter, the pack itself would freeze. The car would need to expend considerable energy heating the battery pack to prevent the electrolyte from passing its high liquidus point and causing the cells to fail. Thus, knowing the liquidus temperature of an electrolyte already in a cell is valuable to the commercial proliferation of Li-ion cells.

Note that, in all cases, the conductivity of the sample dropped several degrees above the liquidus temperature of the electrolyte. This may be due to some change in the electrolyte around the liquidus temperature that causes conductivity fall, other than the phase transition, but is more likely due to experimental error. The conductivity measurements were conducted with a probe that used several milliliters of electrolyte. Thus, as the test was performed by starting at low temperatures and scanning toward higher temperatures, there is a good chance that the electrolyte did not have time to completely melt through the phase transition.

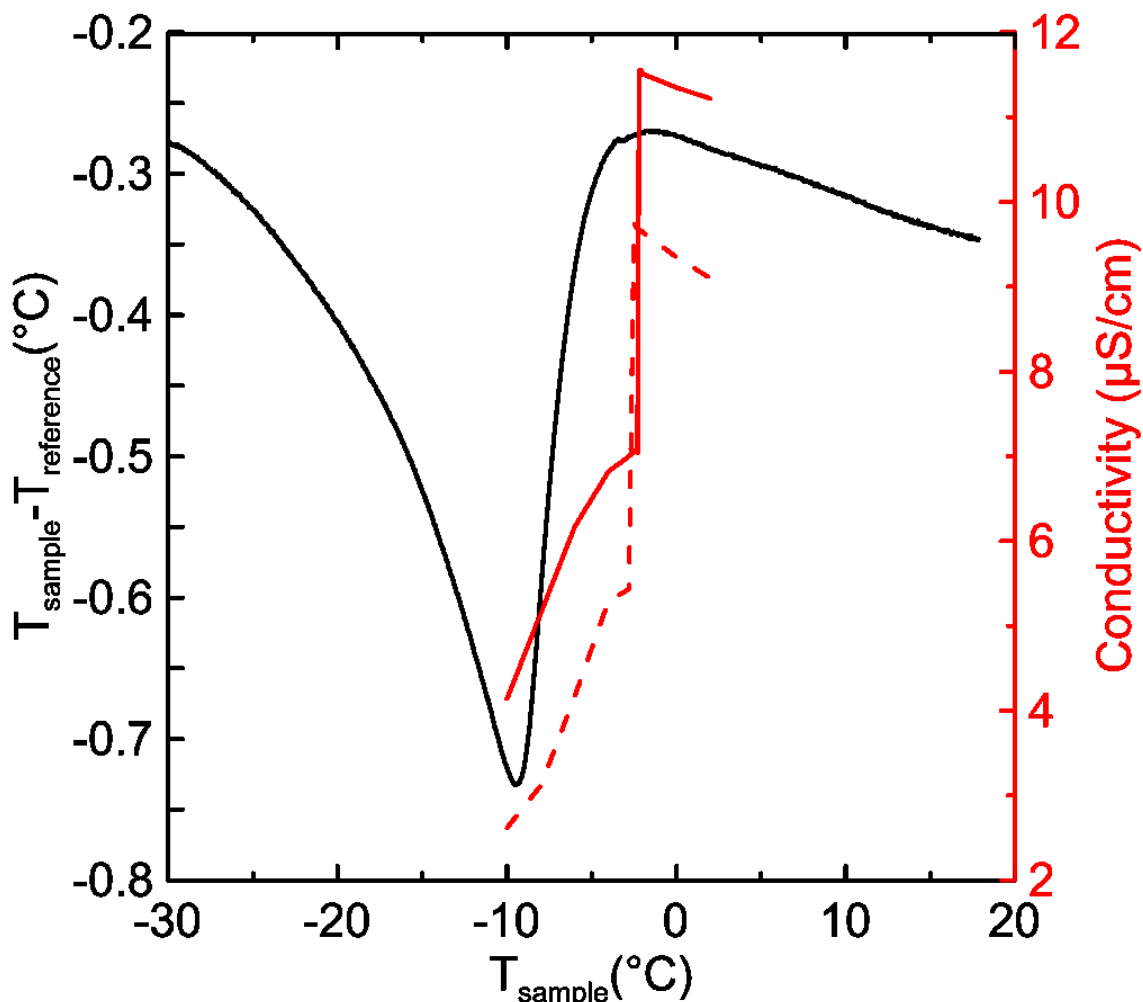


Figure 4.2: The conductivity and DTA curve of 1 M LiPF<sub>6</sub> in 80:10:10 DMC:EC:EMC, against temperature. The solid and dashed red lines represent two tests that conflicted in exact value, but not in the overall trend.

## 4.2 Construction of Phase Diagrams

Compositional phase diagrams can be theoretically modelled, as in Ding's work on binary and ternary solvent-solvent mixtures.<sup>59,60</sup> Though these models are useful, compositional phase diagrams must be measured to be fully reliable. To do so, DTA or DSC tests must be conducted on a sample at each point of interest in compositional space.

When using DTA to create these diagrams, test cells of each composition of interest must be constructed, tested, and the resultant data analyzed. The process of cell creation

is described in section 5.3, the creation of these cells follows that procedure, stopping at the wetting stage. Though the resultant DTA curves may be quite complex, in the case of complex or post-eutectic electrolytes, a liquidus and solidus feature at least can be identified. Then, the liquidus and solidus temperatures can be plotted against the composition of the electrolyte, and a phase diagram can be determined. Distinct states can be identified by the presence of phase transitions, but the physical composition of the electrolyte cannot be determined by DTA.

While solvent-solvent combinations are straightforward, the presence of lithium salts complicates the phase behaviour in unexpected ways. At low concentrations of salt, the liquidus curve is depressed, as in a solvent-solvent system. However, at higher concentrations, beyond the eutectic point, salt-solvent interactions also give rise to more complex behaviour.<sup>7,61,62</sup>

In this thesis, a  $\text{LiPF}_6$ -DMC phase diagram was constructed. For this project, pouch cells were filled with electrolyte composed of DMC and  $\text{LiPF}_6$ , where the molarity varied between 0 and 2 M, at intervals of 0.2 M. Figure 4.3 shows the data produced by tests of these cells.

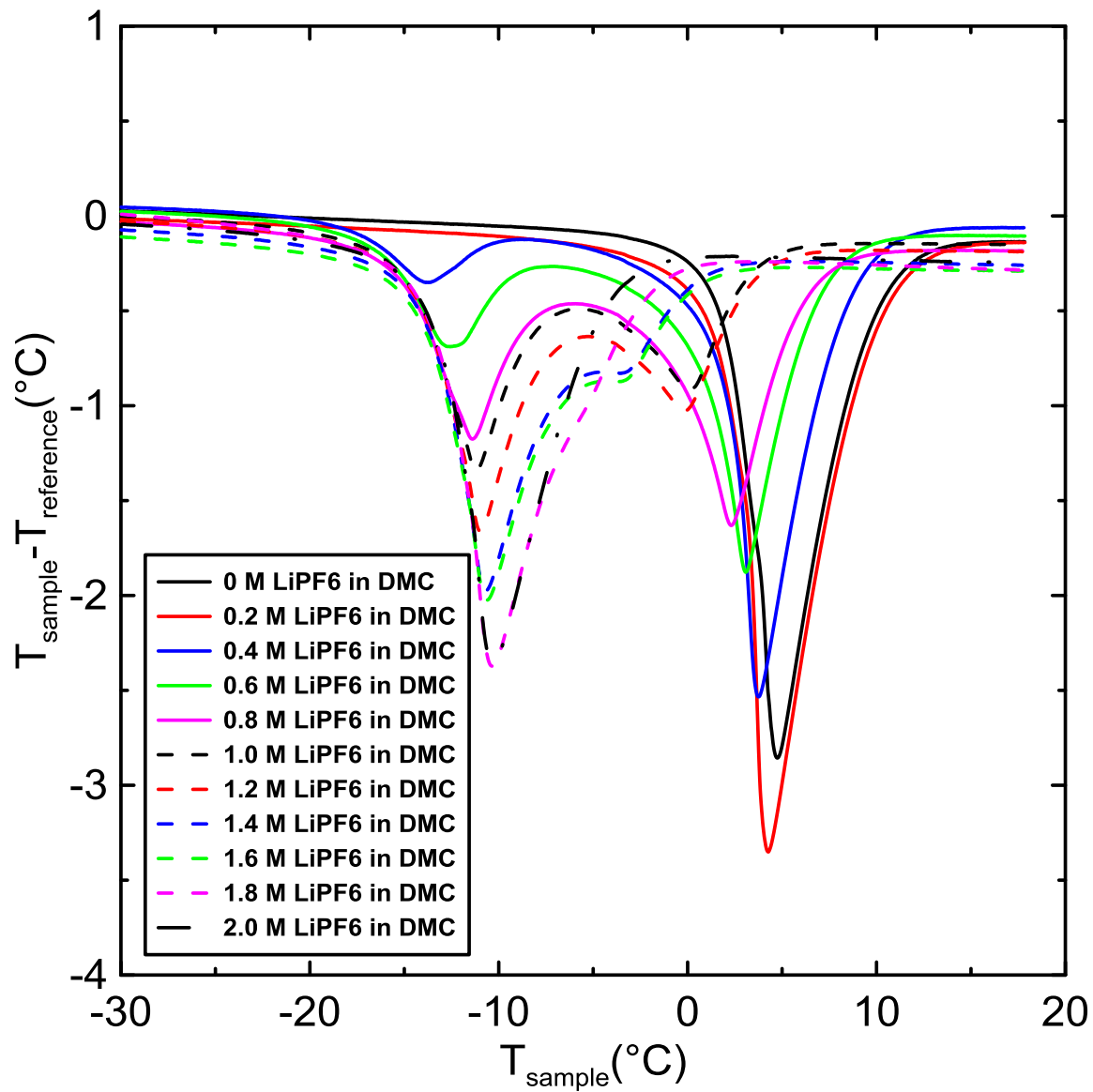


Figure 4.3: A set of DTA curves for LiPF<sub>6</sub>-DMC electrolytes between 0 and 2M, at intervals of 0.2 M.



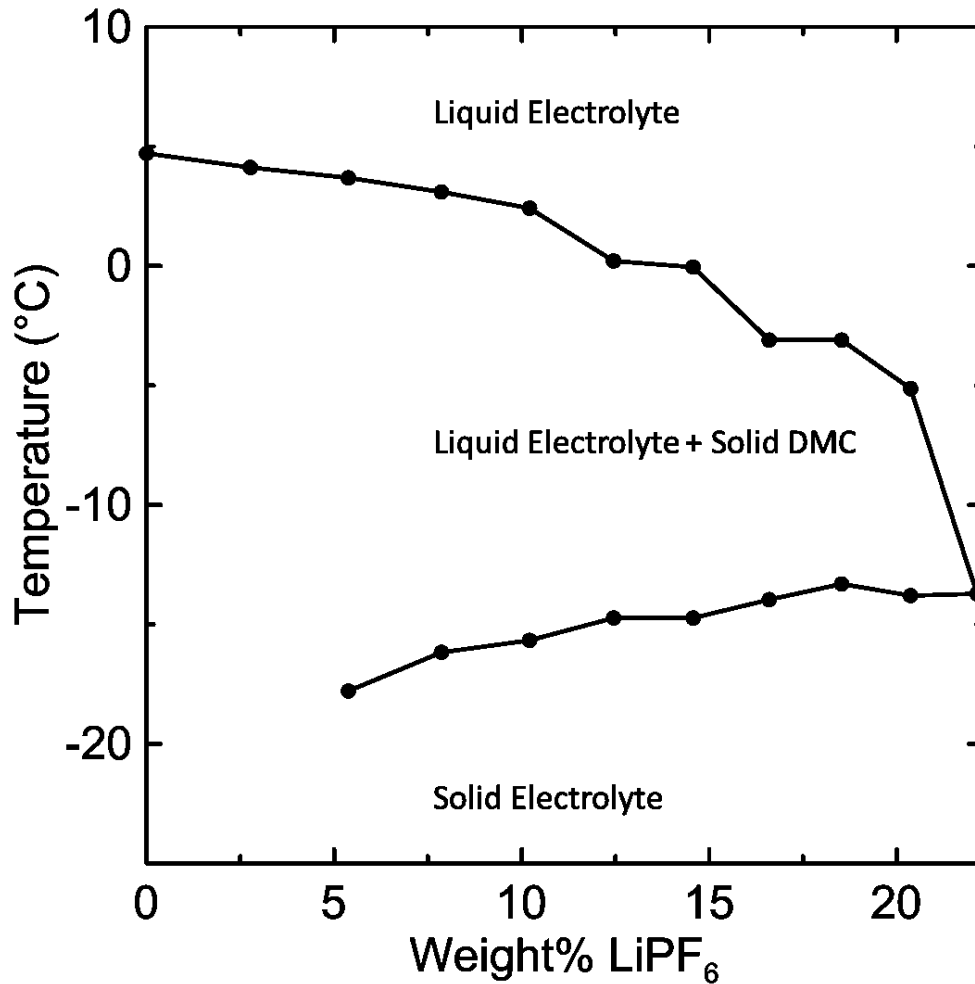


Figure 4.4: The LiPF<sub>6</sub>-DMC phase diagram from 0 to 24% LiPF<sub>6</sub> by weight.

Figure 4.4 shows the pre-eutectic LiPF<sub>6</sub>-DMC phase diagram generated in this work. The liquidus point can be seen to descend from the melting point of DMC, down to the solidus point of the LiPF<sub>6</sub>-DMC mixture. This data suggests that the eutectic of the LiPF<sub>6</sub>-DMC mixture is located at approximately or 22 w% LiPF<sub>6</sub>. As the eutectic is interpreted from DTA curves as being the composition at which all liquid freezes at one time, very careful study must be undertaken to determine its exact location. One feature in a DTA curve can imply the existence of a eutectic, or the existence of two phase transitions, very close to one another.

Though this dataset is informative as to the behaviour of the DMC-LiPF<sub>6</sub> system, it is not practically useful for Li-ion battery development. This electrolyte has a very high liquidus temperature and contains no EC or additives to passivate the negative electrode. However, this data and method serve as a model for how one would develop such datasets for more useful electrolyte systems. Practical systems, e.g. the LiPF<sub>6</sub>-DMC-EC system show more complex behaviour due to the additional degree of freedom of the EC component. This complexity causes these types of systems, called ternary systems, to be far more difficult and time intensive to study.

### **4.3 High Concentration Regions**

At high concentrations of salt, past the eutectic point, the salt-solvent system becomes less well behaved. While before the eutectic the liquidus curve tends smoothly towards the solidus, as in Figure 4.3, post eutectic behaviour introduces several new features that behave in unexpected ways. While a liquidus and solidus features can be identified, the new peaks do not trend toward known boundaries, and thus cannot be easily classified. Figure 4.5 shows data collected from cells with concentrations of LiPF<sub>6</sub> beyond the eutectic.

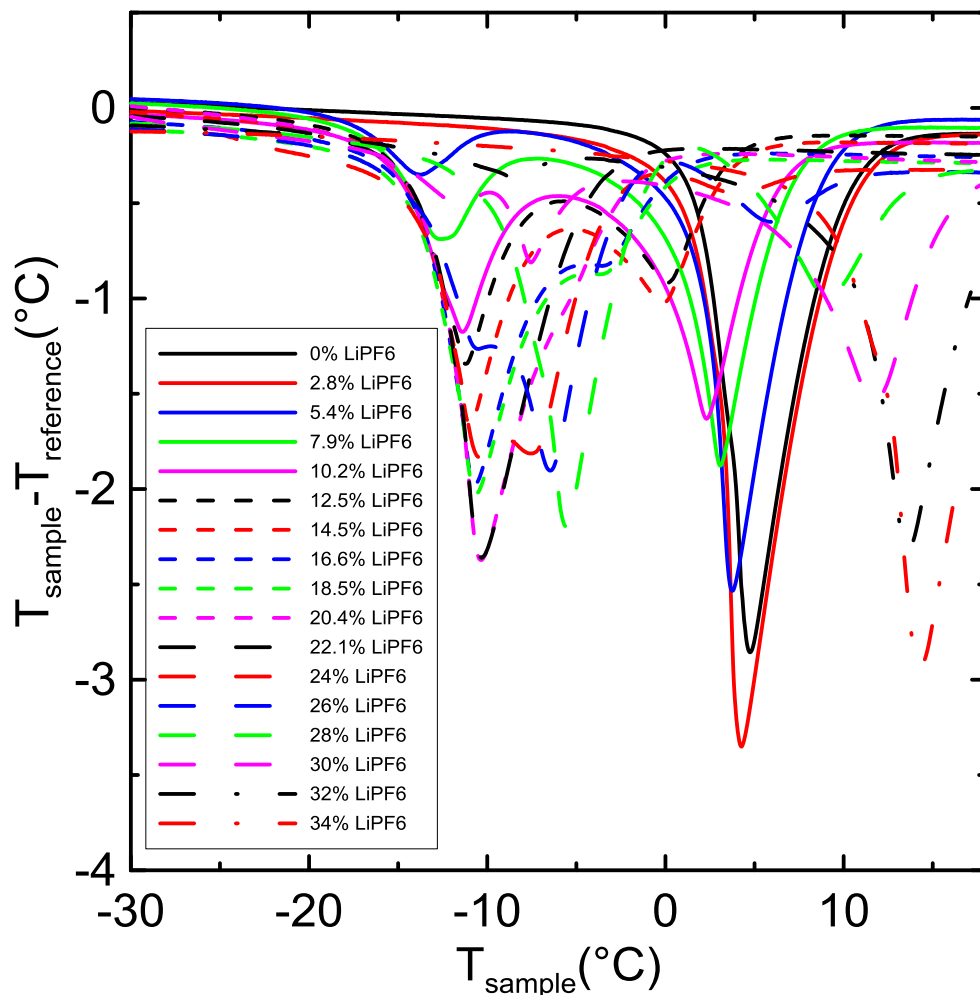


Figure 4.5: Part of the high concentration region of the LiPF<sub>6</sub>-DMC space, alongside the lower concentration data.

It is known, from studies of other salt-solvent phase diagrams,<sup>61,62</sup> that the behaviour of salt-solvent compositions greater than the eutectic concentration is more complex, than those with salt concentrations lower than the eutectic, so the observed behaviour is not without precedent. However, the state of the electrolyte is especially unknown, as the simple model of solvent freezing out of the liquid electrolyte no longer holds. Consideration of the effects of this behaviour is given in section 7.2.8.

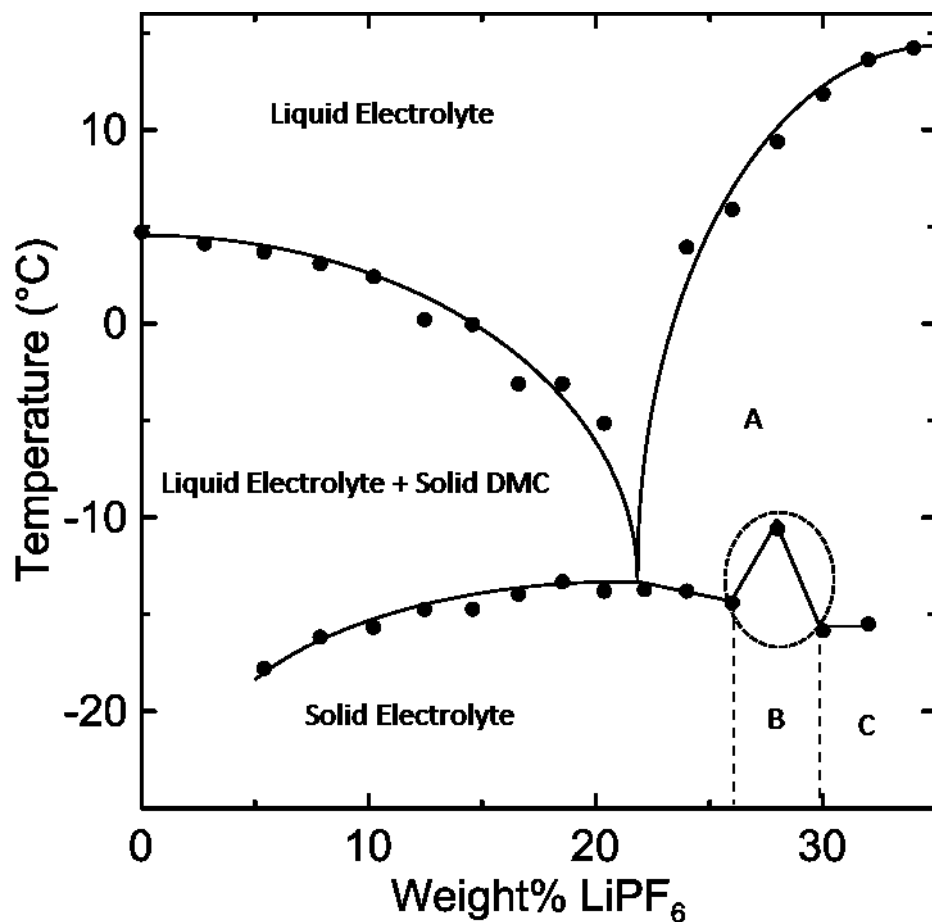


Figure 4.6: A speculative phase diagram of the  $\text{LiPF}_6$ -DMC system that includes regions of very high salt content. The dashed lines represent possible phase transition, given the changes in the solidus at those points. The A, B, and C phases are three phases whose composition cannot be determined by DTA. The ellipse represents a particularly uncertain region in the solidus measurement.

Even so, a speculative diagram for the  $\text{LiPF}_6$ -DMC phase diagram that includes the higher concentration regions can be designed, as shown in Figure 4.6. Note that this figure is somewhat theoretical; it is not known precisely where the eutectic is located, as the DTA features are relatively broad in that concentration region. Further, the solidus in the 22-32%  $\text{LiPF}_6$  region is erratic, which indicates more complex behaviour, or experimental error, as represented in Figure 4.6 by an ellipse.

Figure 4.6 also includes regions labelled A, B, and C. Phases B and C are likely not simply solid electrolyte, as they are divided by changes in the behaviour of the solidus line; as the solidus line changes, the energy needed to break the bonds changes, which indicates a change in the structure of the solid. As well, phase A must be distinct, as it is separated by phase transitions from the other phases. However, though these phases can be speculated to exist, their composition cannot be determined by DTA. Cells were also made and tested up to 42%  $\text{LiPF}_6$ , but these DTA curves displayed significant crystallizations, and were disposed of before the peak removal protocol was devised.

## Chapter 5: Long Term Electrolyte Degradation

The goal of this thesis is to develop and motivate a method by which the state of an electrolyte can be reliably determined solely via DTA. To this end, several cells have been cycled to their complete death, while being tested regularly. These cells were then disassembled, and the remaining electrolyte composition determined via GC/MS and ICP-OES

Once the composition was determined, replica cells with electrolytes of the composition described by GC/MS and ICP-OES were made. These cells were used to verify the interpretation of the Li-ion DTA curves.

### 5.1 Physical Properties of Dry Cells

Cells of two types were produced for this thesis; core-shell cells, and NMC532 cells. Cells of another type, called Rock532 were produced for another project, but tested as part of the greater DTA work, and will be presented here. The name “core-shell” is derived from the positive electrode material, which is composed of a high nickel content core and a high manganese content shell.<sup>63</sup> The core shell cells were chosen for the development of phase diagrams, as they faced an intractable issue of significant gas production at high voltage and were thus unfit for general research, but viable for the creation of phase diagrams, which only require a cell filled with electrolyte. Any pouch cells would suffice, but the core-shell cells were plentiful and not useful for other experiments. The NMC532 cells produced for the long term cycling experiments shown here possess a positive electrode composed of  $\text{Li}(\text{Ni}_{0.5}\text{Mn}_{0.3}\text{Co}_{0.2})\text{O}_2$ . Finally, the Rock532 cells, produced as part of a separate project, are different from the standard NMC532 cells

in that they incorporate a single crystalline cathode structure, as opposed to the polycrystalline structure of the NMC532 cell cathode.

	Core-Shell	NMC532	Rock 532
Positive Electrode	$\text{Li}(\text{Ni}_{1-x-y}\text{Mn}_x\text{Co}_y)\text{O}_2$	$\text{Li}(\text{Ni}_{0.5}\text{Mn}_{0.3}\text{Co}_{0.2})\text{O}_2$	Single Crystal NMC532
PE Loading	16 mg/cm <sup>2</sup>	21.1 mg/cm <sup>2</sup>	21.1 mg/cm <sup>2</sup>
PE Coating	None	Al <sub>2</sub> O <sub>3</sub>	TiO <sub>2</sub>
Negative Electrode	Artificial Graphite	Natural Graphite	Artificial Graphite
NE Loading	9 mg/cm <sup>2</sup>	13.6 mg/cm <sup>2</sup>	13.6 mg/cm <sup>2</sup>

Table 5.1: A brief summary of the physical properties of the cells used in this thesis.

Table 5.1 shows some of the physical properties of the cells used. While the effects of different electrodes on the degradation of electrolyte is complex, it is assumed that different electrodes will not affect the results of tests taken before cycling, as in the determination of the DMC phase diagram.

## 5.2 Electrolyte Produced

The main experiment consisted of forty cells, split into groups based on electrolyte composition and upper cutoff voltage. All cells were the same type, with a natural graphite negative electrode, and a positive electrode composed of  $\text{Li}(\text{Ni}_{0.5}\text{Mn}_{0.3}\text{Co}_{0.2})\text{O}_2$  at a loading of 21.1 mg/cm<sup>2</sup>. All the cells produced for this experiment have a base electrolyte of 1 M LiF<sub>6</sub> in 3:7 w/w EC:EMC. Twenty of the cells use VC, while the other twenty use the PES-211D additive blend. A miscalculation was made during the initial cell creation that led to all additive concentrations being 85% of the correct value; 2%VC becomes 1.7% VC, and so on. This deviation should not lead to significant differences from standard additive

concentrations. The full names, structures, and available melting points of all the chemicals are presented in Table 5.2.

Note that DEC, DMC, VC, PES, DTD, TTSPi, FEC, DMOHC, DEOHC, and EMOHC are sometimes present in the electrolyte in aged cells in small amounts of less than 3% by weight. These are assumed to have negligible effect on the overall DTA signal structure and cell melting points.



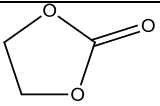
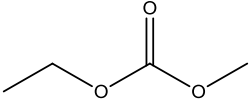
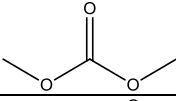
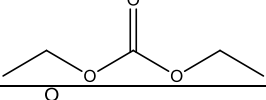
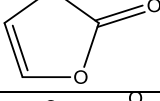
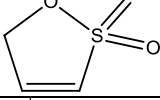
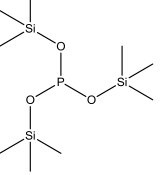
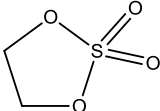
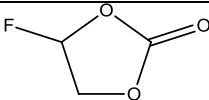
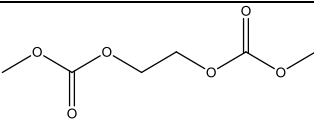
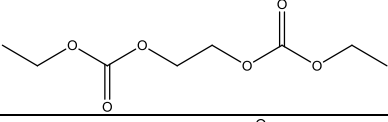
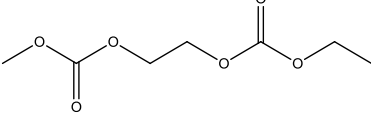
Chemical Name	Abbrev.	Structure	Melting Point
Ethylene Carbonate	EC		36.4°C <sup>5,7,10</sup>
Ethyl Methyl Carbonate	EMC		-53°C <sup>5</sup>
Dimethyl Carbonate	DMC		4.6°C <sup>5</sup>
Diethyl Carbonate	DEC		-74.3°C <sup>7,25</sup>
Vinylene Carbonate	VC		20.5°C <sup>a</sup>
Prop-1-ene-1,3-sultone	PES		Solid at RT
Tris-(trimethylsilyl)-phosphite	TTSPi		Unknown <sup>b</sup>
1,3,2-Dioxathiolane 2, 2-dioxide	DTD		Solid at RT
Fluoroethylene Carbonate	FEC		21.4°C <sup>a</sup>
Dimethyl-2,5-dioxahexane carboxylate	DMOHC		12.1°C <sup>a</sup>
Diethyl-2,5-dioxahexane carboxylate	DEOHC		Unknown <sup>a</sup>
Ethyl Methyl-2,5-dioxahexane carboxylate	EMOHC		Unknown <sup>b</sup>

Table 5.2: Names, structures, and melting points of chemicals discussed in this thesis.

<sup>a</sup> See figures in Appendix A: Solvent Melting Points.

<sup>b</sup> No value in chemical databases, no supply in the lab with which to determine by experiment.

### 5.3 Cell Preparation Method

This work utilizes prismatic, 402035(40 by 20 by 3.5 mm) pouch cells for the study of electrolyte. These cells are used because they can be easily filled with electrolyte, have standardized electrodes, and act as reasonable facsimiles of commercial cells. These cells are received from the manufacturer sealed and dry with no electrolyte. The cells were first dried of any residual water content by cutting the top of the gas bag and vacuum drying in a glovebox antechamber at 100°C for 14 hours. Following the drying process, they were moved into an argon-filled glove box and filled with electrolyte. The filling procedure consists of first using a syringe to fill each cell with 0.9 ml of electrolyte. The cells were then placed in a vacuum wetting canister to draw the electrolyte into the jelly roll, the roll of electrodes and separator in the cell. The cells were then sealed using a vacuum pouch sealer, which puts the cells under a pressure of -90kPa (relative to the glovebox atmosphere, which is at a slightly higher pressure than the outside atmosphere) prior to heat sealing at 160°C for four seconds, to melt the open ends of the cell together.

The cells were then removed from the glove box, placed in lab-built polypropylene cell holders, clamped with rubber blocks and steel shims, and left on a 1.5 V wetting rack in open air for 12-24 hours. This wetting procedure both allows for the electrolyte to suffuse through the jelly roll and prevents the copper foil negative electrode current collector from oxidizing in the electrolyte. Following this, the cells underwent the formation process, which consists of a first charge from 1.5 V to 3.8 V, where it is held for 24 hours, followed by a second charge to the upper cutoff voltage, where it is held for another 24 hours. The cell is then discharged to 3.0 V for cycling. This formation process is optimized to produce a robust SEI.

## 5.4 Cycling Protocol

The cycling protocol used here is called CCCV, which stands for constant current/constant voltage. This is a cycling protocol where a cell is charged to an upper setpoint voltage via a constant current, and then charged with a constant voltage until the current drawn hits 15 mA. After this, the cell is discharged at the same current as its charge process. The cell is cycled to and from its upper cutoff voltage at a standard cycling rate, with one low rate cycle every fifty cycles. In this case, the standard charge rate used was “C/3”, while the low charge rate was “C/20.” The C notation describes the current used with reference to the cell’s initial capacity. A C/3 current will charge the cell in three hours, while the C/20 current will charge it in 20 hours. The cells were cycled at 55°C.

Under normal conditions, these cells would take years to die completely.<sup>7,10</sup> The high temperature was used to kill the cells relatively quickly, as the DTA experiment is interested in the full lifetime of the cell. The single low cycle every twenty cycles can be used to determine valuable information as to the cell’s behaviour. For example, internal impedance will gradually increase, in Li-ion cells undergoing long term cycling. This impedance will prevent higher rate cycling from allowing the cell to reach full capacity. An occasional slower rate cycle will then allow the cell more time to fully charge, allowing for a more accurate determination of the cell’s capacity.

## 5.5 Testing Protocol

For the bulk of the experiment, cells were subjected to DTA on a schedule of cycle time, as opposed to cycle count. The set of cells was split into four cohorts, where the first was tested every two weeks, the second was tested every month, and the third tested every

two months. The fourth set was tested only on death, as a control. The procedure for testing the cells was as described in section 2.1.3. The resultant data was then compared against cycling times, to determine the behaviour of the electrolyte as the cell aged, as discussed in chapter 6.

### 5.5.1 Primary Test - Results

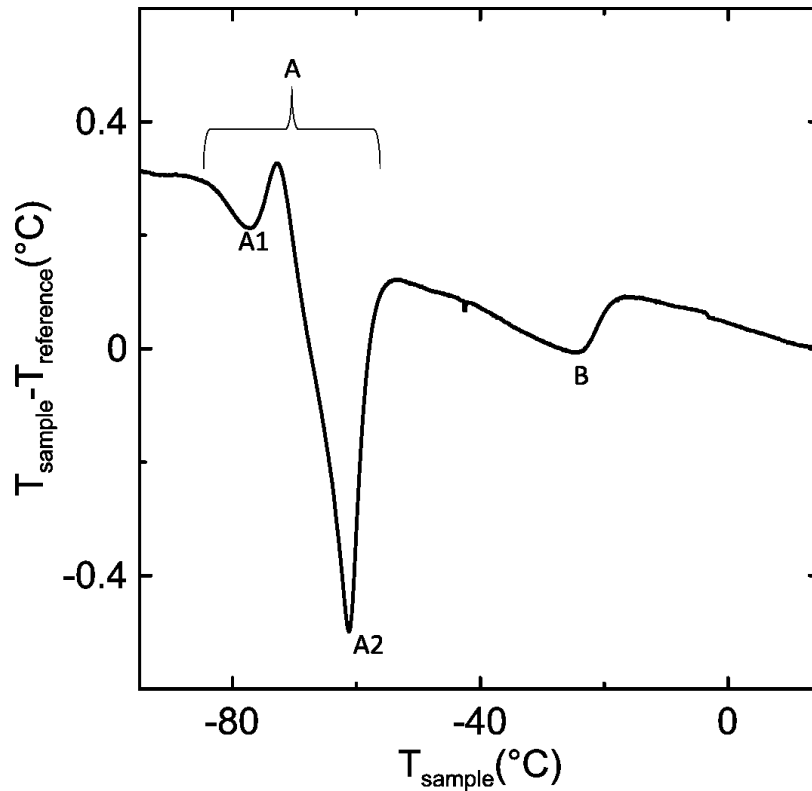


Figure 5.1: A typical DTA curve from a 1 M 3:7 (w%) EC:EMC  $\text{LiPF}_6$  pouch cell. Several features are of note; A denotes the solidus region comprised of a low temperature peak, A1, and a high temperature peak, A2. The third peak, B, is the liquidus feature.

Figure 5.1 shows a typical EC/EMC  $\text{LiPF}_6$  DTA curve. On this curve are labelled the first (feature A1) and second (feature A2) solidus peaks, as well as the liquidus peak (feature B). In most cases, these features will be present in all the data presented in this

section, so these will be the features referenced in their discussion. The 4.1 V datasets for VC and PES-211D show a fresh cell of that type, for reference.

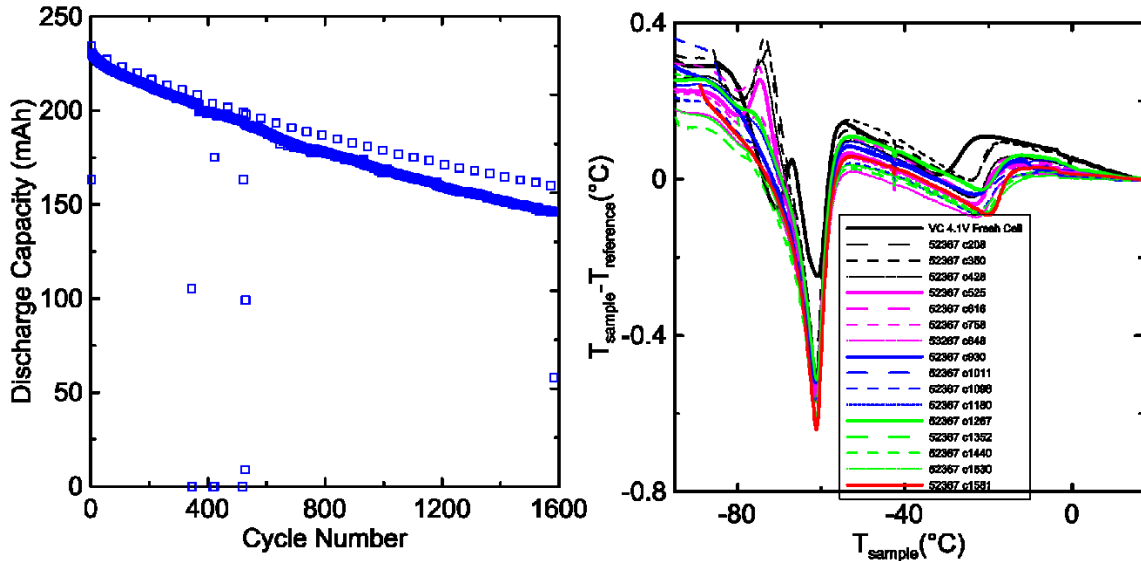


Figure 5.2: Cycling (left) and DTA (right) data for cell 52367, an NMC532/NG cell with 1.0 M LiPF<sub>6</sub> in 3:7 w% EC:EMC + 2VC electrolyte, cycled to 4.1V. The cycle numbers where DTA test occurred are indicated on the legend.

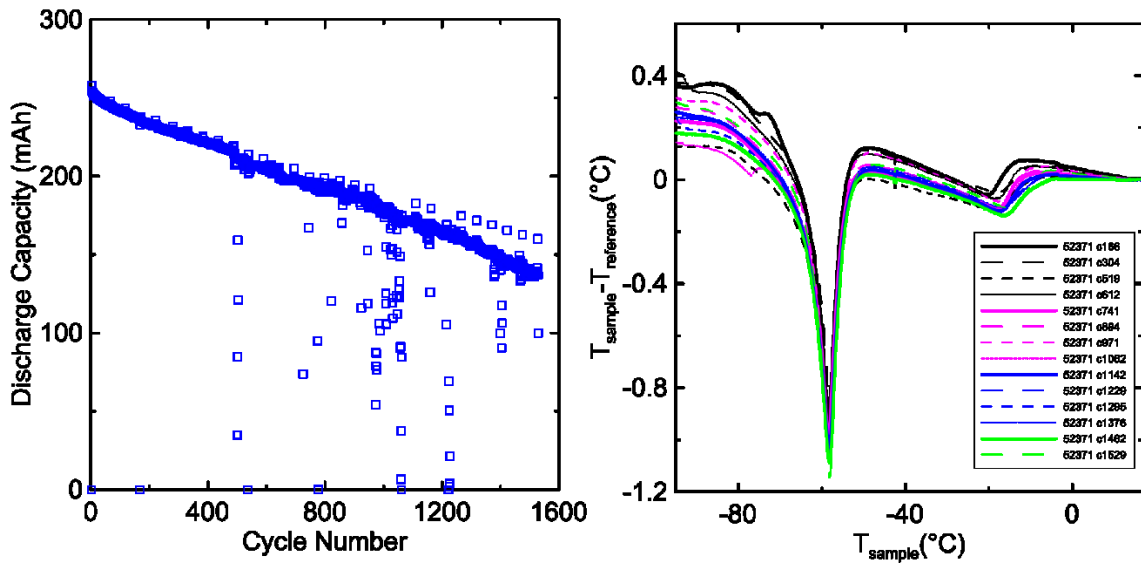


Figure 5.3: Cycling (left) and DTA (right) data for cell 52371, an NMC532/NG cell with 1.0 M LiPF<sub>6</sub> in 3:7 w% EC:EMC + 2VC electrolyte, cycled to 4.2V. The cycle numbers where DTA test occurred are indicated on the legend.

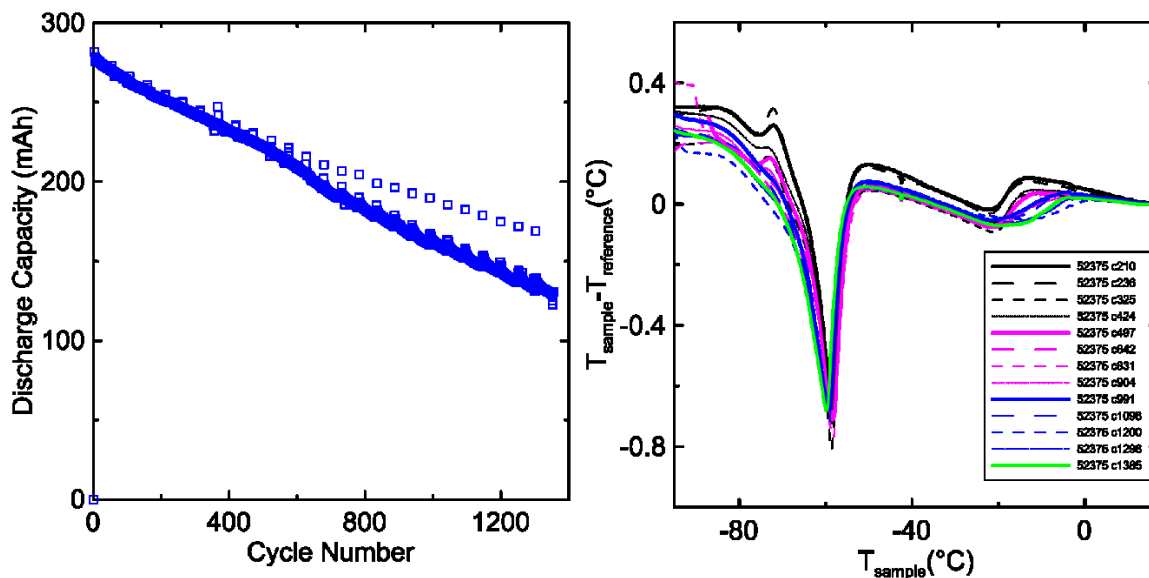


Figure 5.4: Cycling (left) and DTA (right) data for cell 52375, an NMC532/NG cell with 1.0 M LiPF<sub>6</sub> in 3:7 w% EC:EMC + 2VC electrolyte, cycled to 4.3V. The cycle numbers where DTA test occurred are indicated on the legend.

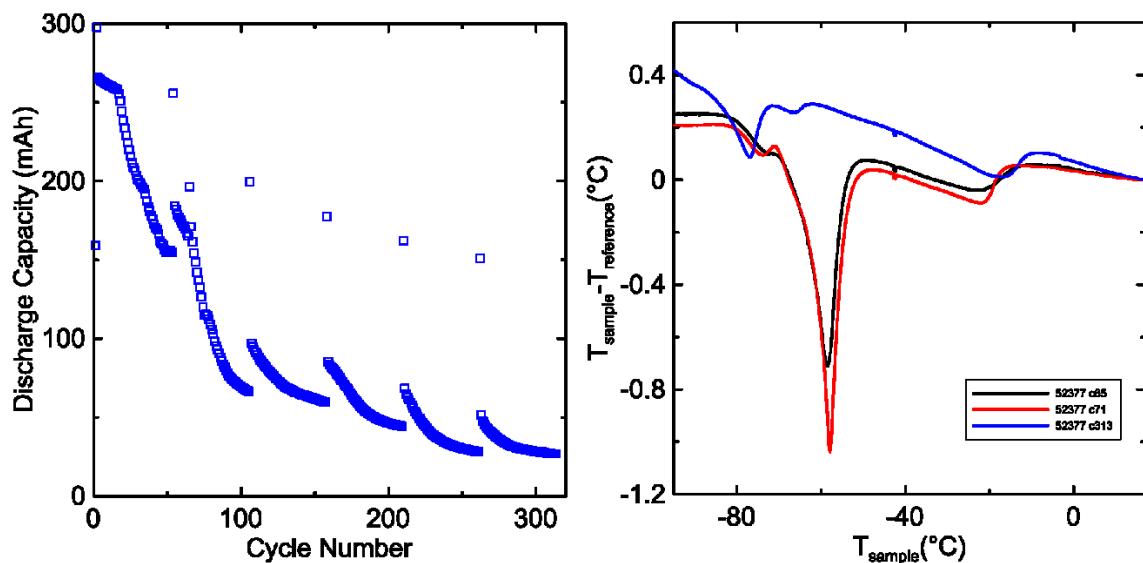


Figure 5.5: Cycling (left) and DTA (right) data for cell 52377, an NMC532/NG cell with 1.0 M LiPF<sub>6</sub> in 3:7 w% EC:EMC + 2VC electrolyte, cycled to 4.4V. The cycle numbers where DTA test occurred are indicated on the legend.

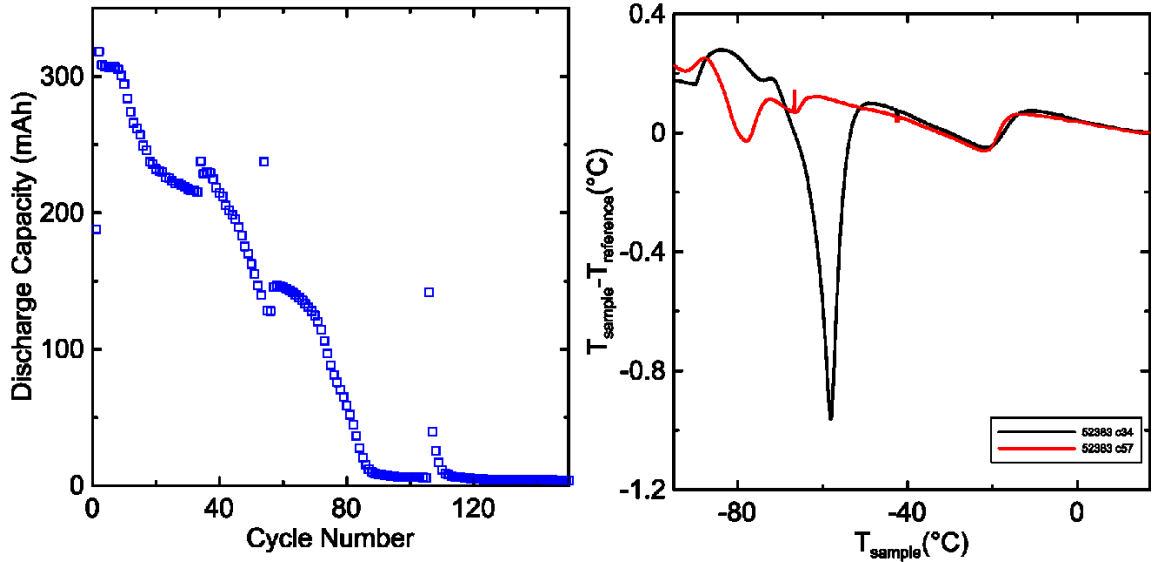


Figure 5.6: Cycling (left) and DTA (right) data for cell 52383, an NMC532/NG cell with 1.0 M LiPF<sub>6</sub> in 3:7 w% EC:EMC + 2VC electrolyte, cycled to 4.1V. The cycle numbers where DTA test occurred are indicated on the legend.

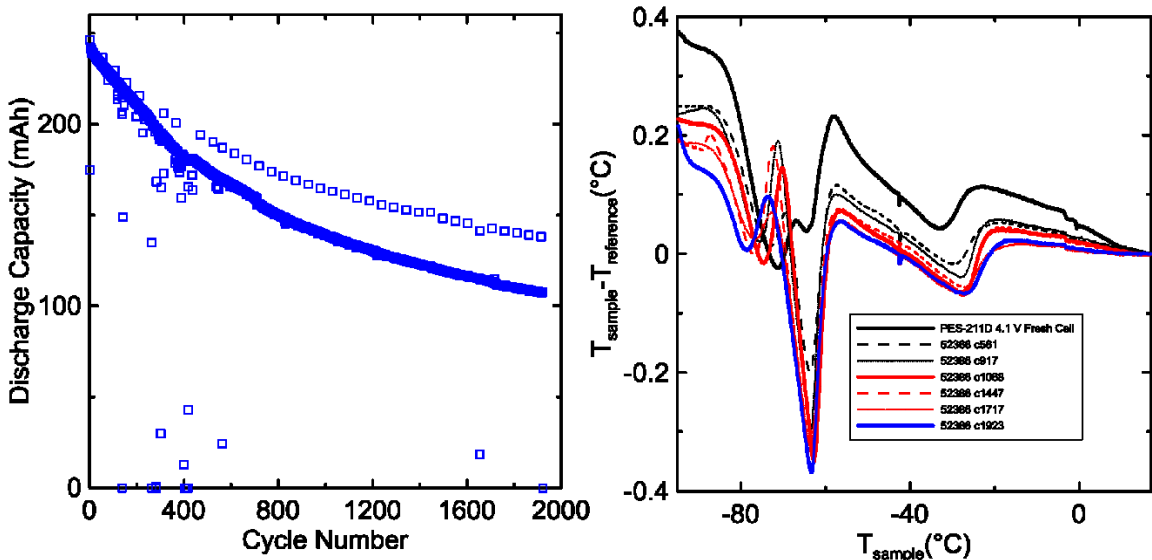


Figure 5.7: Cycling (left) and DTA (right) data for cell 52386, an NMC532/NG cell with 1.0 M LiPF<sub>6</sub> in 3:7 w% EC:EMC + PES-211D electrolyte, cycled to 4.1V. The cycle numbers where DTA test occurred are indicated on the legend.

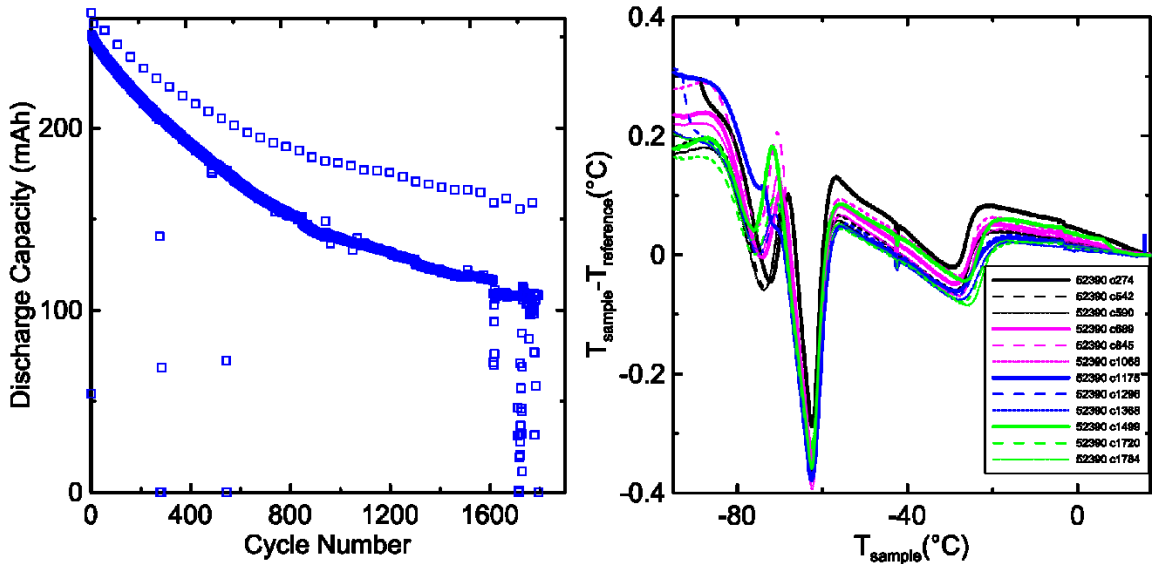


Figure 5.8: Cycling (left) and DTA (right) data for cell 52390, an NMC532/NG cell with 1.0 M  $\text{LiPF}_6$  in 3:7 w% EC:EMC + PES-211D electrolyte, cycled to 4.2V. The cycle numbers where DTA test occurred are indicated on the legend.

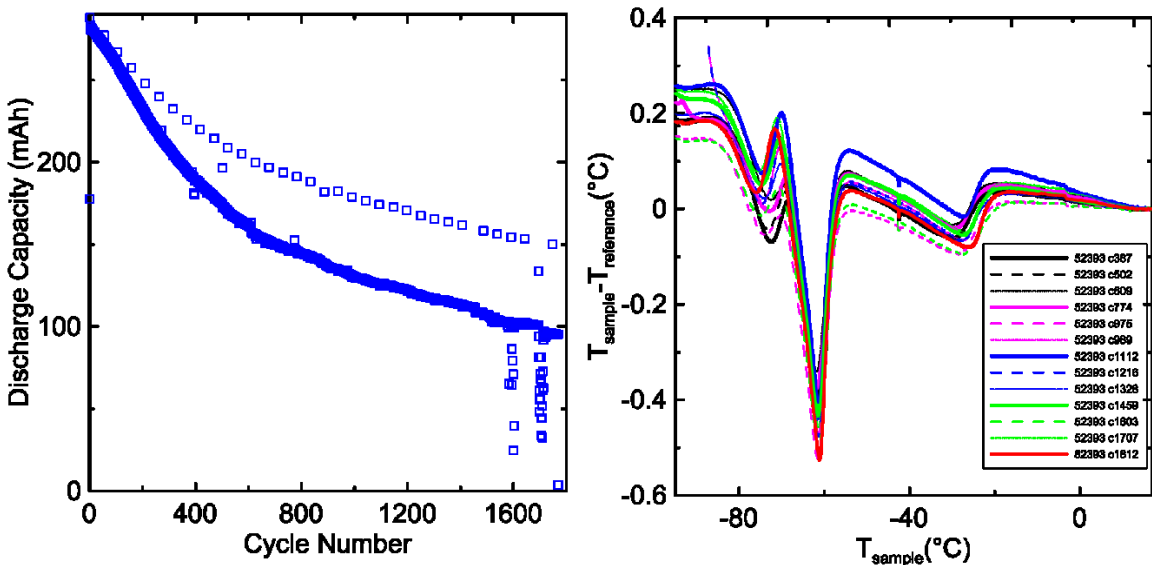


Figure 5.9: Cycling (left) and DTA (right) data for cell 52393, an NMC532/NG cell with 1.0 M  $\text{LiPF}_6$  in 3:7 w% EC:EMC + PES-211D electrolyte, cycled to 4.3V. The cycle numbers where DTA test occurred are indicated on the legend.



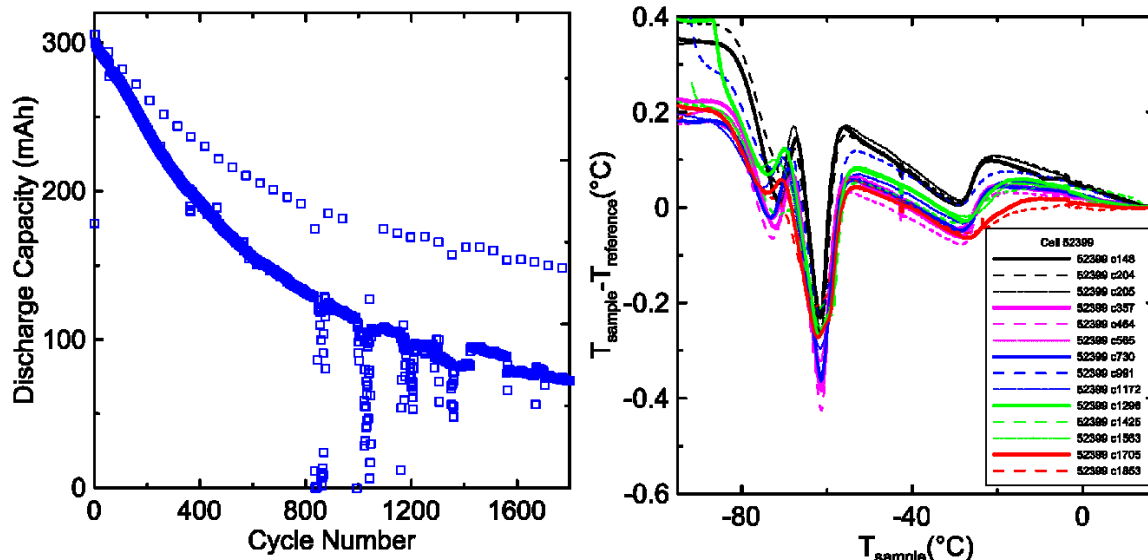


Figure 5.10: Cycling(left) and DTA(right) data for cell 52399, an NMC532/NG cell with 1.0 M LiPF<sub>6</sub> in 3:7 w% EC:EMC + PES-211D electrolyte, cycled to 4.4V. The cycle numbers where DTA test occurred are indicated on the legend.

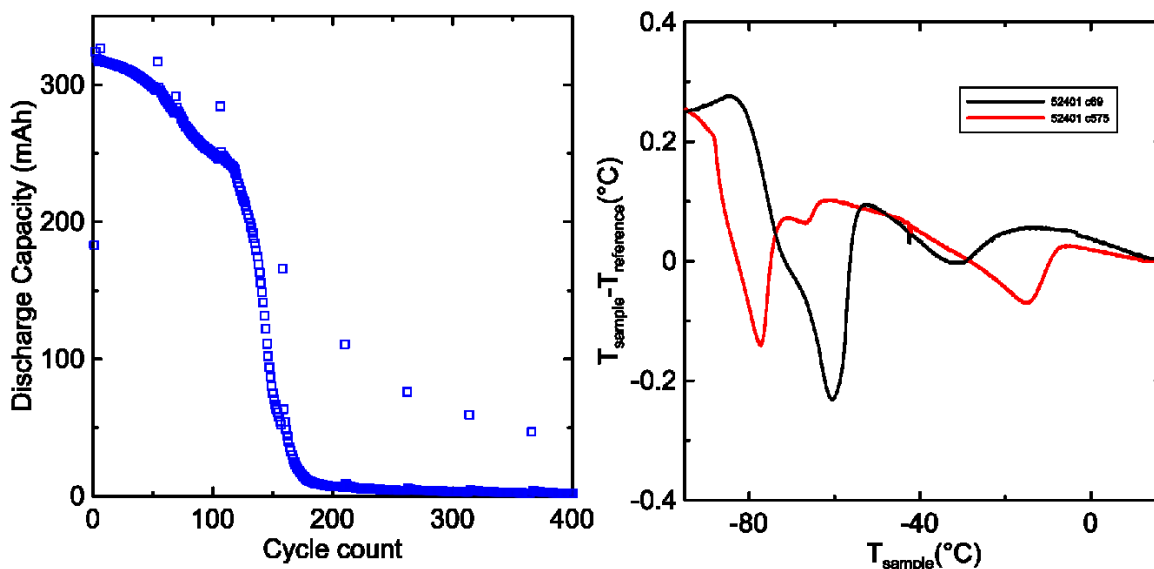


Figure 5.11: Cycling(left) and DTA(right) data for cell 52401, an NMC532/NG cell with 1.0 M LiPF<sub>6</sub> in 3:7 w% EC:EMC + PES-211D electrolyte, cycled to 4.5V. The cycle numbers where DTA test occurred are indicated on the legend.

Figure 5.2 through Figure 5.10 show the results from a selection of the cells with the most DTA testing. Note that the cycling data grows more and more noisy as time goes on, starting after a few hundred cycles have elapsed. This is likely due to the destruction of the positive electrode tab; this tab is composed of thin aluminum and grows weak after

long term storage at high temperature and voltage. As a result, after around six to seven DTA tests, where alligator clips are attached and removed, the positive tab will break off, rendering any further cycling data noisier.

These cells show several systematic trends through the cell death process, including a gradual reduction in size of peak A1, in the case of the VC containing cells. As well, note the gradual increase in temperature of the liquidus peak. This, along with negligible changes in the A region, indicates gradual salt consumption. Figure 5.2 shows this well; though the cell has degraded in performance significantly, only minor changes have occurred in the cell's electrolyte.

Figure 5.5 through 5.6 show similar stories; at voltages above 4.3 V, VC containing cells lose capacity quickly, leading to salt consumption and electrolyte loss. This is consistent with the literature, as VC containing Li-ion cells are known to show significant performance loss above 4.3 V.<sup>64</sup> In contrast, cells with PES-211D continue to perform well at 4.4 V, before undergoing a similarly fast death at 4.5 V.

However, high voltage cells that show catastrophic failure tend to show significant, near instantaneous change in the DTA curve. This is correlated with change to the electrolyte, where significant portions of the EMC component are turned into DMC and DEC, according to the ex situ results. Thus, these radically altered curves no longer hold to the A1, A2, B feature model, as those features are defined with respect to electrolytes dominated by an approximate 3:7 EC:EMC ratio.

### 5.5.2 Secondary Test - 2%VC High Voltage

The 4.5V cells in the primary test were observed to experience dramatic failure within one hundred cycles that, due to time constraints, was not carefully studied. Thus, a secondary test was devised to more carefully examine the behaviour of these cells under high voltage conditions. Thus, two NMC532 cells were filled with 1 M  $\text{LiPF}_6$  in 3:7 EC:EMC + 2%VC, and cycled at 4.5 V. It was hypothesized that the same degradation pathways would be followed as in the primary test, but at a greater rate, due to the elevated voltage. These cells were tested significantly more regularly, in order to capture the dramatic degradation observed in the primary test. Cell 64928 was tested at every loss of five percent discharge capacity, while cell 64929 was tested every twenty percent loss of discharge capacity. The data collected in this test is shown in Figure 5.12, Figure 5.13, and Figure 5.14. The data collected on cell 64928 has been split into two sets of figures, Figure 5.12, Figure 5.13, due to the significant degradation that occurs later in the cell's life.

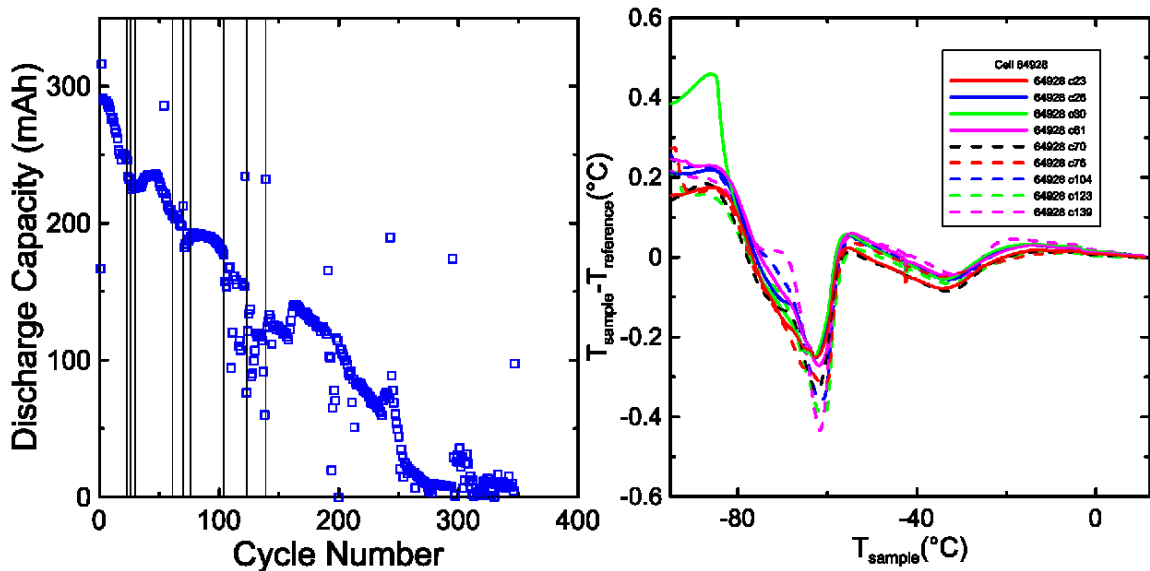


Figure 5.12: Cycling(left) and DTA data(right) from cell 64928, a 1.0 M  $\text{LiPF}_6$  in 3:7 EC:EMC 2VC 4.5 V NMC532/NG cell. The black lines on the cycling data indicate the cycles at which the DTA tests were conducted. This figure shows the first half of the tests conducted on the cell.

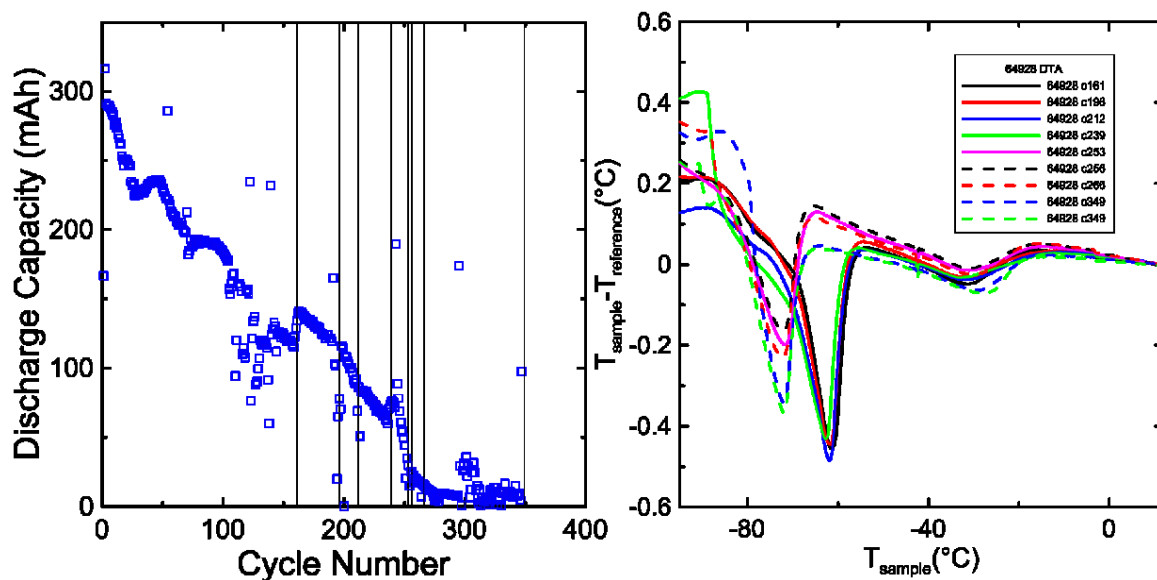


Figure 5.13: Cycling(left) and early DTA data(right) from cell 64928, a 1.0 M  $\text{LiPF}_6$  in 3:7 EC:EMC 2VC 4.5 V NMC532/NG cell. The black lines on the cycling data indicate the cycles at which the DTA tests were conducted. This figure shows the second half of the tests conducted on the cell.

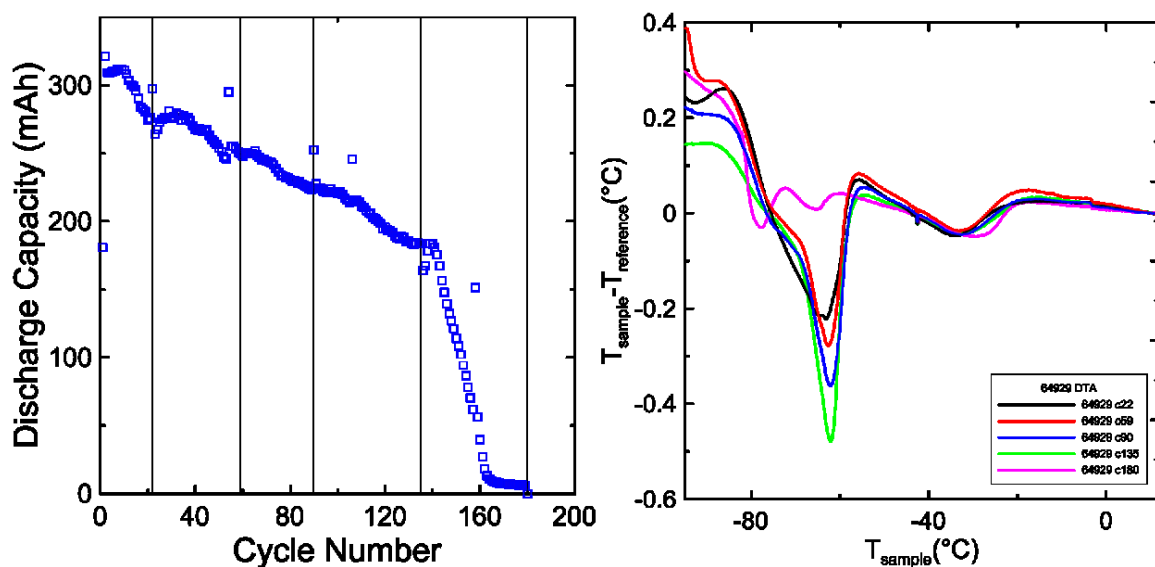


Figure 5.14: Cycling(left) and late DTA data(right) from cell 64929, a 1.0 M  $\text{LiPF}_6$  in 3:7 EC:EMC 2VC 4.5 V NMC532/NG cell. The black lines on the cycling data indicate the cycles at which the DTA tests were conducted. This figure shows all tests conducted on the cell.

There are several things of note in this experiment. The first is the extended lifetime. These cells performed better than their 4.5 V counterparts the primary test, such as the one shown in Figure 5.6, as this cell maintained approximately 60% capacity at 100

cycles, where the 4.5 V cells in the primary test showed near zero capacity at this point. No explanation for this is known. Second is the behaviour at low cycle numbers. The long-lived primary test cells were not tested until several hundred cycles had elapsed, but these cells were tested regularly, from the first cycle forward. Thus, these are the only cells whose early lives were well documented. This early life then tells an interesting story. In both cases, the solidus feature is broad in early tests, before beginning to sharpen as the cell degrades. This would seem to suggest a considerable change in the electrolyte, which conventional DSC wisdom would hold to be an increase in the amount of the material causing the peak; in this case, EMC. However, changes of area like this have recently been determined to be quite complex, as discussed in section 7.2.10. In short, there may be very complex relationships between DTA curve area and the composition of the cell's electrolyte.

## **5.6 Replica Cells**

Once cells have been cycled until death, they are disassembled, and their electrolyte studied through various ex-situ methods. Once this study is completed, cells are made that incorporate the electrolyte composition determined. These cells are referred to as replica cells. While DTA is a powerful tool, it cannot currently be used to quantitatively determine the exact materials in a cell. GC-MS and ICP were used for precise, ex-situ analysis, and the results of those tests were used to create a new set of cells, or replicas. Lauren Thompson did the GC/MS and ICP-OES work to determine the electrolyte composition. These replicas allow for the study of the exact composition of the electrolyte at the time of

death. In this way, the degraded state of the cell can be compared to a fresh cell of the same electrolyte composition, which allows for an interpretation of the Li-ion DTA results.

### **5.6.1 Ex-situ Study of Electrolyte**

The exact procedure used here was performed as described in Ellis *et al.*,<sup>65</sup> using a salt-solvent separation technique developed and published by Petibon *et al.*<sup>49</sup> This method of liquid-liquid extraction separates the solvents from the LiPF<sub>6</sub>, and uses gas chromatography and mass spectrometry to semi-quantitatively study electrolyte. This LiPF<sub>6</sub> separation allows for the LiPF<sub>6</sub> to be analyzed separately, and prevents the damage being done to the GC-MS by buildup of salt or LiF, or direct corrosion by HF or PF<sub>5</sub>.<sup>49</sup> This process, and the results obtained, will be summarized here.

### **5.6.2 Electrolyte Extraction Process**

First, the cells to be studied are discharged to approximately 0 V vs Li/Li<sup>+</sup>, for safety. Then, the tabs and external markings are removed by scissors and acetone, respectively. In order to remove the electrolyte without significant loss, several slits were opened in the top and bottom of the cell, and the cell is placed in a 15 ml polypropylene centrifuge vial and centrifuged at 2200 RPM for 20 minutes at 30°C. The extracted electrolyte was then moved by syringe to samples for GC-MS and ICP-OES study.

### **5.6.3 Use of GC-MS and ICP-OES**

GC-MS sample preparation, as developed by Petibon *et al.*,<sup>48</sup> consists of placing one drop of sample electrolyte in a perfluoroalkoxy polymer centrifuge vial containing 10 ml of dichloromethane and ~0.1 mL of pure water. The dichloromethane serves to extract

the organic components, and the water serves to extract the salt. The sample vials are then shaken for 15 minutes and centrifuged at 2200 rpm for 20 minutes at 20°C. This procedure separates the sample into multiple, visible layers in the vial, the organic component of which can then be extracted into a GC-MS sample vial.

The ICP-OES test samples were prepared by dilution of 0.10 g of each electrolyte in 15 ml vials containing 10 g of 2% HNO<sub>3</sub>.<sup>65</sup> These dilutions give sample concentrations in the measurable range, alongside the three-point calibration in 2% HNO<sub>3</sub>. These samples were measured via a Perkin Elmer Optima 8000 ICP-OES.

As discussed in section 2.2.5, the sample preparation requirement of two dilutions of an already small amount of sample electrolyte introduces considerable error in the measurement.

#### **5.6.4 Results of Ex-Situ Testing**

Cells 52367, 52371, 52371, 52373, 52386, 52390, 52393, 52398, 52375, 52328, and 52329 were studied with ex-situ testing. The results of the ex-situ electrolyte studies were as summarized in Table 5.3 and Table 5.4. While this table does not state this, no cells were found to contain any liquid additive. As stated in section 3.4.2, while EMOHC was expected in these cells, it was not checked for. The % transesterification column is calculated as  $(DMC+DEC)/(DMC+DEC+EMC)$ . Each GC-MS sample was tested twice, while each ICP-OES sample was tested three times, which allowed for the calculation of standard deviations for each value.<sup>66</sup> Though these values have been excluded from Tables 5.3 and 5.4, the *ex situ* results have a mean standard deviation of 0.71%, and a maximum of 3%.

Cell #	Volt.	Li (M)	%EMC	%EC	%DEC	%DMC	%DEOHC	%DMOHC	%Trans.
52367	4.1 V	0.7	60.01	29.07	4.224	3.399	2.06	1.23	11.2
52371	4.2 V	0.42	62.11	26.8	1.96	2.47	4.06	2.628	6.7
52373	4.3 V	0.92	55.71	30	7.008	5.24	1.188	0.8641	18.3
52375	4.3 V	0.42	62.41	30.288	3.02	3	0.81	0.452	8.8
64928	4.5 V	0.19	37.067	30.59	16.9	12.6	1.684	1.15	44.3
64929	4.5 V	0.14	36.0	23.3	20.1	18.2	1.45	1.05	51.6

Table 5.3: The results of the GC-MS and ICP-OES tests conducted on the VC cells ex-situ. The Volt. column describes the upper cutoff voltage of the cell, the Li (M) column describes the post-cycling molarity of the electrolyte, which started at 1.0 M, and the transesterification column is calculated by the ratio of DMC and DEC to DMC, DEC, and EMC. All solvent columns are in weight percentages. All cells started with 1.0 M LiPF<sub>6</sub> in 30:70 w% EC:EMC.

Cell #	Volt.	Li (M)	%EMC	%EC	%DEC	%DMC	%DEOHC	%DMOHC	%Trans.
52386	4.1 V	1.24	59.77	28.72	4.81	3.68	1.832	1.188	12.4
52390	4.2 V	1.12	58.98	31.56	3.595	2.89	1.797	1.173	9.91
52393	4.3 V	1.13	61.7	32.1	2.952	1.969	0.808	0.511	7.39
52398	4.4 V	0.88	59.16	29.3	5.04	3.75	1.641	1.125	12.9

Table 5.4: The results of the GC-MS and ICP-OES tests conducted on the PES-211D cells ex-situ. The Volt. column describes the upper cutoff voltage of the cell, the Li (M) column describes the post-cycling molarity of the electrolyte, which started at 1.0 M, and the transesterification column is calculated by the ratio of DMC and DEC to DMC, DEC, and EMC. All solvent columns are in weight percentages. All cells started with 1.0 M LiPF<sub>6</sub> in 30:70 w% EC:EMC.

There are several important observations to be made from these tables. Of note are the relative amounts of lithium and EMC lost from the electrolyte. The difference in remaining Li content in the PES-211D and VC cells is the most significant. The PES-211D cells show little to no Li consumption, while the VC cells show universal Li consumption. Beyond this, there is very slightly more EMC consumption in the PES-211D cells, and very little EC consumption in either case. Unfortunately, as there are large changes to the electrolyte occurring in the cell, it is difficult to assign the changes in any particular component to a specific degradation process, without extensive further work.



### 5.6.5 Replication of Determined Electrolyte State

Once the state of the electrolyte was determined by GC-MS and ICP-OES, a selection of cells was filled as described. As these cells were not to be cycled or formed, they were made using core-shell cells. Further, to simplify the procedure and analysis somewhat, the DMOHC, EMOHC, and DEOHC components were neglected. As these solvents were determined to be present in concentrations of less than two percent in all but one case, this is not expected to be a significant deviation from the true electrolyte state.

Figure 5.15 through Figure 5.17 show the comparisons between cells 52367, 52373, and 64929 and their replicas. There are several things of note; first is the size of the features in the replica cell DTA curves. In all cases, the replicas are larger than the actual cells. As the replicas were filled with the same amount of electrolyte that the cycled cells were originally filled with, this suggests that the cells did undergo some electrolyte mass loss. Second is the slight offset of the liquidus feature in the 52371 and 52367 cell replicas. This is possibly because the ICP-OES testing protocol used in this work was flawed and overestimated the concentration of lithium in the electrolyte samples.

While 52367 and 52371 show relatively good agreement with the final test conducted on their respective cells, the replicas for cell 64929 are notable in how far off they are. This suggests that some other factor in the cell, that was not included in the replicas, was very significantly influencing the electrolyte's phase transitions. For cell 64929, this is most likely caused by the huge amounts of DEC and DMC created by transesterification which were not included in the replica electrolyte. The replicas for cells 52367 and 52371 also show slightly lower liquidus values than their corresponding cycled cells. This has been correlated with concerns that the ICP-OES sample preparation method

used here is slightly underestimating the  $\text{LiPF}_6$  content of cycled electrolyte samples. Those concerns are now reinforced by the appearance of the replica cells.

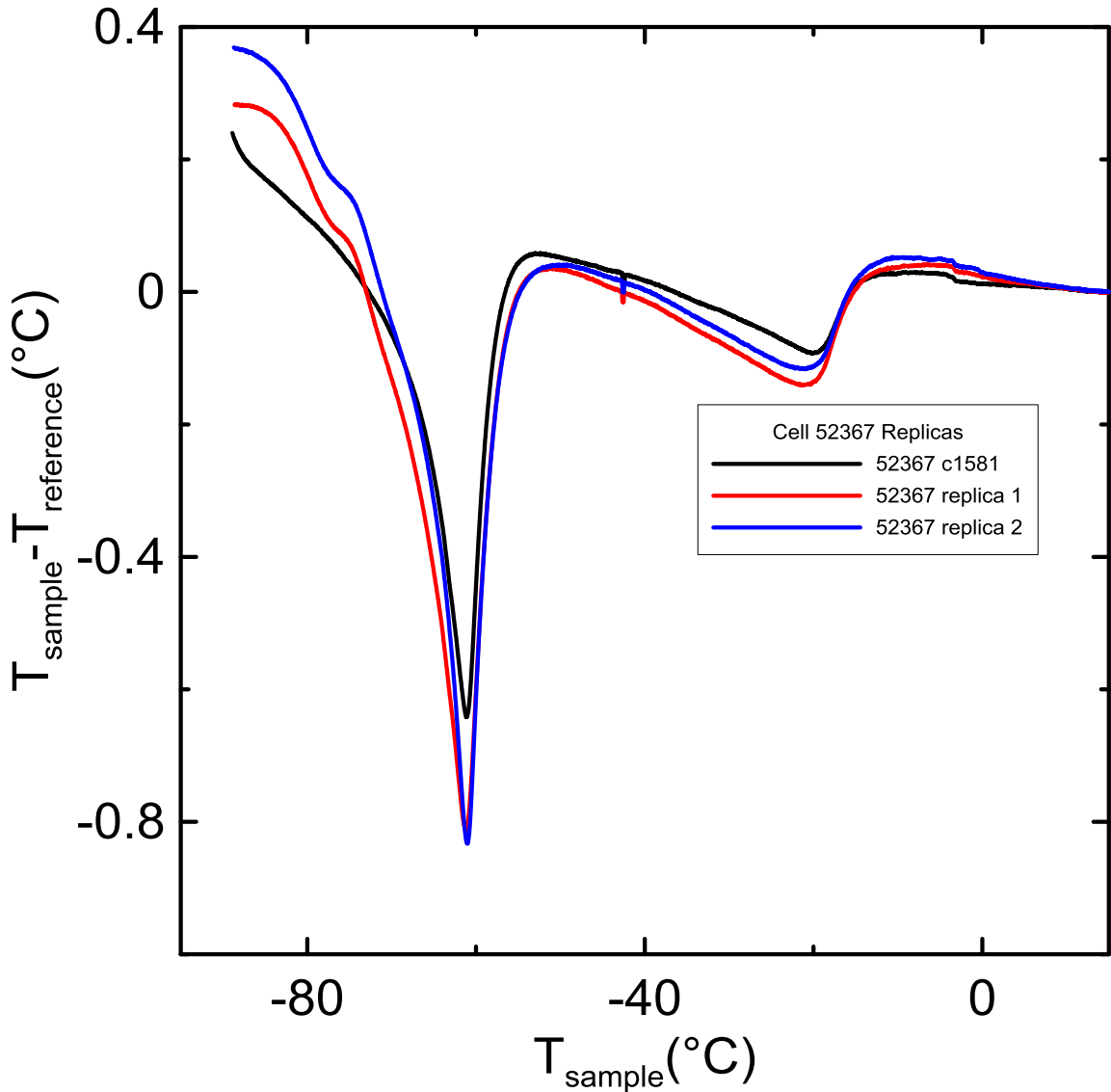


Figure 5.15: A comparison of the DTA data generated by the last test of cell 52367, a 1.0 M  $\text{LiPF}_6$  in 3:7 EC:EMC NMC532/NG cell cycled to 4.1V, and a replica cell made according to the electrolyte composition determined through *ex situ* tests on the same cell.

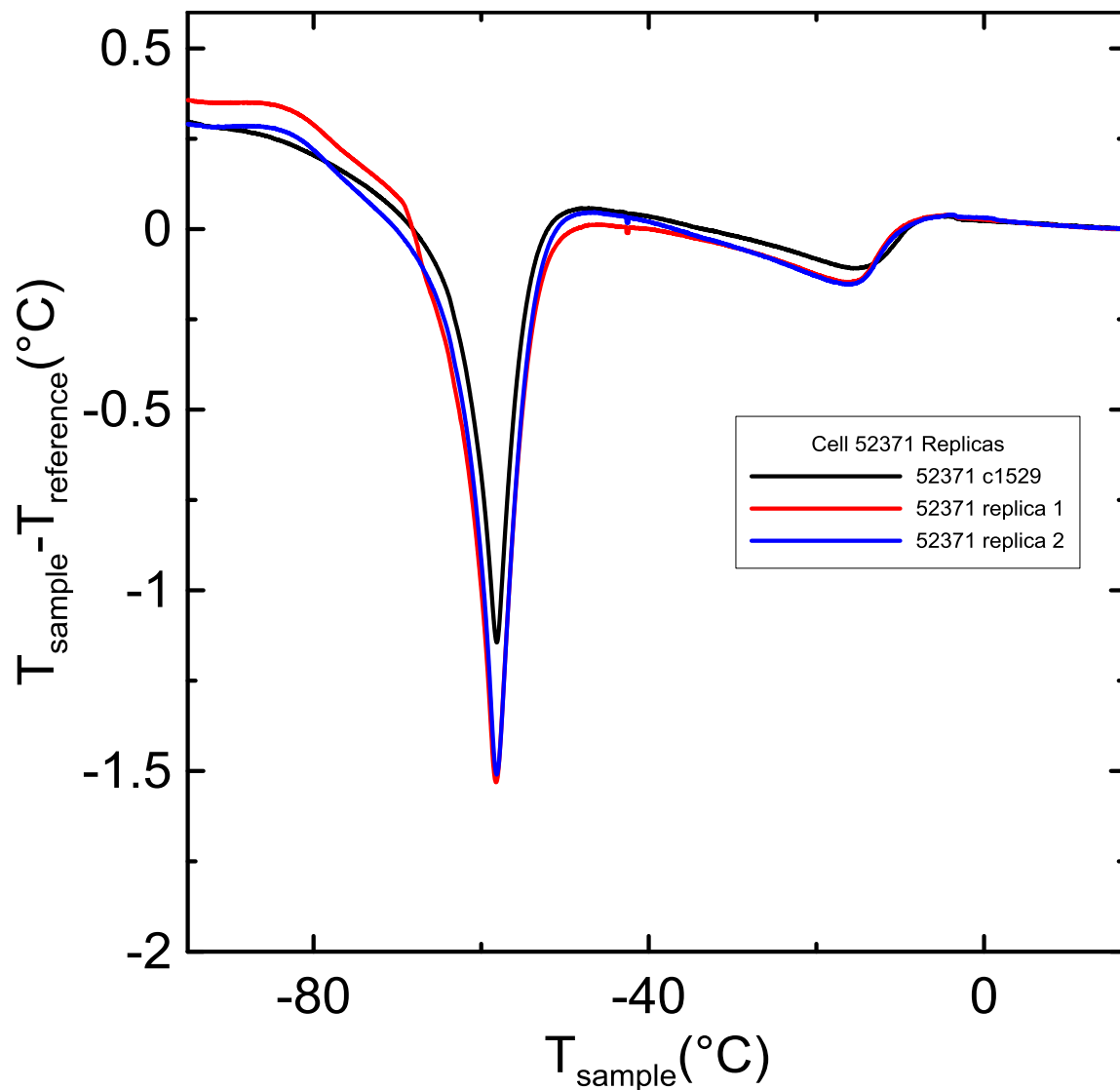


Figure 5.16: A comparison of the DTA data generate by the last test of cell 52371, a 1.0 M  $\text{LiPF}_6$  in 3:7 EC:EMC NMC532/NG cell cycled to 4.2V, and a replica cell made according to the electrolyte composition determined through *ex situ* tests on the same cell.

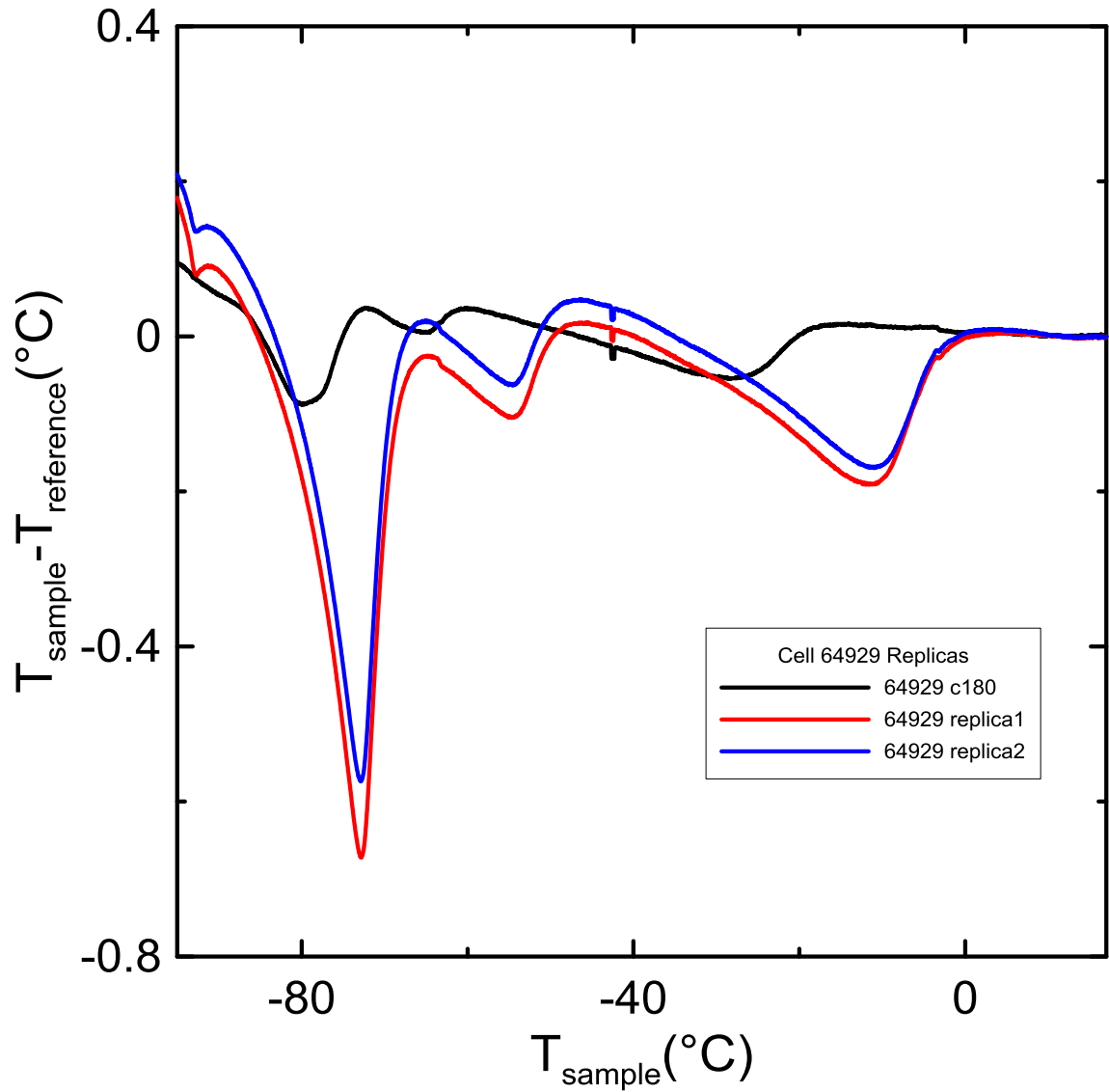


Figure 5.17: A comparison of the DTA data generate by the last test of cell 64929, a 1.0 M  $\text{LiPF}_6$  in 3:7 EC:EMC NMC532/NG cell cycled to 4.5V, and a replica cell made according to the electrolyte composition determined through *ex situ* tests on the same cell.

## Chapter 6: Results and Discussion

### 6.1 Comparison of Primary Test to EC:EMC DTA

Prior to the work done in this thesis, there was an effort to characterize areas of interest in the EC:EMC space. This work was carried out by Ryan Day, Sarah Hyatt, and Asher Wright. This work will be used to study the finer details of the salt loss in the main experiment.

First, it is assumed that the transesterification products, if there are only a few percent of them, will not significantly affect the DTA curve. This can be assumed due to the small effect on the melting point of the bulk solvent by a second material present in concentrations of a few percent, as shown in section 2.1.1. Then, the EC:EMC ratio can be reconstructed, ignoring the transesterification products. This assumption will allow for the comparison to electrolytes of just EC and EMC, as shown in Table 6.1.

VC Cells	Voltage	Li (M)	%EMC	%DEC	%DMC	%EC	%EC: Linear Carbonate
52367	4.1 V	0.70	60.01	4.224	3.399	29.07	30.1
52371	4.2 V	0.42	62.11	1.96	2.47	26.8	28.7
52373	4.3 V	0.92	55.71	7.008	5.24	30	30.6
52375	4.3 V	0.42	62.41	3.03	3	30.288	30.7
PES Cells	Voltage	Li (M)	%EMC	%DEC	%DMC	%EC	%EC: Linear Carbonate
52386	4.1 V	1.24	59.77	4.81	3.68	28.72	29.6
52390	4.2 V	1.12	58.98	3.595	2.89	31.56	32.5
52393	4.3 V	1.13	61.7	2.952	1.969	32.1	32.5
52398	4.4 V	0.88	59.16	5.04	3.75	29.3	30.1

Table 6.1: A comparison of the EC:EMC ratios of the opened cells, in terms of lost EMC content. The Voltage column describes the upper cutoff voltages of the cells, the Li (M) column described the extracted lithium molarity, and the %EC: Linear Carbonate column describes the percent ratio of EC to the linear carbonates DEC, DMC, and EMC.

The “% EC Corrected” column shows the percent of remaining EC in terms of the ratio of EC to EMC, DEC, and DMC, ignoring other transesterification products. Thus, cells studied before death show an increase in EC ratio less than three percent in PES-211D cells, and one percent in VC cells. This can be compared to work done by Asher Wright in the characterization of the changes undertaken by a cell upon  $\text{LiPF}_6$  or EMC consumption as in Figures 6.1 and 6.2, respectively.

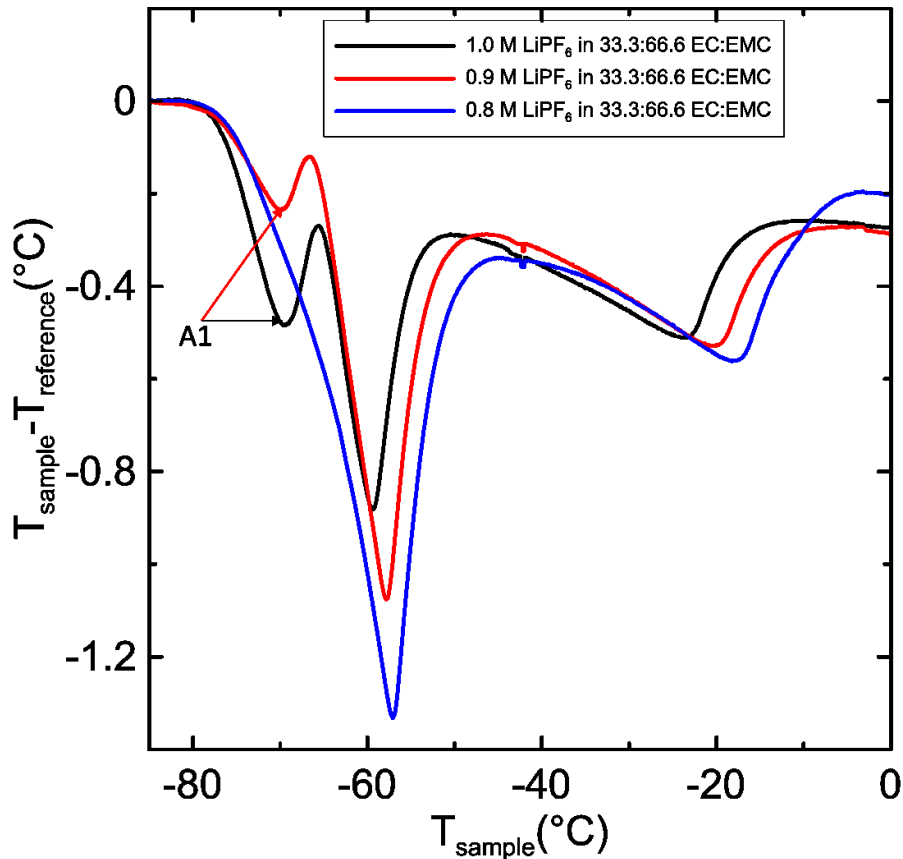


Figure 6.1: DTA data collected on cells with a 33.3:66.6 ratio of EC:EMC and variable amounts of  $\text{LiPF}_6$ . This data represents the effects of salt consumption on the DTA curve of a cell that has undergone minor EMC consumption.

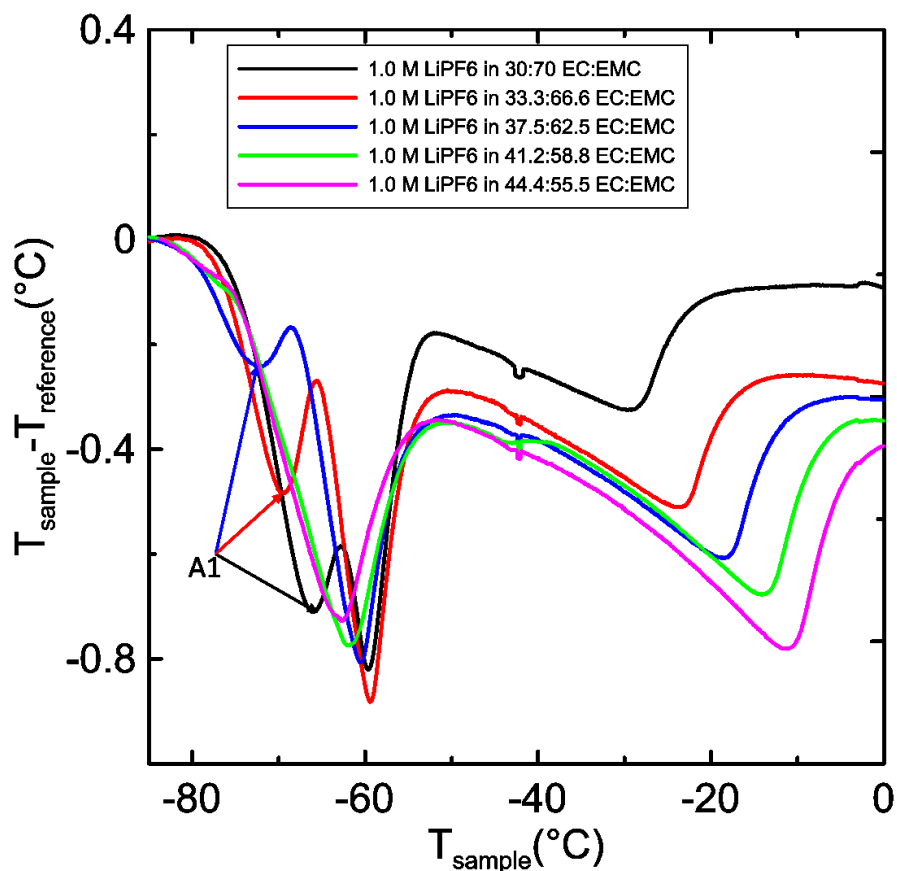


Figure 6.2: DTA data collected on cells with 1.0 M LiPF<sub>6</sub> in EC:EMC cells with variable amounts of EC. This data represents the effects of EMC consumption on a 1.0M EC:EMC solution that starts at 30:70 EC:EMC ratio.

Figures 6.1 and 6.2 show the difficulty in studying the effects of cycling on EC:EMC cells; reduction of LiPF<sub>6</sub> concentration has several similar effects to the consumption of EMC. This is not surprising, as the addition of a salt to a solvent will cause melting point depression similar to the depression caused by the addition of a solvent with a low melting point, such as EMC.

Of note is the minor feature A1. Figure 6.1 shows that this feature disappears with decreasing salt content, but Figure 6.2 shows that it also disappears with decreasing EMC content. However, as in Figure 6.2, the feature does not disappear due to EMC consumption until the EC:EMC ratio reaches 1.4:2. As this ratio is equivalent to 41:59

EC:EMC, and this ratio is far outside those shown by the confirmed *ex situ* data for VC cells which showed disappearance of the A1 feature, it can be assumed that the reduction in size of this peak in the experiments on Li-ion cells is due to the loss of salt. This is further reinforced by the difference observed between VC and PES-211D cells; VC cells saw this peak reduced, while PES-211D cells saw it less affected. While neither showed EMC consumption to that degree, VC cells showed more salt consumption. However, the behaviour of this peak was observed to be less predictable than that of the liquidus feature, and so it was not considered useful.

However, while Figure 6.1 displays similar behaviour to the DTA trends shown in the primary experiment, Figure 6.2 shows that the EMC consumption would cause the liquidus peak to grow, not just shift in temperature. As this was not found in the primary experiment, it can be solidly assumed that the changes observed are due to salt consumption. However, there is some deviation from the 3:7 EC:EMC ratio. Thus, as a solvent composition shift from 30:70 to 33:66 EC:EMC ratio is associated with a liquidus temperature increase of 5.7°C, there should be a 2-3°C change due to ~2% EC:Linear carbonate ratio change in cycled cells. Taking a rough approximation of the average ratio change in VC and PES cells, liquidus errors of 1.5°C on VC cells, 4°C on PES cells can be assumed.

As the EMC consumption rate is rather minor, the most important factor in the movement of the liquidus is the consumption of LiPF<sub>6</sub>. The X M LiPF<sub>6</sub> 3:7 EC:EMC system was explored by Ryan Day, using DSC. Figure 6.3 shows the liquidus vs molarity data for this system. This graph shows that, given negligible change in the EC:EMC ratio,



the change in liquidus point is linearly related to the change in molarity of the electrolyte, in the 0 to 1 M region.

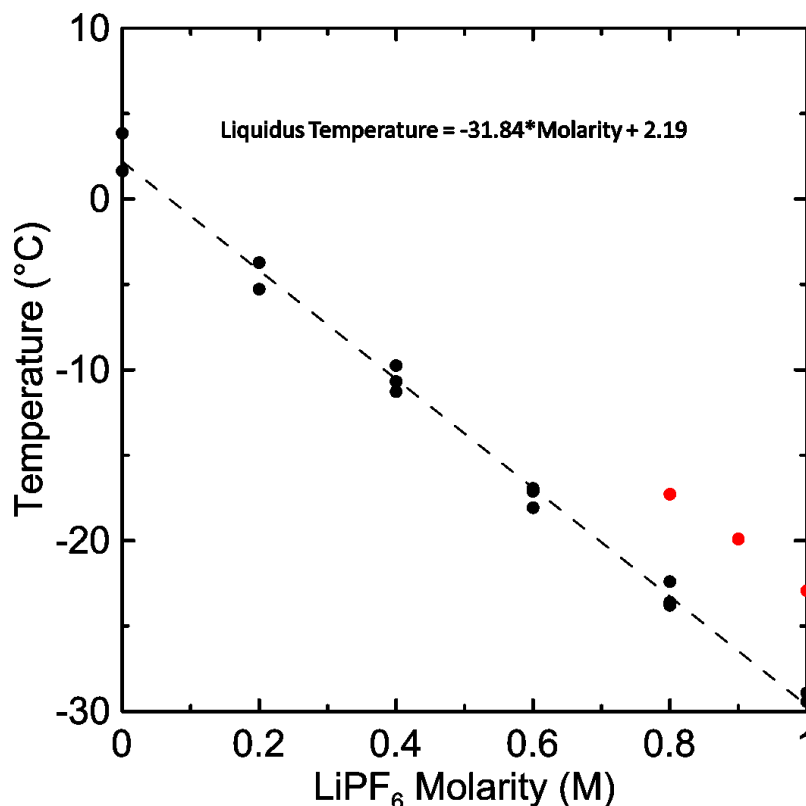


Figure 6.3: The relationship between decreasing LiPF<sub>6</sub> molarity and the liquidus temperature for the 3:7 EC:EMC LiPF<sub>6</sub> electrolyte, as determined by Ryan Day. The red points indicate the liquidus temperatures measured from the DTA curves in Figure 6.1, representing the effects of minor EMC consumption.

## 6.2 Liquidus Point Movement versus Cycle Life

As in section 2.1.5, the peak locations of a DTA curve can be extracted. If these peaks can be associated with any specific component of the electrolyte system, long term trends in the cell's degradation can be described by comparison of DTA curves. In this section, the location of the liquidus point has been signaled out as being an important measure as to the remaining concentration of salt. Figure 6.4 shows the liquidus temperatures of the cells shown in section 5.5.1. There are several aspects of note in this

diagram; first is the uniformity of the data collected on PES-211D cells. This lack of variation in voltage shows that, for PES-211D, the salt content of the electrolyte is not strongly related to the cycling voltage of the cell. Second, the separation between the VC and PES-211D cell data shows that the VC containing cell series has less salt in its electrolyte. This would suggest that cells with VC additive consume more salt in formation, or early cycling.

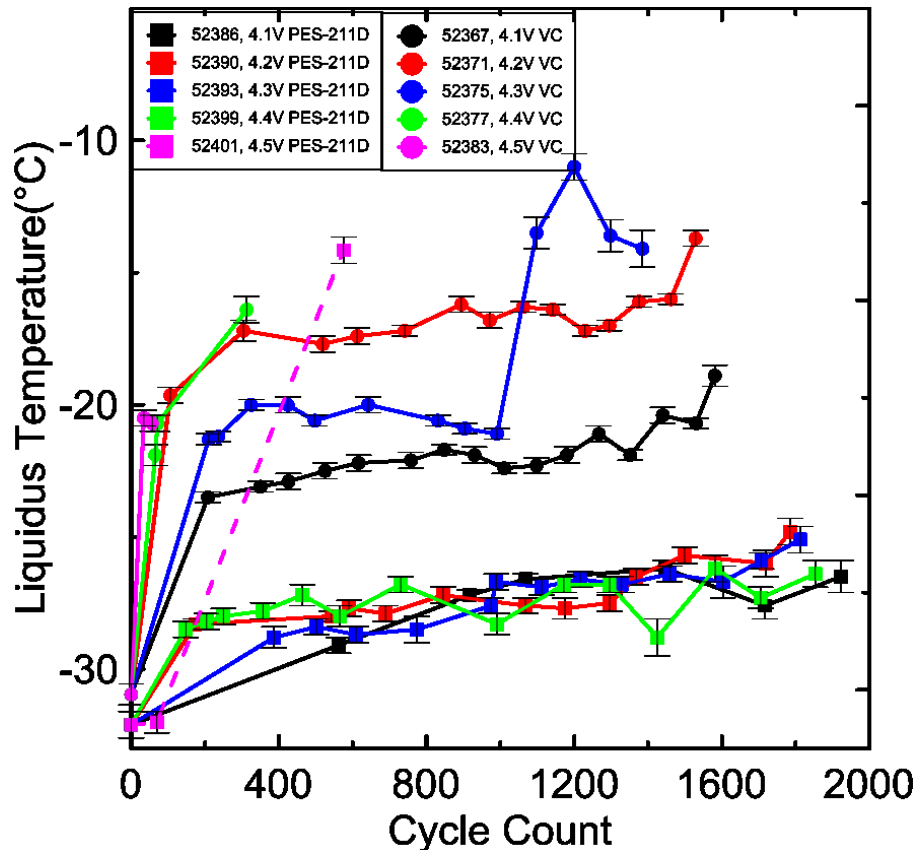


Figure 6.4: Liquidus points versus cycle count for a selection of the cells in the primary test, in shown in section 5.5.1. The error bars arise from an *ad hoc* estimation of the ability of the intersection line method to determine the liquidus point, not of the curve's ability to measure the liquidus temperature of the electrolyte.

Figure 6.4 shows that additives can be ranked in performance and understood in their mechanisms using DTA testing. PES-211D is a better additive set than VC, and this can be shown in-situ by the movement of the liquidus point in terms of cycle lifetime. As

the VC curves show significantly more movement in the liquidus point, it can be concluded that PES-211D prevents salt consumption that occurs throughout the cycle life of the VC cell. Further, as the liquidus points of the PES-211D cells do not move significantly throughout cell lifetime, the EMC consumption observed by ex-situ tests likely occurs at the beginning of cycling. This is also likely to take place in the VC cells, though less clear; the liquidus movement in these cells is due to  $\text{LiPF}_6$  consumption.

As in Tables 5.3 and 5.4, the cells in the primary study did not undergo significant loss of EC, and the ratio of EC to EMC remained relatively stable. Thus, the data shown in Figure 6.4 can be recontextualized to show an approximation of the salt lost over the course of cycling. This comparison is shown in Figure 6.5. Note that each value has an associated error, of 0.12M for PES-211D cells, and 0.48M for 2VC cells, due to the deviation from the ideal 3:7 EC:EMC ratio.

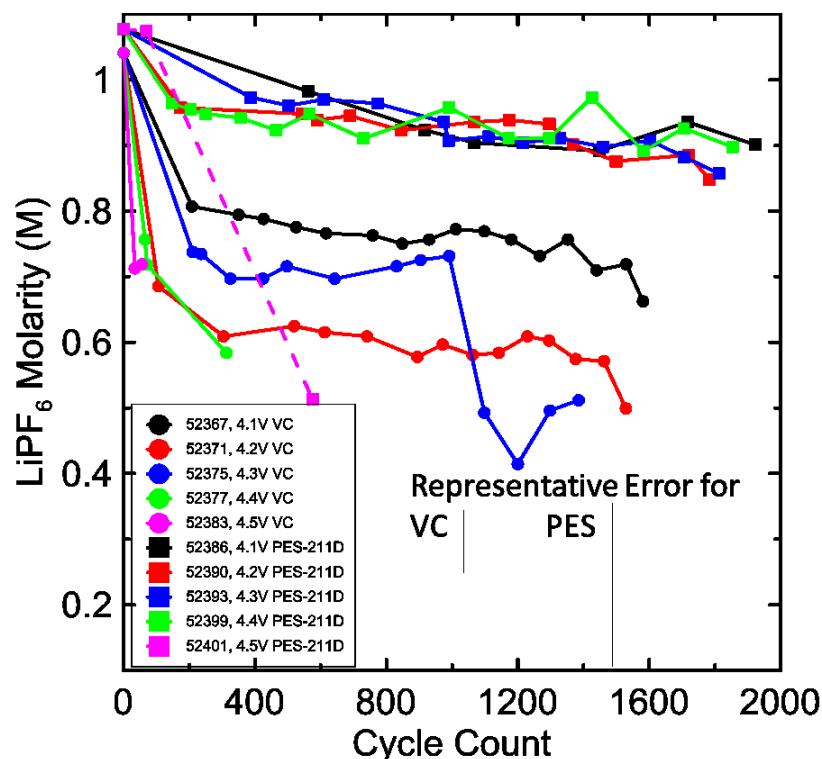


Figure 6.5: Approximate LiPF<sub>6</sub> molarity, calculated by neglecting the influence of EMC loss on the measured liquidus temperature. PES-211D values have an uncertainty of 0.12 M, while VC cells have an error of 0.048 M, as in the representative error bars.

This shows that DTA can be used to test the salt content of the electrolyte *in situ* for the duration of the cell's lifetime. However, this simple model only holds for relatively constant EC:EMC ratios. Salt concentrations in high voltage cells are overestimated. As well, cells that are tested at extremely low capacity are overestimated in Li concentration. Both are due to the occurrence of EMC consumption, which has driven the liquidus temperature off the line expected by the constant ratio assumption. However, as most commercial applications are interested almost exclusively in the performance of cells in the 100-80% capacity range, and the voltages that cause problems are already too high for long cycle lifetimes, the linear molarity-liquidus model is valid.

As mentioned in Chapter 5, there were forty cells created in this series. While one cell of each type was chosen for regular testing, the other cells also underwent DTA testing,

to varying degrees of regularity. Thus, the molarity data from these cells can be extracted, and overlaid on Figure 6.5, as in Figure 6.6.

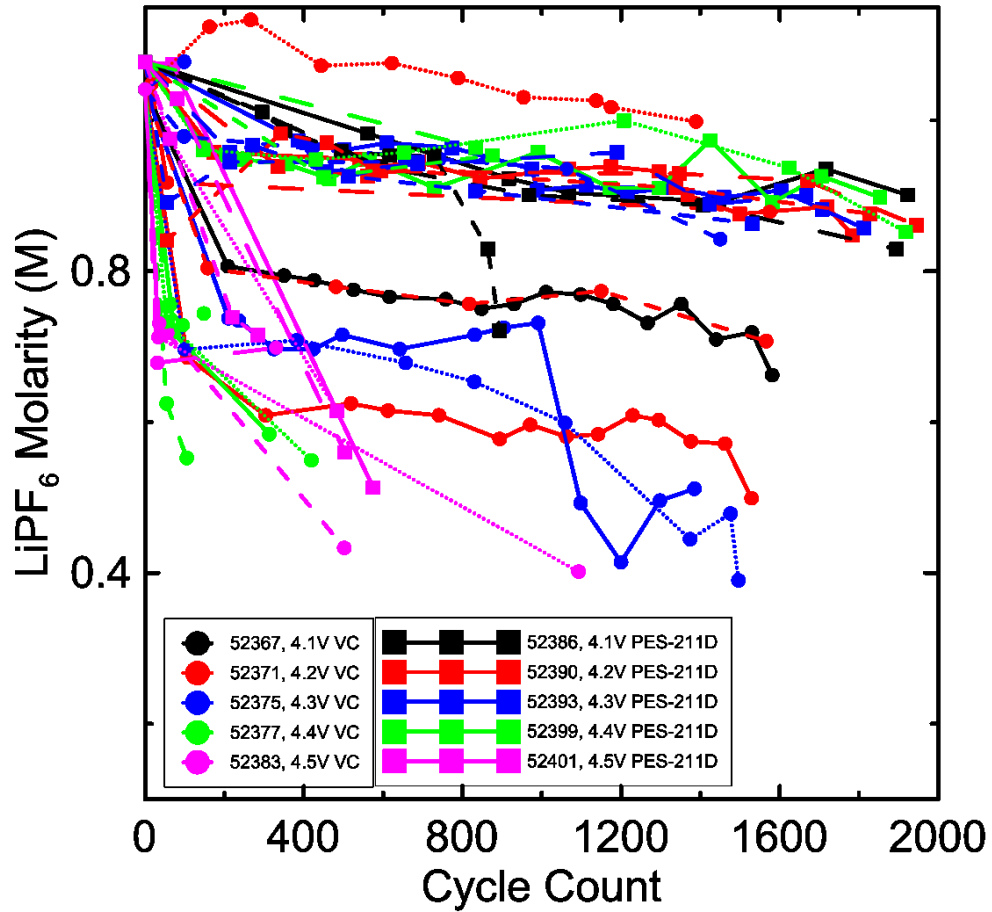


Figure 6.6: The molarity-cycle count data for the less regularly tested cells overlaid against the data shown in Figure 6.5. Dashes of different lengths are used to differentiate between molarity data from like cells.

Solid lines denote cells tested regularly, while dashes of varying lengths have been used to differentiate between the less tested cells. Here, we see that the PES-211D cells show consistent behaviour, regularly consuming little salt, while the VC cells show much more variation in salt consumption. This is particularly clear for the four 4.2 VC cells, where some cells lost little salt and some lost about 0.5 M of salt. This makes little sense,

as experiments should be repeatable. A careful view of the DTA curves for the 4.2 V VC DTA cells (not shown here) shows the following:

1. The DTA curves of cells near cycle 150 for the four 4.2 V cells are not the same. In particular, the solidus features are very different.

2. One cell, given by the red circles in Figure 6.6, shows an increase in apparent salt content compared to cycle 1.

Neither of these observations make sense. As such, they cast into doubt the quality of the VC cells shown in the thesis.

The author of this thesis made the VC cells near the beginning of his tenure in the laboratory. At that time, the author of the thesis did not record the pre and post filling cell weights, or the weights of the cells underwater after filling. It is therefore impossible to be sure that all cells had the same amount of electrolyte added and that a substantial fraction of EC was not pumped away during vacuum sealing in some cells. Such a variation in the initial electrolyte composition could explain the results for the 4.2 V cells in Figure 6.6.

The simple method of determining salt molarity based on liquidus position used here assumes that the initial EC:EMC ratio is the same for all cells during cycling. This may not be the case for the 2% VC cells, but incomplete records mean that there is no way to check this. It is clear that these experiments must be repeated in future in order to gain confidence. Another important learning experience is that the DTA curve of every cell destined for long term testing should be measured immediately after formation to ensure all cells are showing the same initial DTA curve.

### 6.3 Electrolyte Changes in an Improved Cell Chemistry

While the bulk of chapters 5 and 6 have been concerned with cells made during this thesis by the author, many more cells were tested concurrently that were made by others in the same lab. This section details results obtained from one such cell series. This series, cells 63397, 63399, 63401, 63403, 63404, and 63405, were constructed and otherwise tested by Will Stone as part of an unrelated experiment but were deemed valuable for DTA testing. They are all single crystal NMC532 cells, cycled at 55°C, to an endpoint of approximately 700 cycles, using a cycling protocol similar to that used for the cells in the primary and secondary tests, with the same cycle rate and protocol, with upper cutoff voltages between 4.0 and 4.4 V. These cells are quite different from the cells used in the primary and secondary tests, as they use a different positive electrode material, natural instead of artificial graphite, 1.2 M LiPF<sub>6</sub> as opposed to 1.0 M LiPF<sub>6</sub>, and a different additive blend, 2% fluoroethylene carbonate (FEC) + 1% DTD. These cells are, effectively, a more advanced form of the cells used in the primary experiment, as they have better electrodes, additives, and coating, but the same basic salt, solvent, and electrode materials.

The cycling and DTA data from these cells are summarized in Figure 6.7 and Figure 6.8, respectively. As shown in Figure 6.7, these cells are much better than the NMC532 cells used in the primary tests, in terms of cycle lifetime. This is due to the single crystal NMC532 positive electrode being a significant improvement on the standard NMC532 material. As the left panel of Figure 6.8 shows, these cells do not show significant liquidus movement, suggesting little to no salt consumption. However, the right panel shows significant movement in the solidus features at higher voltages. This suggests that this

improved cell chemistry shows little electrolyte salt consumption, but still shows transesterification or parasitic reactions at elevated voltage.

As the electrolyte used in these cells is  $\text{LiPF}_6$  in EC:EMC 3:7, the same liquidus-molarity conversion can be applied here as with the cells in the primary experiment. While these cells were tested at only one point in their cycle life, we can determine the amount of salt lost. These cells have an average molarity of  $1.127 \pm 0.036$  M, while the fresh cell has a molarity of 1.143 M. There may be a very slight linear trend between molarity and cell voltage, but the differences between the determined molarities are smaller than the error. This shows that the salt loss in these cells is so small as to be negligible, in comparison to the state of the salt content of the cells in the primary experiment.

As with the cells in the primary experiment, these cells do not show significant EMC consumption with respect to time. In general, the DTA data of these cells is very similar across the board. The only real difference is in the positive peaks at low temperatures. These show a consistent difference in form between cells at voltages above and below 4.3 V. What this means is not known, but it may point to a more meaningful cause to these peaks.



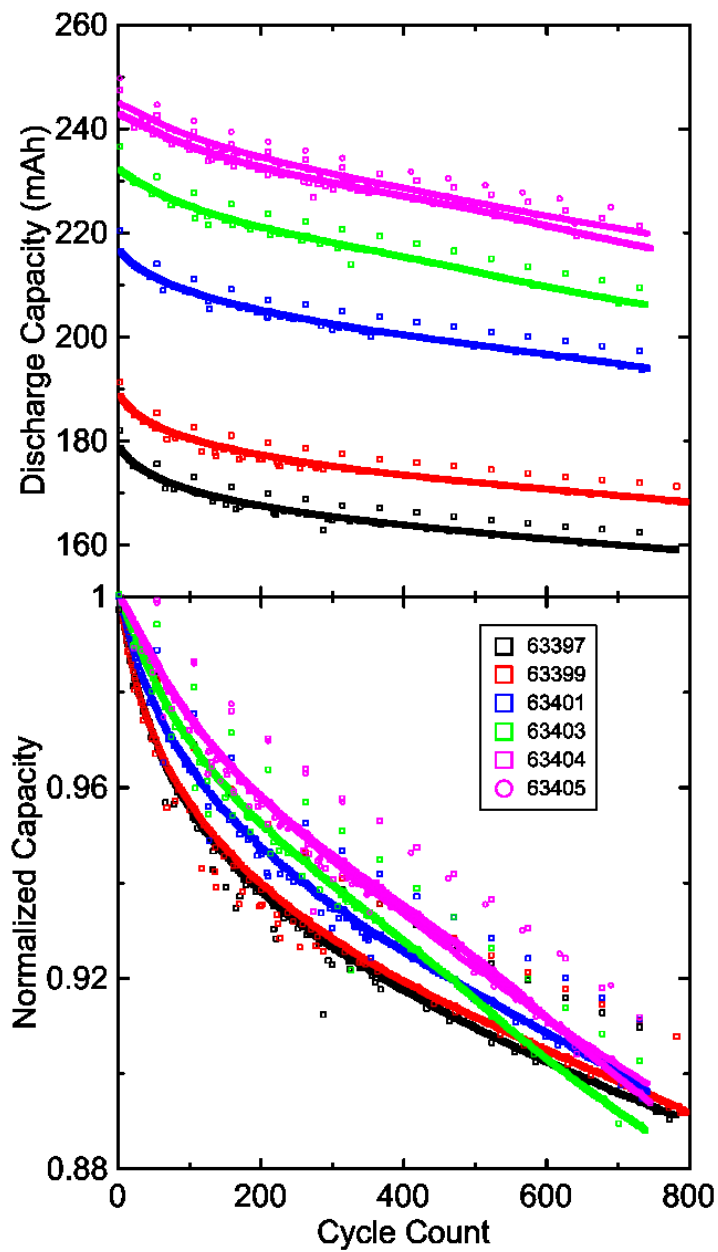


Figure 6.7: Cycling data for cells 63397, 63399, 63401, 63403, 63404, 63405. The upper figure shows absolute capacity, while the lower figure shows normalized capacity over time.

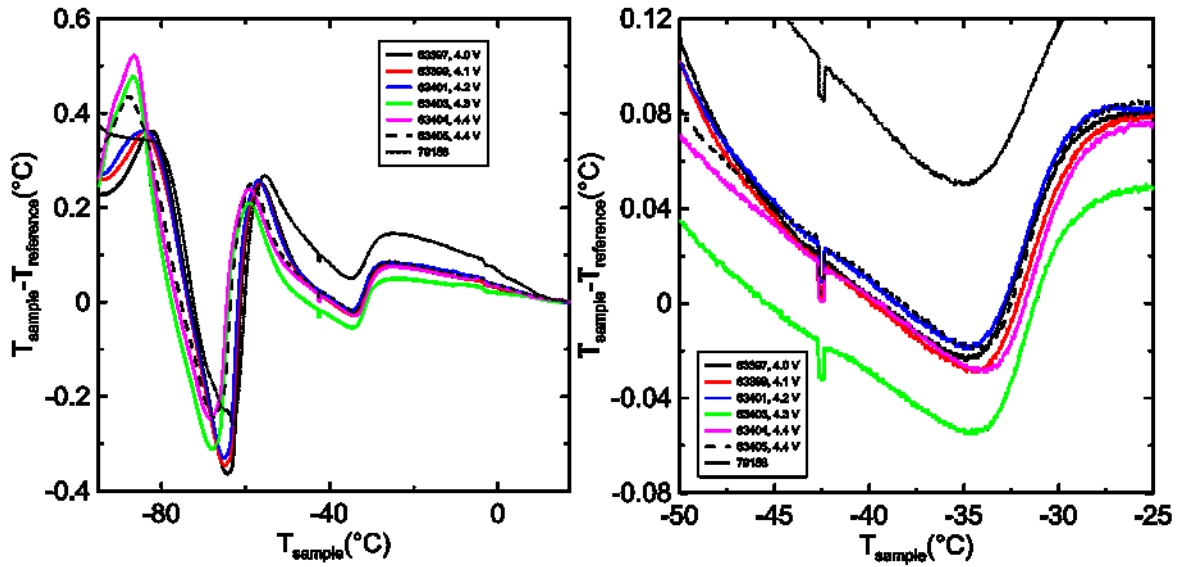


Figure 6.8: DTA data for cells 63397, 63399, 63401, 63403, 63404, and 63405. The left panel shows the DTA data from all the cells, while the right panel shows a closeup of the liquidus feature.

## Chapter 7: Conclusion

### 7.1 Conclusions

Li-ion cells can be developed for a wide variety of applications and uses. This wide variety of uses necessitates a wide variety of Li-ion cell configurations, including many complex electrolyte chemistries. Conventional testing of these electrolytes is laborious, and often destructive to the cell. Li-ion DTA can be used to test Li-ion cell electrolytes *in situ*, with no damage to the cell's performance or overall health. Further, as has been shown in this thesis, DTA can be used to probe the degradation mechanisms at work during long term, high temperature cycling.

Several important conclusions can be taken from the results of this work. It has been found that even small changes in the electrolyte can be associated with significant loss of cell performance. As well, it has been found that, in the cells tested here, there are only very minor changes to the amount of liquid in the cell's electrolyte; though there are certainly parasitic reactions occurring, the liquid electrolyte mass is roughly conserved through most of the cell's life.

It has also been found that electrolytes in identical cells containing VC and PES-211D additives will follow distinct electrolyte degradation pathways. While this can be found using GC-MS, this determination shows that DTA can be used to study these pathways without destruction of the cells. This validates one of the more important questions of the method; whether it can be used to study differences in electrolyte degradation caused just by different additives. This will allow the method to be used to directly study the ways additives affect cell degradation and help advance the understanding of Li-ion additives in general.

The exception to this is the cell's behaviour near death. When a cell, especially a high voltage cell, is near death, it is prone to rapid degradation in cycling capacity; a cell is more likely to decrease in performance rapidly after a period of slow degradation, than to degrade down to zero capacity in a consistent manner. Though the exact mechanisms of this rapid degradation were not explored, it has been correlated to a rapid change in electrolyte over the same span of time.

Finally, it has been shown that DTA can be used to determine the remaining Li content of cycled cells *in situ*, using a simple linear relationship between the liquidus point of the DTA curve, and the molarity of the electrolyte. This simple model performs well over the majority of the cell's life, where the EC:EMC ratio is relatively constant, but fails at the end of the cell's life, where EMC consumption proceeds faster than EC consumption.

## **7.2 Future Work**

While the work outlined in this thesis was ongoing, there were several other projects undertaken that used the DTA apparatus to various degrees. While these projects are also ongoing, the work there has led to several prospective future projects. This section outlines several of these and describes what might be learned or obtained from their completion.

### **7.2.1 Development of Additional Phase Diagrams**

DTA requires robust phase diagrams so the result of a given test can be properly interpreted. Unfortunately, compositional phase diagrams are very labor intensive to develop. As of this writing, work is underway in the development of a phase diagram for EC:DMC:LiPF<sub>6</sub> using DTA, and while this is one of the most commonly used electrolyte

compositions, there are many more. These phase diagrams would allow for rapid analysis of the state of the electrolyte in any cell containing the same original electrolyte, provided the solvents do not change substantially by transesterification to other solvents not included in the phase diagram.

As this thesis shows, electrolyte in good Li-ion cells does not change significantly throughout cycling. Thus, though a full phase diagram would be of scholarly value, the practical Li-ion development process would be more interested in a very high resolution diagram, based around the region of the phase space through which an electrolyte degrades. Thus, to design a useful phase diagram, a series of cells would need to be studied via GC-MS, to determine how the EC:DMC ratio changes between the first and last cycle.

### **7.2.2 Observation of Dramatic Changes in the Electrolyte**

Over the course of this work, there have been several occasions where the capacity of a cell decreased sharply, and the state of the electrolyte changed dramatically, at the same time. Figure 7.1 shows an example of this change that occurred in cell 64928. Unfortunately, this event was not successfully observed. However, there are several important aspects of this change that can be noted.

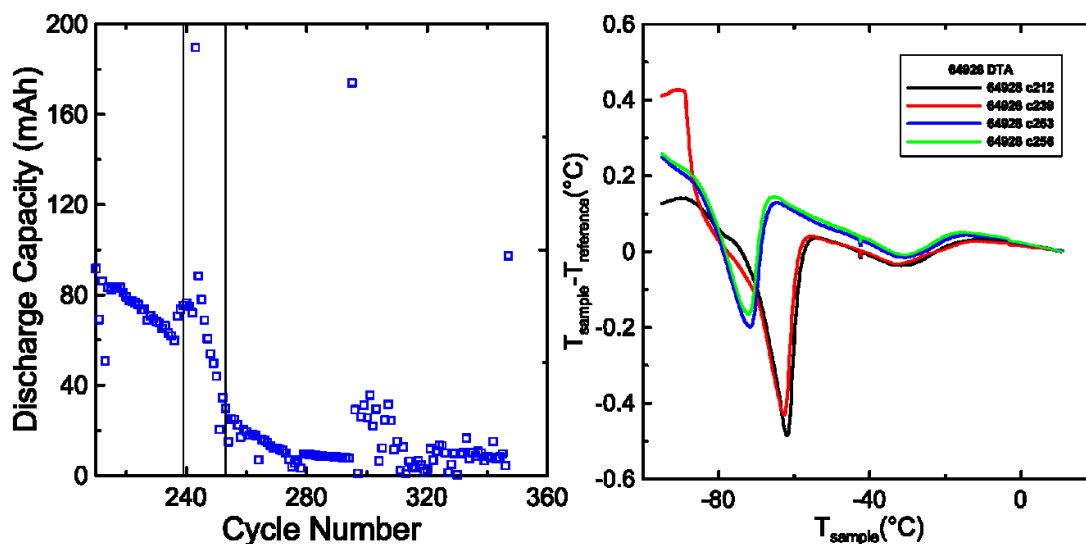


Figure 7.1: A closeup of the cycling data and the relevant DTA curves of cell 64928, a 4.5 V VC cell, when it went through rapid changes in electrolyte composition. The black lines on the cycling data graph indicate cycles 239 and 253, before and after the significant change in electrolyte state.

First, is that the breadth of the region over which the change occurs means that no determination of the order of the events can be made. That is, the causal relationship between the loss of capacity and the change in electrolyte, if there is one, cannot be studied. However, one hypothesis is that this is caused by transesterification induced by Li plating. Li plating is a process where active lithium, instead of intercalating into an electrode, deposits on the surface. As this layer is not passivated, lithium alkoxides are created, and transesterification proceeds. A number of further observations also back this up.

Second, in most cases, while the cells had very poor capacity at  $C/3$  cycling rate, they still displayed capacity at a  $C/20$  cycling rate, as indicated by the capacity data points above the main  $C/3$  data in Figure 7.1. This disparity indicates that cells that undergo this change still possess most of their capacity but have developed significant internal impedance. While it is possible that electrochemical impedance spectroscopy could be

used to study the source of the impedance, and whether it could be associated with the electrolyte or the electrodes, the cells shown here no longer exist.

Third, while the state of the electrolyte was observed before and after the change, no intermediate measurement was made. Thus, nothing is known about how the electrolyte changes from one curve to the other. The features are shown to both shrink and move, indicating both a change in composition as well as a possible loss of liquid state solvent. However, this could also indicate that the final state is one with a significantly lower enthalpy of fusion, as in section 7.2.10.

Fourth, as the event has never been directly observed, the speed at which the change occurs is not known. Cell 64928 was observed to change dramatically over the course of fourteen cycles. However, this still leaves a window of about fourteen hours where the electrolyte could have changed. This may seem like a short amount of time, but while the cell was cycling at C/3, it has lost significant capacity, and so each cycle lasts about one hour on average.

Fifth, the lack of change in the liquidus feature might indicate little consumption of lithium salt. As in Figure 7.1, these sorts of rapid changes in electrolyte often leave the liquidus unmoved, which indicates that the salt concentration was not decreased significantly. Thus, this is likely not a sudden increase in salt consuming parasitic reactions.

Sixth, there is significant change in behaviour in the solidus feature, both in location and size. This would indicate either some significantly increased rate of a parasitic reaction involving solvent, or some reaction, like transesterification changing the solvent into some other molecule.

Thus, it is likely that this change is brought on by a rapid increase in the rate of transesterification reactions. This would indicate some significant increase in the relative amount of lithium alkoxides, which might be related to the rapid loss of capacity. Some reaction using inventory  $\text{Li}^+$  like Li plating to create lithium alkoxides would explain most of the behaviour seen here.

In general, a better understanding of this phenomenon, if it could be obtained, could lead to a more complete understanding of the interactions between the electrolyte and cell. However, commercial interest in cells is generally limited to the 100-70% range of initial storage capacity of a cell's lifetime, and this phenomenon has been, almost exclusively, observed at >50% capacity.

### **7.2.3 Low Salt Tests**

The relationships between electrolyte salt molarity and Li-ion cell performance are not well known, beyond the ionic conductivity and viscosity of the electrolyte. To start, it has been shown that cells with lower salt molarity experience dramatic capacity loss earlier than identical cells with greater salt molarities. However, the observed change in salt concentration was relatively small in relation to the difference between the initial salt concentrations, as in Figure 7.2. Thus, this failure is not due to some critical lack of salt. Note that the terms “hold” and “OCV” in Figure 7.2 refer to protocols where a cell is brought up to the described voltage, and either held at that voltage, or allowed to self-discharge in open circuit conditions.



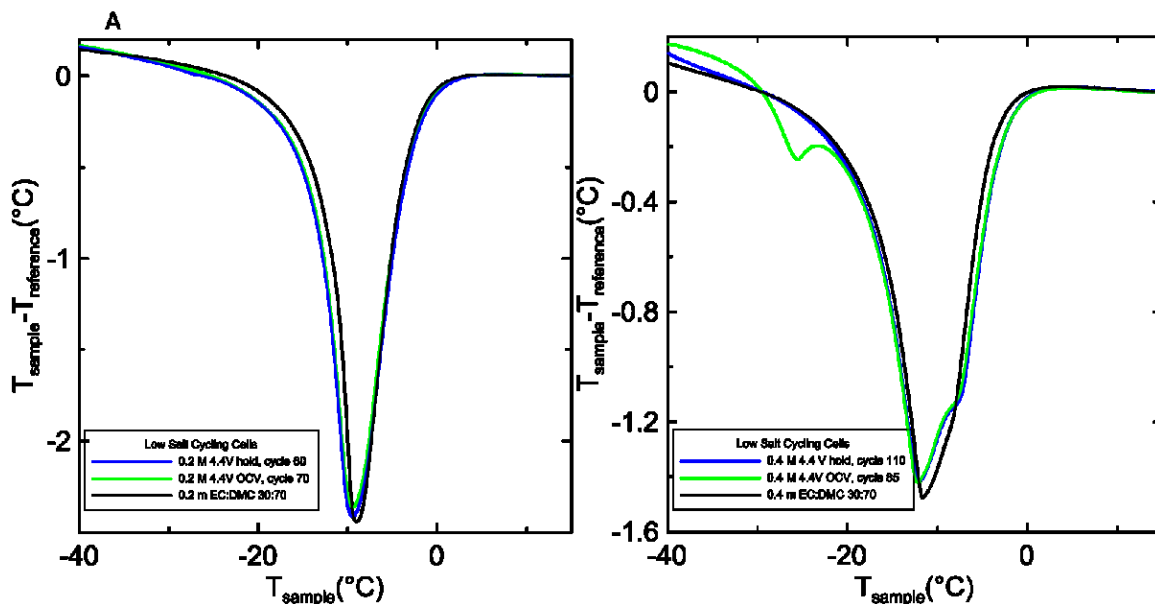


Figure 7.2: DTA curves of low salt tests. All cycled cells were taken off after they reached 80% of initial capacity. Note that, this significant loss of capacity is correlated with minimal change in the electrolyte.

As of this writing, several tests are being conducted on the effects of salt content on the function of li-ion cells. These tests are being conducted on 30:70 EC:DMC, with salt concentrations varying between 0.2 and 0.8 M  $\text{LiPF}_6$ . Thus far, DTA has been used to test the 0.2 and 0.4 M cells once they reached 80% of their initial capacity and were considered dead. Further work in this area will consist of tests on the rest of the cells once they reach death, and study of the remaining salt content, as determined by comparison to the EC:DMC  $\text{LiPF}_6$  phase diagram currently in construction. This project hopes to determine if there is a link between the behaviour of an Li-ion cell near its death and the salt content at that point and in the cell's history.

#### 7.2.4 Cylindrical Cell Performance Post DTA

It has been observed, as in Figure 7.3, that some heavily cycled cylindrical cells report a slight improvement in capacity and voltage hysteresis post DTA testing.

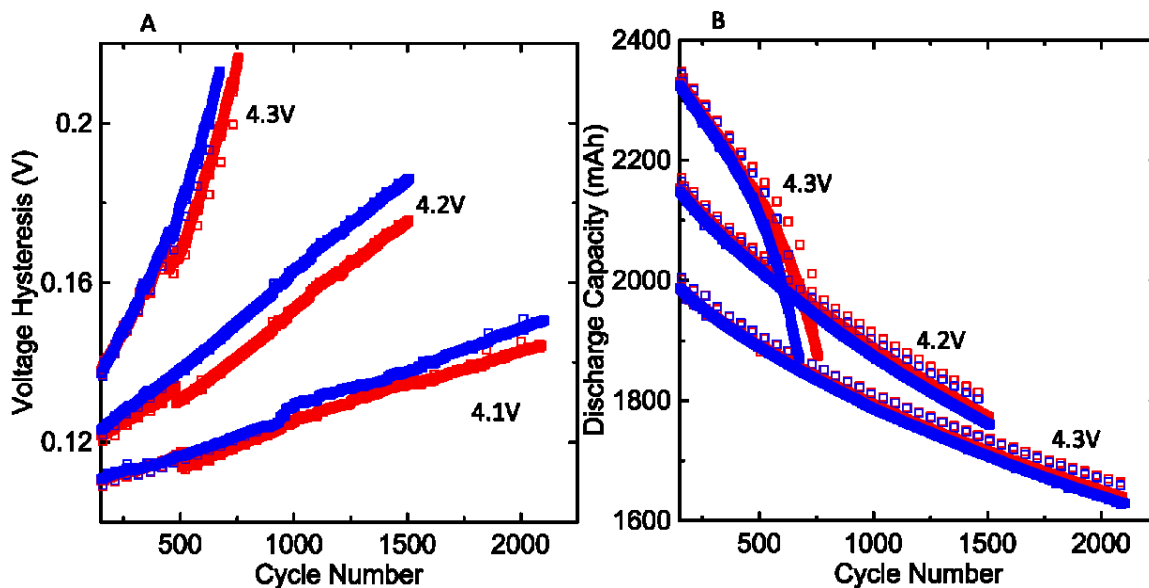


Figure 7.3: Cycling data from cylindrical cells that displayed slight improvement after DTA testing (red) at approximately 400 cycles, in comparison to cells that did not undergo testing (blue), both in voltage hysteresis (A) and in the discharge capacity(B), especially at high voltages.

This initial improvement was followed by long term improvement in lifetime, by 10%. No difference in behaviour was observed in cells that were tested with DTA while fresh and went on to long term cycling. The effect has also not been observed to occur twice in one cell, or at all, in the case of pouch cells. This fact leads to the hypothesis that the effect is related to some difference between the pouch and cylindrical cell form factors, or their treatment. The only non-scale differences between pouch and cylinder form factors are pressure and electrode winding. This then leads to the hypothesis that the effect could be related to internal cell pressure in some way.

Though this behaviour was of interest, it was not determined what could have caused it. The hypotheses considered as of this writing were, 1) that the contraction and expansion during freezing experienced by the electrolyte somehow damaged the SEI in such a way as to increase the reversible capacity of the cell and 2) that the decrease in

temperature might have affected solvation of pressurized gas products in the cell, changing its performance through modification of the electrolyte.

If this process were better understood, it might be optimized for a considerable increase in the cycling lifetime of Li-ion cells.

### **7.2.5 Exploration of Ternary Phase Diagrams**

While data on the phase diagrams of binary solvents in electrolytes system is very valuable, there are several chemistries of interest composed of three solvents and one salt. Two such chemistries are 70:5:25 DMC:EMC:EC, and 80:10:10 DMC:EC:EMC, both with LiPF<sub>6</sub>. While the corresponding solvent systems can be computed theoretically,<sup>57</sup> the solvent-salt systems must be investigated experimentally. Unfortunately, a full survey of the systems would be prohibitively time intensive. Direct study of the entire ternary solvent space would require several hundred cells, each requiring hours of DTA channel time. A more practical survey would be the investigation of the regions of the ternary space surrounding the chemistries in question. For example, if cells were to be made with solvent and salt concentrations within a few percent of the original composition at four concentrations for EMC, DMC, and LiPF<sub>6</sub> separated by 5% weight percent each, one could develop a reasonably robust partial phase diagram that could describe small changes in the electrolyte reasonably well. Such a project, assuming four data points in three degrees of freedom, would require only 64 cells. This would cut down on the time requirement, while producing a phase diagram that would be more practical for the study of these ternary systems, at the cost of the ability to look at the greater picture of the ternary space.

### **7.2.6 Additive Study**

One of the unexplored uses of DTA is the in-situ study of the effects of additives on formation. In this case, DTA could be used to study the effect of different additives on the electrolyte composition post-formation. If the base electrolyte were known, and phase diagrams for said electrolyte were developed, a formed cell could undergo a DTA test, and the resultant signal could be used to roughly determine the compounds removed from the electrolyte during the formation process. As the only change in formation is the creation of the SEI, this data would then grant information as to the composition of the SEI. This would be valuable, as the composition of the SEI is very difficult to study. This method could find a niche use in the early evaluation of the behaviour of additives in Li-ion cells, where the exact behaviour of an additive blend is not always well understood.

Further, DTA could be used to study the amount of additive required to modify the SEI. The ideal case for additives is to add as little as possible, so as to not disturb the properties of the bulk electrolyte. A comparison of DTA tests on cells with a range of concentrations of an additive could be used to determine how much additive must be used to prevent SEI formation from consuming bulk solvent.

### **7.2.7 Software Development**

MATLAB Software has been developed to that can take a set of given DTA files, in all currently used formats, and extract the data of interest, sort the resultant DTA curves by age, record said data in a separate file, and graph in a MATLAB exported image. Software is being developed that can determine the slopes, background subtracted signal, peak locations and feature areas with some user input. Of interest would be software that

could receive a set of data set against cycle lifetime, and determine changes in peak area, peak location, and peak features in a relatively automated manner. This could then be combined with phase diagram databases for rapid analysis of DTA curves.

Further work would be in peak fitting. While the solidus features of a DTA curve are generally not single Gaussians, they may be pseudo-Voight peaks, some other kind of standard curve, or a combination of multiple gaussians. If this is the case, a program could be developed that would take in a background subtracted DTA signal and, with some user assistance, determine the exact features of the peaks. This would make the signal analysis more robust. The liquidus peaks, on the other hand, are very asymmetric, and probably cannot be fit with any common type of curve.

### **7.2.8 Concentration Gradients and Room Temperature Cell Failure**

In some applications, Li-ion cells must be charged, discharged, and recharged rapidly. In these cases, the lithium cell is rapidly intercalating and deintercalating lithium at the electrodes. If the electrolyte is not given time to equilibrate, the cell can generate a concentration gradient of  $\text{Li}^+$  across the electrolyte. If the cell has a high relative amount of a high freezing point solvent, this gradient may generate small areas where the electrolyte has a liquidus temperature at or near room temperature. As discussed in section 4.1, this would lead to a rapid drop in ionic conductivity, and thus a drop-off in cell performance. This situation would be of interest to DTA, as studies could be made to determine how concentrated common electrolytes must become before room temperature failure becomes a present issue. From this, charging procedures and cell chemistries could be developed that would prevent these concentrations from arising.

## 7.2.9 Heat Capacity/Background Slope

It has been assumed, in previous work, that the background of a DTA curve was linear, and its slope irrelevant. However, some recent tests have shown systematic relationships between electrolyte degradation and an increase in the slope of the background.

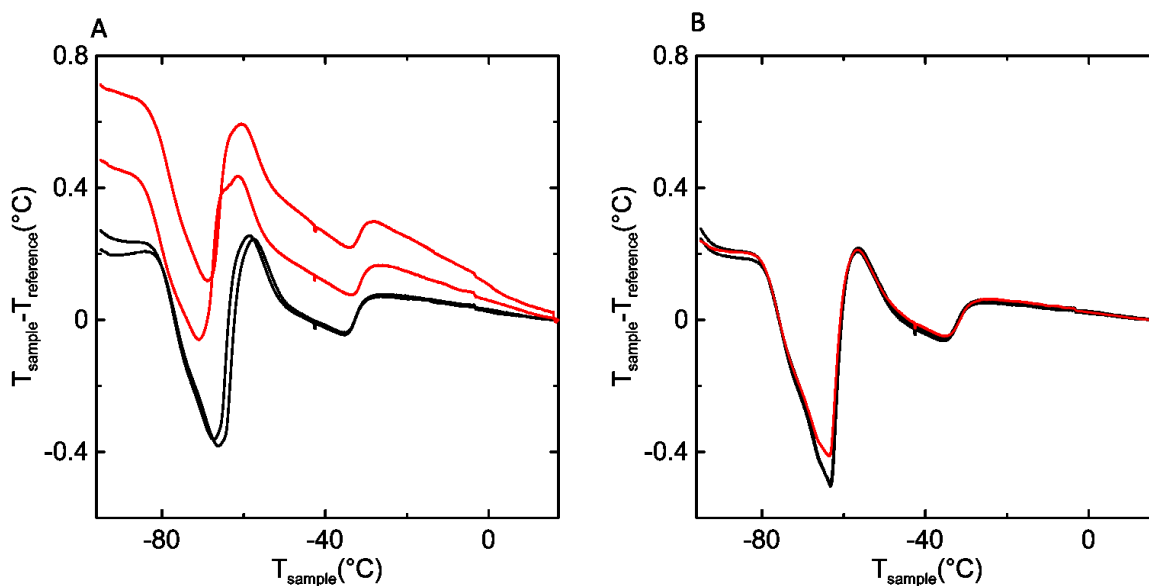


Figure 7.4: A comparison of the background slopes observed in cells with different chemistries. The black curves show DTA data for cells after three months of cycling, where the red curves are cells of the same chemistry after six months. The cells in A and B have different additives and electrode chemistries, but identical cycling procedures and conditions.

As shown in Figure 7.4, this relationship is consistent. Some cells start with lower background slopes that gradually increase over the course of months of testing, while cells with other chemistries do not change in the same way. As this behaviour has been observed to be systematic, it should be related to some deeper metric of cell degradation. If this were understood, it could be used to study the degradation of a cell.

Determining what this process may be is not simple, but hypotheses can be made. From the data in Figure 7.4, it has been observed that sample cells with degraded electrolyte start a DTA heating curve at a higher temperature than the reference, and end with temperatures much lower than the reference. This relationship would seem to represent a situation where the sample cell has a larger heat capacity than the reference. However, tests have been done on cells with different amounts of electrolyte, which do not show this background behaviour.

### **7.2.10 Enthalpy of Fusion vs Composition**

Though the integral of the DTA curve is thought to represent the latent heat of the associated phase transition, the sizes of the peaks have been found to change in unexpected ways, in relation to the composition of the electrolyte. This has been especially apparent in high salt concentration systems, where the area of the peak shrinks dramatically at high salt concentrations, before growing at even higher concentrations. This behaviour has serious implications toward the use of DTA for testing the amount of electrolyte remaining in a cell; if the area of the peak changes with composition as well as with the amount of electrolyte remaining, analysis becomes considerably more difficult. Figure 7.5 shows this trend. The curves in this figure represent cells with the same base electrolyte and different amounts of salt, but the phase transitions involve very different enthalpies of fusion. Further, these enthalpies shrink towards 1.4 m LiPF<sub>6</sub>, and then grow towards 1.8 m.

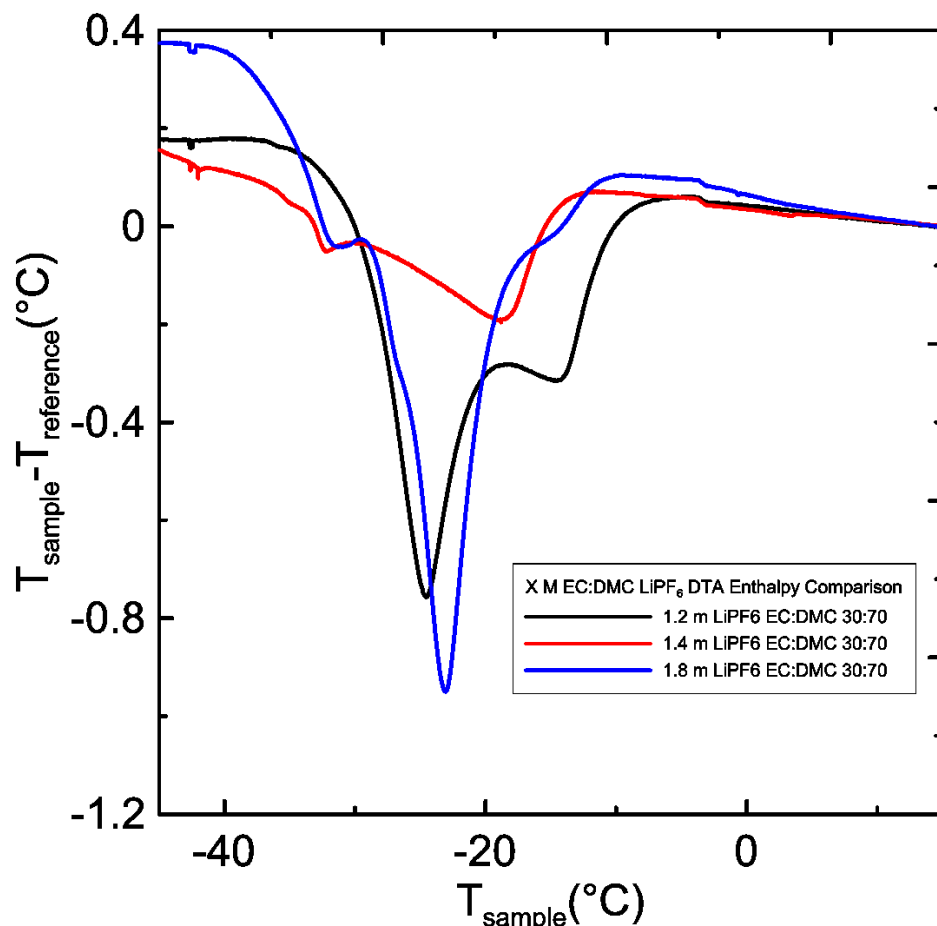


Figure 7.5: A comparison of the DTA curves of three cells with different salt concentrations and identical solvent compositions. Note the significant changes in area, indicating significant changes in enthalpy of fusion.

The trend shown in Figure 7.5 is not the only example of this sort of area change behaviour, simply one of the more dramatic examples. This region of inquiry is new and will require significant work to determine the underlying behaviour. This would likely be studied alongside the broader composition matrices.

### 7.2.11 Finer Study of Post-Eutectic Regions

Recently, work has been published on the phase diagrams of high salt content electrolytes.<sup>61,62</sup> Han *et al.* and Seo *et al.* show phase diagrams for high salt concentration systems determined by DSC, as well as physical models for the behaviour. These models



rely on the existence of multiple configurations of solvent and salt molecules which then give rise to multiple phases.

DTA has not been shown to do a good job of resolving features in the high salt concentration region, both due to the complexity of phase transition behaviour at those ranges, and the elevated phase transition temperatures of the high salt concentration solutions being difficult to reach with the DTA apparatus. However, an adaptation of this work, using DSC, applied to very high salt concentration LiPF<sub>6</sub>:DMC, or LiPF<sub>6</sub>:DMC:EC could be used to better understand the DTA data at those regions. As a final note, Han *et al.* and Seo *et al.* only study interactions between single salts and single solvents; they do not have data for the effects of salt concentration in a binary solvent system, which is of interest to DTA.

#### **7.2.12 Extended Tests of Binary Phase Diagrams**

While DTA can be used to create compositional phase diagrams, another way to create phase diagrams is by DSC. DSC does not require creation of Li-ion cells, is faster, uses significantly less electrolyte – samples on the order of milligrams vs a full gram – and is developed specifically for the testing of fresh electrolytes. This is in opposition to DTA, which is a more specialized tool for testing degraded cells. Thus, work is being done to generate phase diagrams via DSC for use by DTA. As of this writing, a DMC:EC:LiPF<sub>6</sub> phase diagram is being developed. If this diagram can be shown to be identical to the diagram generated by DTA, finer study can be taken in the regions of interest. For example, as this work has shown that relatively minor changes to the DTA curve can be correlated to significant cell performance degradation, DSC could be used to perform very

fine studies, on the order of differences of 1-2%, in the region of common electrolyte compositions.

Further, while the tests presented here have only used  $\text{LiPF}_6$ , there are other salts in use in this lab, and more in use outside of it. It has previously been assumed that the salt-solvent interaction was independent of the anion contributed by the salt, but this may not be the case. It has been suggested that anion-cation coordination systems within the solvent may be the cause of new phases in high salt concentration systems.<sup>61</sup> If this is correct, then  $\text{LiPF}_6$  may have a very different effect on the melting behaviour of a solvent than, say,  $\text{LiTFSI}$ , which has a much larger anion. One new project might be to test a simple salt-solvent combination, whose  $\text{LiPF}_6$  equivalent has been well understood, such as the  $\text{LiBOB-DMC}$  or  $\text{LiTFSI-DMC}$  phase diagram and check to see if it matches the already known diagrams.

### **7.2.13 Careful Study of Early Cell Life**

All cells in the secondary experiment, outlined in section 5.5.2 show changes in the first few cycles in a cell. These changes were not documented in the primary experiment. This suggest that there may be early life behaviour in these cells, at lower voltages that was not observed. One possibility is that, at high temperatures,  $\text{LiPF}_6$  may decompose until an equilibrium is reached between  $\text{LiPF}_6$ ,  $\text{LiF}$  and  $\text{PF}_5$ , thus driving transesterification to some upper limit, or higher voltages induce a brief period of accelerated parasitic reactions in these cells, which tapers off. If either of these were correct, or if some other mechanism could be understood, this could lead to a better understanding of the early life of Li-ion electrolyte, and how it might relate to long term degradation and cycle life.

This early lifetime degradation would not be difficult to study but would be time consuming. A small series of identical, simple electrolyte cells could be made, set to a series of voltages and temperatures, and tested in the first few weeks of their lifetimes. One possible test that could be used could be a set of cells cycled to 4.3 V, 4.4 V, and 4.5 V, at 20, 40, and 55°C, tested every ten or twenty cycles, until the cells had reached one hundred cycles. If the cells were started on a staggered schedule to prevent significant backup, then this would require 45 to 90 tests, and take around a month, with full use of one DTA apparatus.

#### **7.2.14 Storage versus Cycling**

While it may be assumed that the most damaging process a Li-ion cell can undergo is high voltage and high temperature cycling, work done concurrently with this thesis has shown high voltage storage to be similarly damaging. This is concerning to the development of Li-ion cells, as many applications require extended time at high voltage, especially the grid level storage required for large scale renewable energy implementation.

This behaviour has been reflected in DTA tests, in a large experiment with cycling and storage cells. This suggests that, while some electrolyte degradation is related to the number of cycles a cell has undergone, some of the degradation is dependent on time, or average voltage over a cell's lifetime. This is another area where DTA can help to diagnose degradation effects. As long term storage cells, by nature, do not have much electrochemical data, DTA can be used to study their health post-test, and to determine the effects of different additives or cell chemistries on electrolyte degradation.

### **7.2.15 Methyl Acetate Cells**

Methyl acetate (MA) has been shown to grant some beneficial features to Li-ion cells. As it is a very low viscosity solvent, it will drive the total electrolyte viscosity down, when used as a cosolvent in concentration ranges of 10-20%, and thus drive up ionic conductivity, as in section 3.3.3. This would be of use when designing a cell that could charge quickly. However, MA carries its own challenges when being considered for testing in DTA sample cells; MA is the reference currently used to test other cells. Thus, a cell containing MA would not freeze completely when using standard DTA temperature ranges. Depending on what degradation processes are present in these cells, that lack of freezing may occlude important data.

This leads to two possible paths, if DTA testing is intended to be used on MA containing cells. The first is finding a new reference cell electrolyte. This may not be simple, as such an electrolyte would ideally need to be similar to the solvents used in Li-ion cells, in terms of heat capacity. If no such solvent is found, these cells could be run against dry pouch cells. The resultant data would not be perfect, but the thermal mass of the dry cell would be close to the sample cell, giving acceptable results. The third option is to simply ignore the component that does not freeze, and interpret the data based on the component that does.

### **7.2.16 Anode Free Cells**

Though general development of Li-ion cells requires very broad development across many areas of performance, there are niche areas where one aspect of Li-ion cell capability can be promoted at the cost of others. One such niche is extremely high energy

density cells that are used disposably. A Li-ion technology for this niche is the so called “anode free” configuration. This class of cell is not anode free in that it has no anode at all, but in that it uses no negative intercalation material to store lithium. Instead, this type of battery plates and strips metallic lithium directly on the negative current collector, or on a thin coating on said current collector. This type of cell can achieve massive energy densities, but has a very short lifetime, usually on the order of a few dozen cycles.

These cells are in development, and efforts are being made to extend their lifetime as much as possible. As these cells are a relatively new form of Li-ion cell, every aspect must be optimized, from the negative “electrode” surface, to the salts, solvents, and additives used. While these cells are new, and their degradation not well understood, it has been hypothesized that a possible cause of death is a sudden lack of solvent with which to create new SEI. As lithium is being repeatedly plated and stripped, the cell is constantly creating new SEI material, and consuming electrolyte. When the electrolyte is gone, the cell fails, or so goes the hypothesis. If this is the case, DTA could be used to determine the remaining solvent mass, how that mass relates to the death of the cell, and how variations in cell and electrolyte design affect the process.

#### **7.2.17 Positive Peak Investigation**

Though the cells tested in the main experiment do not show them, the presence of positive peaks in DTA data has plagued various cell series in recent years of DTA testing. Though a protocol has been devised to counteract these features, as described in section 2.1.4, there may yet be some physical meaning to these features. For example, in Figure 6.8, these features show up in all cells, but are markedly different in cells cycled to voltages

above and below 4.3 V. Further, the fact that no cells in the primary experiment show consistent positive peaks, while other data taken, but not shown here, shows positive peaks in every cell, suggests that there is a systematic cause to these features.

The first step in a study of this phenomenon would be the characterization of which cells do and do not show these features. This would involve a close study of the data collected thus far in the DTA project, and a comparison against all factors that have been observed to differ between cells that do and do not show these features. This includes positive electrode, negative electrode, additive, upper cutoff voltage, cycle temperature, cycle lifetime, electrolyte composition, and testing protocol. Only then could the development of a system of understanding regarding what might be causing these features to be developed.

Like many aspects of DTA, this could possibly be leveraged to the development of a new understanding of Li-ion cells, or a deeper understanding of the interactions present in Li-ion cell electrolyte.

#### **7.2.18 Melting Points of Linear Carbonates**

While the work done in and around this project has illuminated many, potentially very useful projects that could be undertaken to further broad understanding of Li-ion cells, it has also brought to light a more pedantic issue in the literature surrounding this space. Namely, many chemical databases are incorrect about the melting points of linear carbonate solvents used in Li-ion cells. If one searches for these values either on the internet or in a conventionally trusted database like the CRC Handbook of Chemistry and Physics, one may find that DMC, DEC, and EMC melt at 0.5, -43, and -14.5°C, where the

actual melting points are 4.6, -74.3, and -55.6°C. In the case of DEC, the value came from one paper published over a century ago, whose results were either never questioned, or repeated erroneously, and accepted into the literature. It is likely that the rest of these errors stem from similar situations. Though the same errors do not seem to be present for cyclic carbonates such as ethylene or propylene carbonate, the presence of the linear carbonate errors calls into question the literature values for other classes of solvents.

It may be of value to conduct a test on the melting points of these materials, either with DSC or DTA, and publish a correction to this error in the literature. Whether or not such a publication would be noticed by the groups assembling chemical databases is another matter.

#### **7.2.19 Electrolyte Evolution of EC:DMC**

The Dahn Lab is moving towards electrolytes based on EC and DMC. To this end, an experiment like the primary one described here could be conducted on EC:DMC cells. This degradation would likely be considerably clearer, as cells that do not have EMC cannot, to the current understanding, undergo transesterification to create other linear carbonates. This then means that the interpretation of the DTA curves resulting from such an experiment would be uncluttered by quite so many reaction products.

There are also a few lessons to be taken from the experiment in this thesis, for consideration when designing further experiments of this kind. First, the experiment does not require four duplicates of each cell type. This redundancy leads to an unmanageable number of cells, that cannot be studied meaningfully. This difficulty may be alleviated by a higher throughput of DTA, that could be accomplished using multiple devices. Second,

the cells that will die quickly should be tested first. High upper cutoff voltage can be used to accelerate death and therefore show meaningful change very fast, but the early changes in the lower voltage cells is also of interest. Starting all cells at once, as was done in this thesis, will likely lead to an attempt to record the degradation of the cells that die quickly, at the expense of the longer lived cells that may be degrading in informative ways.



## Bibliography

- [1] R.P. Day, J. Xia, R. Petibon, J. Rucska, H. Wang, A.T.B. Wright, J.R. Dahn, Differential Thermal Analysis of Li-Ion Cells as an Effective Probe of Liquid Electrolyte Evolution during Aging, *Journal of The Electrochemical Society*. 162 (2015) A2577–A2581. doi:10.1149/2.0181514jes.
- [2] M.S. Ding, K. Xu, T.R. Jow, Liquid-Solid Phase Diagrams of Binary Carbonates for Lithium Batteries, *Journal of The Electrochemical Society*. 147 (2000) 1688–1694. doi:10.1149/1.1393419.
- [3] J.R. Dahn, R.E. Mar, M.D. Fleischauer, M.N. Obrovac, The Impact of the Addition of Rare Earth Elements to  $\text{Si}_{1-x}\text{Sn}_x$  Negative Electrode Materials for Li-Ion Batteries, *J. Electrochem. Soc.* 153 (2006) A1211–A1220. doi:10.1149/1.2194631.
- [4] J.R.A. Carlsson, J.-E. Sundgren, X.-H. Li, L.D. Madsen, H.T.G. Hentzell, Predicting the crystallization temperature variation with composition for amorphous silicon-based binary alloy thin films, *Journal of Applied Physics*. 81 (1997) 1150–1156. doi:10.1063/1.363860.
- [5] M.S. Ding, K. Xu, T.R. Jow, Liquid-Solid Phase Diagrams of Binary Carbonates for Lithium Batteries, *Journal of The Electrochemical Society*. 147 (2000) 1688. doi:10.1149/1.1393419.
- [6] G.W.H. Höhne, W. Hemminger, H.-J. Flammersheim, *Differential Scanning Calorimetry: An Introduction for Practitioners*, Springer, 1996.
- [7] K. Xu, Nonaqueous Liquid Electrolytes for Lithium-Based Rechargeable Batteries, *Chemical Reviews*. 104 (2004) 4303–4418. doi:10.1021/cr030203g.
- [8] D.C. Harris, *Quantitative Chemical Analysis*, Eighth, W. H. Freeman and Company, New York, 2010.
- [9] R. Petibon, STUDY OF THE REACTIVITY OF ELECTROLYTE SOLVENTS AND ADDITIVES IN LI-ION CELLS AND DESIGN OF NEW ELECTROLYTE BLENDS, (2016). <https://DalSpace.library.dal.ca/xmlui/handle/10222/71986> (accessed August 26, 2018).
- [10] J. Reddy, *Linden's Handbook of Batteries*, Fourth Edition, McGraw-Hill, 2011.
- [11] M.S. Whittingham, Lithium Batteries and Cathode Materials, *Chem. Rev.* 104 (2004) 4271–4302. doi:10.1021/cr020731c.
- [12] T. Marks, S. Trussler, A.J. Smith, D. Xiong, J.R. Dahn, A Guide to Li-Ion Coin-Cell Electrode Making for Academic Researchers, *Journal of The Electrochemical Society*. 158 (2011) A51. doi:10.1149/1.3515072.

- [13] A.J. Smith, J.C. Burns, D. Xiong, J.R. Dahn, Interpreting High Precision Coulometry Results on Li-ion Cells, *J. Electrochem. Soc.* 158 (2011) A1136–A1142. doi:10.1149/1.3625232.
- [14] J.B. Goodenough, K.-S. Park, The Li-Ion Rechargeable Battery: A Perspective, *J. Am. Chem. Soc.* 135 (2013) 1167–1176. doi:10.1021/ja3091438.
- [15] J.R. Dahn, Phase diagram of  $\text{Li}_x\text{C}_6$ , *Phys. Rev. B.* 44 (1991) 9170–9177. doi:10.1103/PhysRevB.44.9170.
- [16] A. Dębski, W. Zakulski, Ł. Major, A. Góral, W. Gąsior, Enthalpy of formation of the  $\text{Li}_{22}\text{Si}_5$  intermetallic compound, *Thermochimica Acta.* 551 (2013) 53–56. doi:10.1016/j.tca.2012.10.015.
- [17] L.Y. Beaulieu, K.W. Eberman, R.L. Turner, L.J. Krause, J.R. Dahn, Colossal Reversible Volume Changes in Lithium Alloys, *Electrochem. Solid-State Lett.* 4 (2001) A137–A140. doi:10.1149/1.1388178.
- [18] D. Larcher, S. Beattie, M. Morcrette, K. Edström, J.-C. Jumas, J.-M. Tarascon, Recent findings and prospects in the field of pure metals as negative electrodes for Li-ion batteries, *J. Mater. Chem.* 17 (2007) 3759–3772. doi:10.1039/B705421C.
- [19] N. Nitta, F. Wu, J.T. Lee, G. Yushin, Li-ion battery materials: present and future, *Materials Today.* 18 (2015) 252–264. doi:10.1016/j.mattod.2014.10.040.
- [20] K. Mizushima, P.C. Jones, P.J. Wiseman, J.B. Goodenough,  $\text{Li}_x\text{CoO}_2$  ( $0 < x < 1$ ): A new cathode material for batteries of high energy density, *Materials Research Bulletin.* 15 (1980) 783–789. doi:10.1016/0025-5408(80)90012-4.
- [21] D. Aurbach, K. Gamolsky, B. Markovsky, Y. Gofer, M. Schmidt, U. Heider, On the use of vinylene carbonate (VC) as an additive to electrolyte solutions for Li-ion batteries, *Electrochimica Acta.* 47 (2002) 1423–1439.
- [22] J. Tu, X.B. Zhao, G.S. Cao, D.G. Zhuang, T.J. Zhu, J.P. Tu, Enhanced cycling stability of  $\text{LiMn}_2\text{O}_4$  by surface modification with melting impregnation method, *Electrochimica Acta.* 51 (2006) 6456–6462. doi:10.1016/j.electacta.2006.04.031.
- [23] P. Arora, Z. (John) Zhang, Battery Separators, *Chem. Rev.* 104 (2004) 4419–4462. doi:10.1021/cr020738u.
- [24] R. Fong, U. von Sacken, J.R. Dahn, Studies of lithium intercalation into carbons using nonaqueous electrochemical cells, *Journal of The Electrochemical Society.* 137 (1990) 2009–2013.
- [25] M.S. Ding, K. Xu, S. Zhang, T.R. Jow, Liquid/Solid Phase Diagrams of Binary Carbonates for Lithium Batteries Part II, *J. Electrochem. Soc.* 148 (2001) A299–A304. doi:10.1149/1.1353568.

- [26] M.N. Obrovac, V.L. Chevrier, Alloy Negative Electrodes for Li-Ion Batteries, *Chem. Rev.* 114 (2014) 11444–11502. doi:10.1021/cr500207g.
- [27] J. Xia, R. Petibon, D. Xiong, L. Ma, J.R. Dahn, Enabling linear alkyl carbonate electrolytes for high voltage Li-ion cells, *Journal of Power Sources.* 328 (2016) 124–135. doi:10.1016/j.jpowsour.2016.08.015.
- [28] E. Logan, E. M. Tonita, K. L. Gering, J. Li, X. Ma, L. Y. Beaulieu, J. R. Dahn, A Study of the Physical Properties of Li-Ion Battery Electrolytes Containing Esters, *Journal of The Electrochemical Society.* 165 (2018) A21–A30. doi:10.1149/2.0271802jes.
- [29] K.H. Seng, L. Li, D.-P. Chen, Z.X. Chen, X.-L. Wang, H.K. Liu, Z.P. Guo, The effects of FEC (fluoroethylene carbonate) electrolyte additive on the lithium storage properties of NiO (nickel oxide) nanocuboids, *Energy.* 58 (2013) 707–713. doi:10.1016/j.energy.2013.06.011.
- [30] R.S. Arumugam, L. Ma, J. Li, X. Xia, J.M. Paulsen, J.R. Dahn, Special Synergy between Electrolyte Additives and Positive Electrode Surface Coating to Enhance the Performance of Li[Ni<sub>0.6</sub>Mn<sub>0.2</sub>Co<sub>0.2</sub>]O<sub>2</sub>/Graphite Cells, *J. Electrochem. Soc.* 163 (2016) A2531–A2538. doi:10.1149/2.0171613jes.
- [31] X. Li, Z. Yin, X. Li, C. Wang, Ethylene sulfate as film formation additive to improve the compatibility of graphite electrode for lithium-ion battery, *Ionics.* 20 (2014) 795–801. doi:10.1007/s11581-013-1036-5.
- [32] J. Xia, N.N. Sinha, L.P. Chen, J.R. Dahn, A Comparative Study of a Family of Sulfate Electrolyte Additives, *J. Electrochem. Soc.* 161 (2014) A264–A274. doi:10.1149/2.015403jes.
- [33] L. Ma, L. Ellis, S.L. Glazier, X. Ma, Q. Liu, J. Li, J.R. Dahn, LiPO<sub>2</sub>F<sub>2</sub> as an Electrolyte Additive in Li[Ni<sub>0.5</sub>Mn<sub>0.3</sub>Co<sub>0.2</sub>]O<sub>2</sub>/Graphite Pouch Cells, *J. Electrochem. Soc.* 165 (2018) A891–A899. doi:10.1149/2.0381805jes.
- [34] H.-H. Lee, Y.-Y. Wang, C.-C. Wan, M.-H. Yang, H.-C. Wu, D.-T. Shieh, The function of vinylene carbonate as a thermal additive to electrolyte in lithium batteries, *J Appl Electrochem.* 35 (2005) 615–623. doi:10.1007/s10800-005-2700-x.
- [35] J.C. Burns, R. Petibon, K.J. Nelson, N.N. Sinha, A. Kassam, B.M. Way, J.R. Dahn, Studies of the Effect of Varying Vinylene Carbonate (VC) Content in Lithium Ion Cells on Cycling Performance and Cell Impedance, *Journal of The Electrochemical Society.* 160 (2013) A1668–A1674.
- [36] T. Sasaki, T. Abe, Y. Iriyama, M. Inaba, Z. Ogumi, Suppression of an Alkyl Dicarboxate Formation in Li-Ion Cells, *J. Electrochem. Soc.* 152 (2005) A2046–A2050. doi:10.1149/1.2034517.

- [37] B. Li, Y. Wang, H. Rong, Y. Wang, J. Liu, L. Xing, M. Xu, W. Li, A novel electrolyte with the ability to form a solid electrolyte interface on the anode and cathode of a  $\text{LiMn}_2\text{O}_4$ /graphite battery, *J. Mater. Chem. A*. 1 (2013) 12954–12961. doi:10.1039/C3TA13067C.
- [38] J. Xia, L. Ma, C.P. Aiken, K.J. Nelson, L.P. Chen, J.R. Dahn, Comparative Study on Prop-1-ene-1,3-sultone and Vinylene Carbonate as Electrolyte Additives for  $\text{Li}(\text{Ni}_{1/3}\text{Mn}_{1/3}\text{Co}_{1/3})\text{O}_2$ /Graphite Pouch Cells, *J. Electrochem. Soc.* 161 (2014) A1634–A1641. doi:10.1149/2.0541410jes.
- [39] N.N. Sinha, J.C. Burns, J.R. Dahn, Comparative Study of Tris(trimethylsilyl) Phosphate and Tris(trimethylsilyl) Phosphite as Electrolyte Additives for Li-Ion Cells, *J. Electrochem. Soc.* 161 (2014) A1084–A1089. doi:10.1149/2.087406jes.
- [40] D.Y. Wang, J. Xia, L. Ma, K.J. Nelson, J.E. Harlow, D. Xiong, L.E. Downie, R. Petibon, J.C. Burns, A. Xiao, others, A Systematic Study of Electrolyte Additives in  $\text{Li}[\text{Ni}_{1/3}\text{Mn}_{1/3}\text{Co}_{1/3}]\text{O}_2$  (NMC)/Graphite Pouch Cells, *Journal of The Electrochemical Society*. 161 (2014) A1818–A1827.
- [41] A.J. Smith, J.C. Burns, J.R. Dahn, A High Precision Study of the Coulombic Efficiency of Li-Ion Batteries, *Electrochem. Solid-State Lett.* 13 (2010) A177–A179. doi:10.1149/1.3487637.
- [42] J. Vetter, P. Novák, M.R. Wagner, C. Veit, K.-C. Möller, J.O. Besenhard, M. Winter, M. Wohlfahrt-Mehrens, C. Vogler, A. Hammouche, Ageing mechanisms in lithium-ion batteries, *Journal of Power Sources*. 147 (2005) 269–281. doi:10.1016/j.jpowsour.2005.01.006.
- [43] D. Abraham, D. W. Dees, J. Knuth, E. Reynolds, R. Gerald, Y.-E. Hyung, I. Belharouak, M. Stoll, E. Sammann, S. MacLaren, R. Haasch, R. Twisten, M. Sardela, V. Battaglia, E. Cairns, J. Kerr, M. Kerlau, R. Kosteki, J. Lei, L. Norin, Diagnostic examination of Generation 2 lithium-ion cells and assessment of performance degradation mechanisms., (2005). doi:10.2172/861617.
- [44] C.P. Aiken, J. Xia, D.Y. Wang, D.A. Stevens, S. Trussler, J.R. Dahn, An Apparatus for the Study of In Situ Gas Evolution in Li-Ion Pouch Cells, *Journal of The Electrochemical Society*. 161 (2014) A1548–A1554.
- [45] M. Broussely, S. Herreyre, P. Biensan, P. Kasztejna, K. Nechev, R.J. Staniewicz, Aging mechanism in Li ion cells and calendar life predictions, *Journal of Power Sources*. 97–98 (2001) 13–21. doi:10.1016/S0378-7753(01)00722-4.
- [46] N.N. Sinha, A.J. Smith, J.C. Burns, G. Jain, K.W. Eberman, E. Scott, J.P. Gardner, J.R. Dahn, The use of elevated temperature storage experiments to learn about parasitic reactions in wound  $\text{LiCoO}_2$ /graphite cells, *Journal of The Electrochemical Society*. 158 (2011) A1194–A1201.

- [47] L.J. Krause, L.D. Jensen, J.R. Dahn, Measurement of Parasitic Reactions in Li Ion Cells by Electrochemical Calorimetry, *J. Electrochem. Soc.* 159 (2012) A937–A943. doi:10.1149/2.021207jes.
- [48] L.E. Downie, J.R. Dahn, Determination of the Voltage Dependence of Parasitic Heat Flow in Lithium Ion Cells Using Isothermal Microcalorimetry, *J. Electrochem. Soc.* 161 (2014) A1782–A1787. doi:10.1149/2.0301412jes.
- [49] R. Petibon, L. Rotermund, K.J. Nelson, A.S. Gozdz, J. Xia, J.R. Dahn, Study of Electrolyte Components in Li Ion Cells Using Liquid-Liquid Extraction and Gas Chromatography Coupled with Mass Spectrometry, *Journal of the Electrochemical Society.* 161 (2014) A1167–A1172. doi:10.1149/2.117406jes.
- [50] V. Agubra, J. Fergus, Lithium Ion Battery Anode Aging Mechanisms, *Materials (Basel).* 6 (2013) 1310–1325. doi:10.3390/ma6041310.
- [51] S.E. Sloop, J.B. Kerr, K. Kinoshita, The role of Li-ion battery electrolyte reactivity in performance decline and self-discharge, *Journal of Power Sources.* 119–121 (2003) 330–337. doi:10.1016/S0378-7753(03)00149-6.
- [52] H. Yoshida, T. Fukunaga, T. Hazama, M. Terasaki, M. Mizutani, M. Yamachi, Degradation mechanism of alkyl carbonate solvents used in lithium-ion cells during initial charging, *Journal of Power Sources.* 68 (1997) 311–315. doi:10.1016/S0378-7753(97)02635-9.
- [53] H. Kim, S. Grugeon, G. Gachot, M. Armand, L. Sannier, S. Laruelle, Ethylene bis-carbonates as telltales of SEI and electrolyte health, role of carbonate type and new additives, *Electrochimica Acta.* 136 (2014) 157–165. doi:10.1016/j.electacta.2014.05.072.
- [54] T. Sasaki, T. Abe, Y. Iriyama, M. Inaba, Z. Ogumi, Formation mechanism of alkyl dicarbonates in Li-ion cells, *Journal of Power Sources.* 150 (2005) 208–215. doi:10.1016/j.jpowsour.2005.02.021.
- [55] E.S. Takeuchi, H. Gan, M. Palazzo, R.A. Leising, S.M. Davis, Anode Passivation and Electrolyte Solvent Disproportionation: Mechanism of Ester Exchange Reaction in Lithium-Ion Batteries, *J. Electrochem. Soc.* 144 (1997) 1944–1948. doi:10.1149/1.1837726.
- [56] B. Strehle, S. Solchenbach, M. Metzger, K.U. Schwenke, H.A. Gasteiger, The Effect of CO<sub>2</sub> on Alkyl Carbonate Trans-Esterification during Formation of Graphite Electrodes in Li-Ion Batteries, *J. Electrochem. Soc.* 164 (2017) A2513–A2526. doi:10.1149/2.1001712jes.
- [57] X. Zhang, P.N. Ross, R. Kosteki, F. Kong, S. Sloop, J.B. Kerr, K. Striebel, E.J. Cairns, F. McLarnon, Diagnostic Characterization of High Power Lithium-Ion

- Batteries for Use in Hybrid Electric Vehicles, *J. Electrochem. Soc.* 148 (2001) A463–A470. doi:10.1149/1.1362541.
- [58] R. Petibon, J. Xia, L. Ma, M.K.G. Bauer, K.J. Nelson, J.R. Dahn, Electrolyte System for High Voltage Li-Ion Cells, *J. Electrochem. Soc.* 163 (2016) A2571–A2578. doi:10.1149/2.0321613jes.
- [59] M.S. Ding, Liquid-Solid Phase Diagrams of Ternary and Quaternary Organic Carbonates, *J. Electrochem. Soc.* 151 (2004) A731–A738. doi:10.1149/1.1690782.
- [60] M.S. Ding, Liquid–Solid Phase Equilibria and Thermodynamic Modeling for Binary Organic Carbonates, *J. Chem. Eng. Data.* 49 (2004) 276–282. doi:10.1021/je034134e.
- [61] S.-D. Han, O. Borodin, J.L. Allen, D.M. Seo, D.W. McOwen, S.-H. Yun, W.A. Henderson, Electrolyte Solvation and Ionic Association: IV. Acetonitrile-Lithium Difluoro(oxalato)borate (LiDFOB) Mixtures, *Journal of the Electrochemical Society.* 160 (2013) A2100–A2110. doi:10.1149/2.094309jes.
- [62] D.M. Seo, J.L. Allen, L.A. Gardner, S.-D. Han, P.D. Boyle, W.A. Henderson, Electrolyte Solvation and Ionic Association: Cyclic Carbonate and Ester-LiTFSI and -LiPF<sub>6</sub> Mixtures, *ECS Transactions.* 50 (2013) 375–380. doi:10.1149/05026.0375ecst.
- [63] J. Li, R. Doig, H. Liu, G. Botton, J.R. Dahn, The Effect of Interdiffusion on the Properties of Lithium-Rich Core-Shell Cathodes, *J. Electrochem. Soc.* 163 (2016) A2841–A2848. doi:10.1149/2.1231613jes.
- [64] K.J. Nelson, G.L. d’Eon, A.T.B. Wright, L. Ma, J. Xia, J.R. Dahn, Studies of the Effect of High Voltage on the Impedance and Cycling Performance of Li[Ni<sub>0.4</sub>Mn<sub>0.4</sub>Co<sub>0.2</sub>]O<sub>2</sub>/Graphite Lithium-Ion Pouch Cells, *J. Electrochem. Soc.* 162 (2015) A1046–A1054. doi:10.1149/2.0831506jes.
- [65] L.D. Ellis, S. Buteau, S.G. Hames, L.M. Thompson, D.S. Hall, J.R. Dahn, A New Method for Determining the Concentration of Electrolyte Components in Lithium-Ion Cells, Using Fourier Transform Infrared Spectroscopy and Machine Learning, *Journal of The Electrochemical Society.* 165 (2018) A256–A262. doi:10.1149/2.0861802jes.
- [66] L. Thompson, CHANGES TO THE ELECTROLYTE IN AGED LI-ION CELLS, (2018). <https://DalSpace.library.dal.ca/xmlui/handle/10222/74109> (accessed August 25, 2018).

## Appendix A: Solvent Melting Points

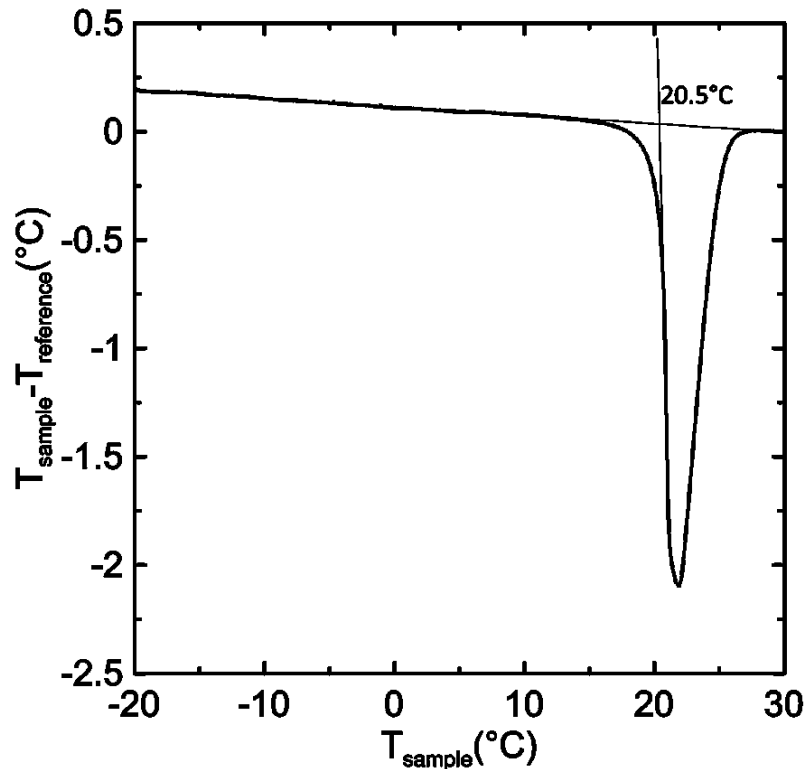


Figure B.1: A DTA test of a core-shell cell filled with VC, run at 0.25°C/min.

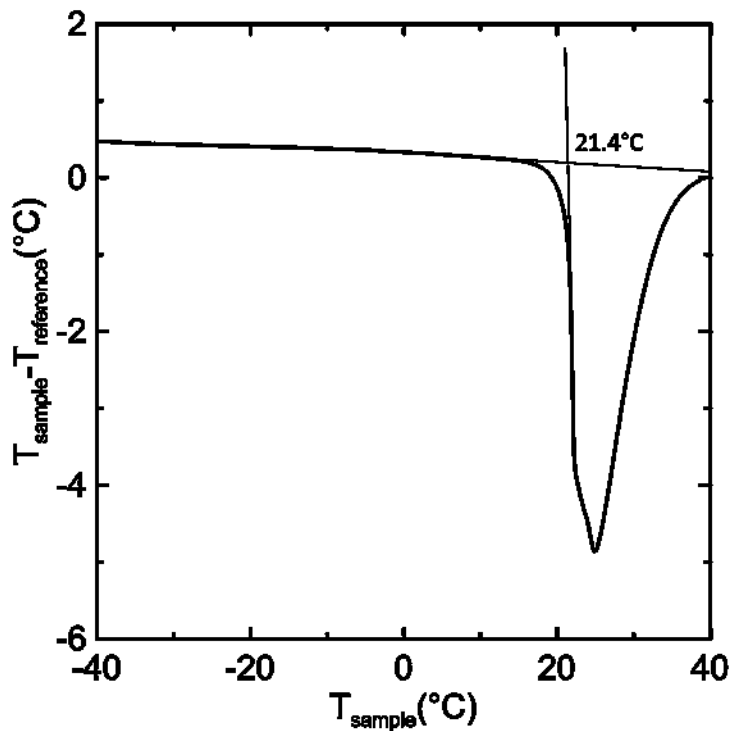


Figure B.2: A DTA test of a core shell cell filled with FEC, run at 1.0°C/min.

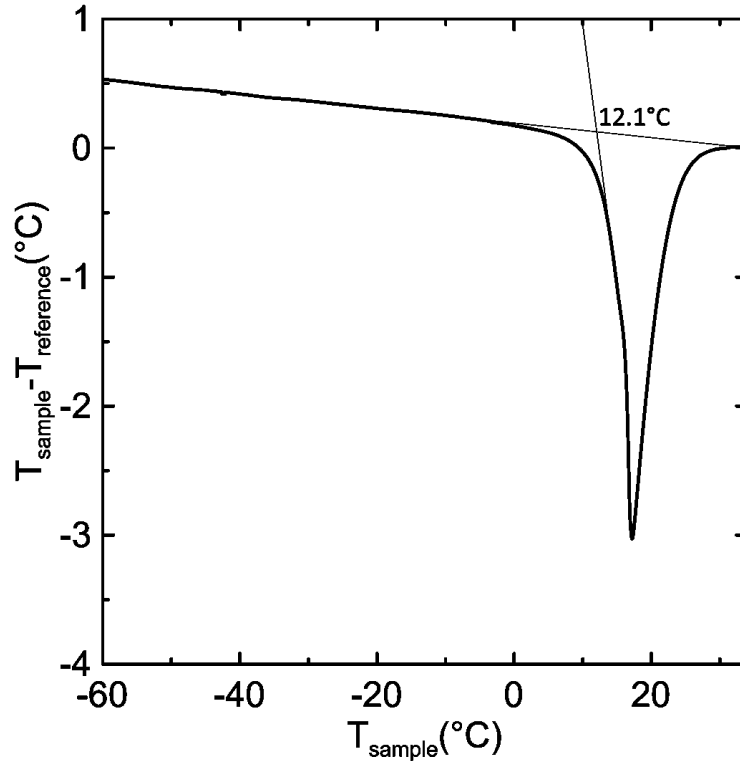


Figure B.3: A DTA test of a core shell cell filled with DMOHC, run at 1.0°C/min.

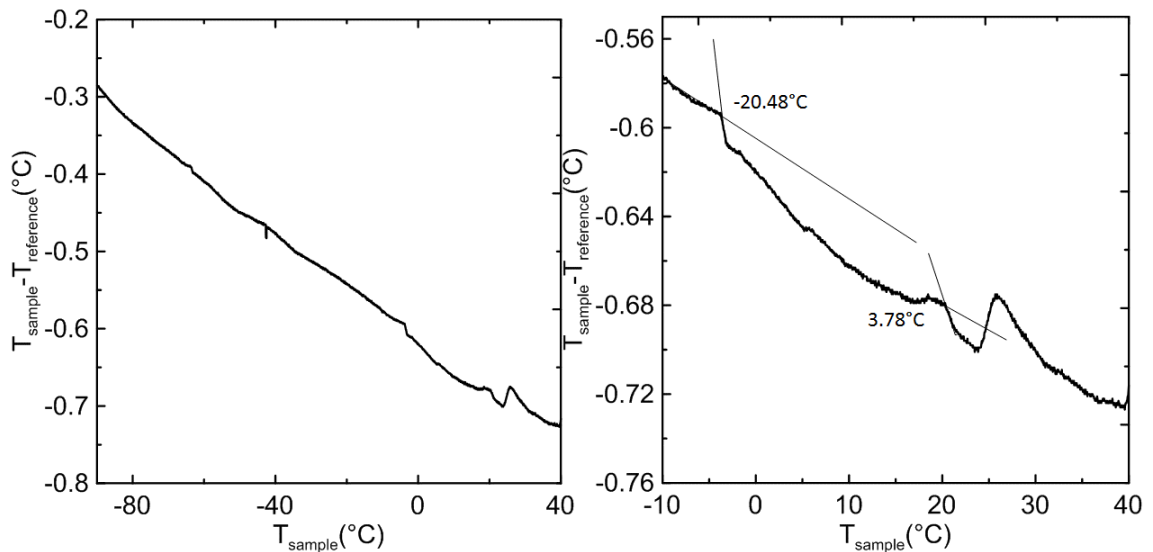


Figure B.4: A DTA test of a core shell cell filled with DEOHC, tested at 1.0°C/min. There may be a freezing point at -20.48°C, or 3.78°C, but the extremely small size makes these difficult to interpret, or justify that these are not just noise. A second cell of this type was filled and tested down to -180°C, with no apparent phase transitions; if these are not phase transitions, then DEOHC does not freeze until some temperature below -180°C.



## Appendix B: Permissions

dejun.xiong@capchem.com  
Tue 06-26, 4:35 AM

Sure



熊得军 Dejun Xiong  
研发中心 R&D Center  
研发副总监 Vice R&D Director

Mobile: 0086-136-0260-1140(座号: 6293)

E-mail: dejun.xiong@capchem.com

地址: 深圳市坪山区马峦街道沙壙同富裕工业区  
Add: Shabo Tongfuyu Industry Zone, Maluan Subdistrict,  
Pingshan District, Shenzhen City, PRC  
Zip Code: 518118  
Tel: 0086-(0)755-8992-3768  
Fax: 0086-(0)755-8992-4533  
Web: www.capchem.com

\*\*\*

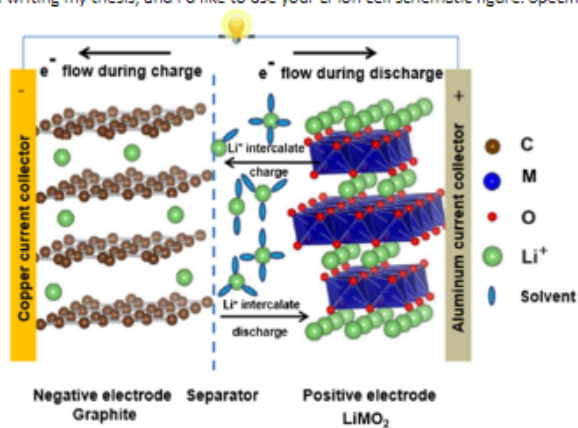
Michael Bauer

Mon 06-25, 1:52 PM

dejun.xiong@capchem.com

Hello

I'm writing my thesis, and I'd like to use your Li-ion cell schematic figure. Specifically, this one:



May I have your permission to use this figure?

Michael Bauer

Electrochemical Society, Inc LICENSE  
TERMS AND CONDITIONS

Jul 23, 2018

This is a License Agreement between Michael K Bauer ("You") and Electrochemical Society, Inc ("Electrochemical Society, Inc") provided by Copyright Clearance Center ("CCC"). The license consists of your order details, the terms and conditions provided by Electrochemical Society, Inc, and the payment terms and conditions.

**All payments must be made in full to CCC. For payment instructions, please see information listed at the bottom of this form.**

License Number	4394920628299
License date	Jul 17, 2018
Licensed content publisher	Electrochemical Society, Inc
Licensed content title	Journal of the Electrochemical Society
Licensed content date	Jan 1, 1948
Type of Use	Thesis/Dissertation
Requestor type	Academic institution
Format	Print, Electronic
Portion	chart/graph/table/figure
Number of charts/graphs/tables/figures	2
The requesting person/organization is:	Michael Bauer
Title or numeric reference of the portion(s)	Chapter 2, Figure 2.1, Chapter 2, Figure 2.3
Title of the article or chapter the portion is from	Liquid-Solid Phase Diagrams of Binary Carbonates for Lithium Batteries
Editor of portion(s)	N/A
Author of portion(s)	Michael S. Ding, Kang Xu, and T. Richard Jow
Volume of serial or monograph.	147
Issue, if republishing an article from a serial	5
Page range of the portion	1689-1690
Publication date of portion	January 1, 2000
Rights for	Main product
Duration of use	Current edition and up to 5 years
Creation of copies for the disabled	no
With minor editing privileges	no
For distribution to	Worldwide
In the following language(s)	Original language of publication
With incidental promotional use	no
The lifetime unit quantity of new product	Up to 499
Title	STUDYING LONG TERM LI-ION ELECTROLYTE DEGRADATION USING LITHIUM ION DIFFERENTIAL THERMAL ANALYSIS
Instructor name	Jeff Dahn
Institution name	Dalhousie University
Expected presentation date	Aug 2018
Billing Type	Invoice
Billing Address	Michael K Bauer 6369 Coburg Road Apartment 304  Halifax, NS B3H 4J7 Canada Attn: Michael Bauer
Total (may include CCC user fee)	0.00 USD
Terms and Conditions	

Electrochemical Society, Inc LICENSE  
TERMS AND CONDITIONS

Jul 23, 2018

This is a License Agreement between Michael K Bauer ("You") and Electrochemical Society, Inc ("Electrochemical Society, Inc") provided by Copyright Clearance Center ("CCC"). The license consists of your order details, the terms and conditions provided by Electrochemical Society, Inc, and the payment terms and conditions.

**All payments must be made in full to CCC. For payment instructions, please see information listed at the bottom of this form.**

License Number	4394920629713
License date	Jul 17, 2018
Licensed content publisher	Electrochemical Society, Inc
Licensed content title	Journal of the Electrochemical Society
Licensed content date	Jan 1, 1948
Type of Use	Thesis/Dissertation
Requestor type	Academic institution
Format	Print, Electronic
Portion	chart/graph/table/figure
Number of charts/graphs/tables/figures	1
The requesting person/organization is:	Michael Bauer
Title or numeric reference of the portion(s)	Chapter 2, Figure 2.12
Title of the article or chapter the portion is from	Differential Thermal Analysis of Li-Ion Cells as an Effective Probe of Liquid Electrolyte Evolution during Aging
Editor of portion(s)	N/A
Author of portion(s)	R. P. Day, J. Xia, R. Petibon, J. Rucska, H. Wang, A. T. B. Wright and J. R. Dahn
Volume of serial or monograph.	162
Issue, if republishing an article from a serial	14
Page range of the portion	A2579
Publication date of portion	October 9, 2015
Rights for	Main product
Duration of use	Current edition and up to 5 years
Creation of copies for the disabled	no
With minor editing privileges	no
For distribution to	Worldwide
In the following language(s)	Original language of publication
With incidental promotional use	no
The lifetime unit quantity of new product	Up to 499
Title	STUDYING LONG TERM LI-ION ELECTROLYTE DEGRADATION USING LITHIUM ION DIFFERENTIAL THERMAL ANALYSIS
Instructor name	Jeff Dahn
Institution name	Dalhousie University
Expected presentation date	Aug 2018
Billing Type	Invoice
Billing Address	Michael K Bauer 6369 Coburg Road Apartment 304  Halifax, NS B3H 4J7 Canada Attn: Michael K Bauer
Total (may include CCC user fee)	0.00 USD
Terms and Conditions	

## TERMS AND CONDITIONS

The following terms are individual to this publisher:

None

### Other Terms and Conditions:

#### STANDARD TERMS AND CONDITIONS

1. Description of Service; Defined Terms. This Republication License enables the User to obtain licenses for republication of one or more copyrighted works as described in detail on the relevant Order Confirmation (the "Work(s)"). Copyright Clearance Center, Inc. ("CCC") grants licenses through the Service on behalf of the rightsholder identified on the Order Confirmation (the "Rightsholder"). "Republication", as used herein, generally means the inclusion of a Work, in whole or in part, in a new work or works, also as described on the Order Confirmation. "User", as used herein, means the person or entity making such republication.

2. The terms set forth in the relevant Order Confirmation, and any terms set by the Rightsholder with respect to a particular Work, govern the terms of use of Works in connection with the Service. By using the Service, the person transacting for a republication license on behalf of the User represents and warrants that he/she it (a) has been duly authorized by the User to accept, and hereby does accept, all such terms and conditions on behalf of User, and (b) shall inform User of all such terms and conditions. In the event such person is a "freelancer" or other third party independent of User and CCC, such party shall be deemed jointly a "User" for purposes of these terms and conditions. In any event, User shall be deemed to have accepted and agreed to all such terms and conditions if User republishes the Work in any fashion.

#### 3. Scope of License; Limitations and Obligations.

3.1 All Works and all rights therein, including copyright rights, remain the sole and exclusive property of the Rightsholder. The license created by the exchange of an Order Confirmation (and/or any invoice) and payment by User of the full amount set forth on that document includes only those rights expressly set forth in the Order Confirmation and in these terms and conditions, and conveys no other rights in the Work(s) to User. All rights not expressly granted are hereby reserved.

3.2 General Payment Terms: You may pay by credit card or through an account with us payable at the end of the month. If you and we agree that you may establish a standing account with CCC, then the following terms apply: Remit Payment to: Copyright Clearance Center, 29118 Network Place, Chicago, IL 60673-1291. Payments Due: Invoices are payable upon their delivery to you (or upon our notice to you that they are available to you for downloading). After 30 days, outstanding amounts will be subject to a service charge of 1-1/2% per month or, if less, the maximum rate allowed by applicable law. Unless otherwise specifically set forth in the Order Confirmation or in a separate written agreement signed by CCC, invoices are due and payable on "net 30" terms. While User may exercise the rights licensed immediately upon issuance of the Order Confirmation, the license is automatically revoked and is null and void, as if it had never been issued, if complete payment for the license is not received on a timely basis either from User directly or through a payment agent, such as a credit card company.

3.3 Unless otherwise provided in the Order Confirmation, any grant of rights to User (i) is "one-time" (including the editions and product family specified in the license), (ii) is non-exclusive and non-transferable and (iii) is subject to any and all limitations and restrictions (such as, but not limited to, limitations on duration of use or circulation) included in the Order Confirmation or invoice and/or in these terms and conditions. Upon completion of the licensed use, User shall either secure a new permission for further use of the Work(s) or immediately cease any new use of the Work(s) and shall render inaccessible (such as by deleting or by removing or severing links or other locators) any further copies of the Work (except for copies printed on paper in accordance with this license and still in User's stock at the end of such period).

3.4 In the event that the material for which a republication license is sought includes third party materials (such as photographs, illustrations, graphs, inserts and similar materials) which are identified in such material as having been used by permission, User is responsible for identifying, and seeking separate licenses (under this Service or otherwise) for, any of such third party materials; without a separate license, such third party materials may not be used.

3.5 Use of proper copyright notice for a Work is required as a condition of any license granted under the Service. Unless otherwise provided in the Order Confirmation, a proper copyright notice will read substantially as follows: "Republished with permission of [Rightsholder's name], from [Work's title, author, volume, edition number and year of copyright]; permission conveyed through Copyright Clearance Center, Inc." Such notice must be provided in a reasonably legible font size and must be placed either immediately adjacent to the Work as used (for example, as part of a by-line or footnote but not as a separate electronic link) or in the place where substantially all other credits or notices for the new work containing the republished Work are located. Failure to include the required notice results in loss to the Rightsholder and CCC, and the User shall be liable to pay liquidated damages for each such failure equal to twice the use fee specified in the Order Confirmation in addition to the use fee itself and any other fees and charges specified.

3.6 User may only make alterations to the Work if and as expressly set forth in the Order Confirmation. No Work may be used in any way that is defamatory, violates the rights of third parties (including such third parties' rights of copyright, privacy, publicity, or other tangible or intangible property), or is otherwise illegal, sexually explicit or obscene. In addition, User may not conjoin a Work with any other material that may result in damage to the reputation of the Rightsholder. User agrees to inform CCC if it becomes aware of any infringement of any rights in a Work and to cooperate with any reasonable request of CCC or the Rightsholder in connection therewith.

4. Indemnity: User hereby indemnifies and agrees to defend the Rightsholder and CCC, and their respective employees and directors, against all claims, liability, damages, costs and expenses, including legal fees and expenses, arising out of any use of a Work beyond the scope of the rights granted herein, or any use of a Work which has been altered in any unauthorized way by User, including claims of defamation or infringement of rights of copyright, publicity, privacy or other tangible or intangible property.

5. Limitation of Liability. UNDER NO CIRCUMSTANCES WILL CCC OR THE RIGHTSHOLDER BE LIABLE FOR ANY DIRECT, INDIRECT, CONSEQUENTIAL OR INCIDENTAL DAMAGES (INCLUDING WITHOUT LIMITATION DAMAGES FOR LOSS OF BUSINESS PROFITS OR INFORMATION, OR FOR BUSINESS INTERRUPTION) ARISING OUT OF THE USE OR INABILITY TO USE A WORK, EVEN IF ONE OF THEM HAS BEEN ADVISED OF THE POSSIBILITY OF SUCH DAMAGES. In any event, the total liability of the Rightsholder and CCC (including their respective employees and directors) shall not exceed the total amount actually paid by User for this license. User assumes full liability for the actions and omissions of its principals, employees, agents, affiliates, successors and assigns.

6. Limited Warranties. THE WORK(S) AND RIGHT(S) ARE PROVIDED "AS IS". CCC HAS THE RIGHT TO GRANT TO USER THE RIGHTS GRANTED IN THE ORDER CONFIRMATION DOCUMENT. CCC AND THE RIGHTSHOLDER DISCLAIM ALL OTHER WARRANTIES RELATING TO THE WORK(S) AND RIGHT(S), EITHER EXPRESS OR IMPLIED, INCLUDING WITHOUT LIMITATION IMPLIED WARRANTIES OF MERCHANTABILITY OR FITNESS FOR A PARTICULAR PURPOSE. ADDITIONAL RIGHTS MAY BE REQUIRED TO USE ILLUSTRATIONS, GRAPHS, PHOTOGRAPHS, ABSTRACTS, INSERTS OR OTHER PORTIONS OF THE WORK (AS OPPOSED TO THE ENTIRE WORK) IN A MANNER CONTEMPLATED BY USER: USER UNDERSTANDS AND AGREES THAT NEITHER CCC NOR THE RIGHTSHOLDER MAY HAVE SUCH ADDITIONAL RIGHTS TO GRANT.

7. Effect of Breach. Any failure by User to pay any amount when due, or any use by User of a Work beyond the scope of the license set forth in the Order Confirmation and/or these terms and conditions, shall be a material breach of the license created by the Order Confirmation and these terms and conditions. Any breach not cured within 30 days of written notice thereof shall result in immediate termination of such license without further notice. Any unauthorized (but licensable) use of a Work that is terminated immediately upon notice thereof may be liquidated by payment of the Rightsholder's ordinary license price therefor, any unauthorized (and unlicensable) use that is not terminated immediately for an reason (including, for example, because materials containing the Work cannot reasonably be recalled) will be subject to all remedies available at law or in equity, but in no event to a payment of less than three times the Rightsholder's ordinary license price for the most closely analogous licensable use plus Rightsholder's and/or CCC's costs and expenses incurred in collecting such payment.

#### 8. Miscellaneous.

8.1 User acknowledges that CCC may, from time to time, make changes or additions to the Service or to these terms and conditions, and CCC reserves the right to send notice to the User by electronic mail or otherwise for the purposes of notifying User of such changes or additions; provided that any such changes or additions shall not apply to permissions already secured and paid for.

8.2 Use of User-related information collected through the Service is governed by CCC's privacy policy, available online here:

<http://www.copyright.com/content/cc3/en/tools/footer/privacypolicy.html>

8.3 The licensing transaction described in the Order Confirmation is personal to User.

Therefore, User may not assign or transfer to any other person (whether a natural person or an organization of any kind) the license created by the Order Confirmation and these terms and conditions or any rights granted hereunder; provided, however, that User may assign such license in its entirety on written notice to CCC in the event of a transfer of all or substantially all of User's rights in the new material which includes the Work(s) licensed under this Service.

8.4 No amendment or waiver of any terms is binding unless set forth in writing and signed by the parties. The Rightsholder and CCC hereby object to any terms contained in any writing prepared by the User or its principals, employees, agents or affiliates and purporting to govern or otherwise relate to the licensing transaction described in the Order Confirmation, which terms are in any way inconsistent with any terms set forth in the Order Confirmation and/or in these terms and conditions or CCC's standard operating procedures whether such writing is prepared prior to, simultaneously with or subsequent to the Order Confirmation, and whether such writing appears on a copy of the Order Confirmation or in separate instrument.

8.5 The licensing transaction described in the Order Confirmation document shall be governed by and construed under the law of the State of New York, USA, without regard to the principles thereof of conflicts of law. Any case, controversy, suit, action, or proceeding arising out of, in connection with, or related to such licensing transaction shall be brought, CCC's sole discretion, in any federal or state court located in the County of New York, State of New York, USA, or in any federal or state court whose geographical jurisdiction covers the location of the Rightsholder set forth in the Order Confirmation. The parties expressly submit to the personal jurisdiction and venue of each such federal or state court. If you have any comments or questions about the Service or Copyright Clearance Center, please contact us at 978-750-8400 or send an e-mail to [info@copyright.com](mailto:info@copyright.com).

v 1.1

Questions? [customerscare@copyright.com](mailto:customerscare@copyright.com) or +1-855-239-3415 (toll free in the US) or +1-978-646-2777.